NUMERICAL SIMULATION OF SINGLE PHASE AND BOILING MICROJET IMPINGEMENT

A

THESIS

Presented to the Faculty

of the University of Alaska Fairbanks

in Partial Fulfillment of the Requirements

for the Degree of

DOCTOR OF PHILOSOPHY

By

Srivathsan Ragunathan, M.S.

Fairbanks, Alaska

December 2008

NUMERICAL SIMULATION OF SINGLE PHASE AND BOILING MICROJET IMPINGEMENT

By

Srivathsan Ragunathan

RECOMMENDED:

Advisory Committee Chair

Chair, Department of Mechanical Engineering

APPROVED:

Dean, College of Engineering and Mines

Dean of the Graduate School

Dec 12, 2008

Date

Abstract

This work presents results from the numerical simulation of single phase and boiling microjets primarily for high density electronics cooling. For the single phase microjets, numerical simulation results for the flow fields and heat transfer characteristics in a laminar, confined microjet (76 μm in diameter) impingement arrangement are presented. The parameters varied included the jet Reynolds Number, the fluid Prandtl Number and the ratio of the nozzle-to-plate distance to the jet diameter. Primary and secondary recirculation zones were observed in the stagnation region and the radial outflow region which had a significant impact on the local Nusselt Number distribution on the heated surface. The location and the displacement of the primary and secondary recirculation zones are of particular importance and are associated with secondary peaks in the Nusselt Number similar to those observed for turbulent jet impingement in larger conventional jets.

Numerical simulation results are presented for boiling microjet impingement in a confined arrangement. The Renssealer Polytechnic Institute (RPI) model was modified for laminar flow boiling for simulating these types of flows. The model primarily proposes three different heat transfer components, the single phase heat transfer, the quenching heat transfer and the evaporative heat transfer. The model was first validated with experimental results from the literature and then extended to study the effects of liquid subcooling, microjet Reynolds Number based on the nozzle inlet, and heat flux levels. The simulation results were in good agreement with results from comparable experiments in the literature. The average wall temperature increases as the applied wall heat flux is increased. The slopes of the temperature curves in the radial direction flatten out at higher heat fluxes and lower levels of subcooling indicating the effectiveness of boiling heat transfer. For the cases considered in this study, the single phase heat transfer

component dominates the other two modes of heat transfer The liquid velocity profile has a considerable impact on the vapor bubble nucleation, vapor drag and the bubble departure diameter. Lower levels of subcooling are associated with boiling inception and more vigorous boiling in the vicinity of the stagnation zone rather than those with higher levels of subcooling. The degree of subcooling emerged as the single largest factor controlling the lateral temperature rise in an electronic chip cooled by a single, confined impinging microjet. Increases in the jet inlet Reynolds Number for the same heat flux and subcooling levels increased the dominance of forced convection heat transfer over the boiling heat transfer. Lower Reynolds Number flows are marked by partial nucleate boiling in contrast to higher Reynolds Number flows marked by forced convection boiling. For all the cases considered in this work, the single phase heat transfer component dominated the other two modes of heat transfer. The evaporative mode dominates the quenching heat transfer mode, an observation that is markedly different from those observed for turbulent evaporative jets found in the literature.

Table of Contents

Page

Page

Page

List of Figures

Page

Page

List of Tables

Page

Nomenclature

T	Temperature (K)
V	Velocity (m/s)
P	Pressure (N/m^2)
q	Applied Wall Heat Flux (W/m^2)
h	Heat Transfer Coefficient (W/m^2K)
d	Diameter (m)
z	Nozzle to Heated Plate Distance (m)
Nu	Nusselt Number
Ja	Jakob Number
Re	Reynolds Number
Pr	Prandtl Number
n	Nucleation Site Density
f	Bubble Departure Frequency (Hz)
C_d	Drag Cofficient
Ω	Effective Wall Area Occupied by the boiling sites
n	Nucleation Site Density
f	Bubble Departure Frequency
ρ	Density (kg/m^3)
L	Latent Heat (J/kg)
U	Local Liquid Velocity (m/s)
ν	Kinematic Viscosity (m^2/s)
$\dot{m}$	Mass Flow Rate (kg/s)
α	Volume Fraction
h	Enthalpy (J/kg)
A	Area (m^2)

C_p	Specific Heat Capacity at Constant Pressure (J/kgK)
t	Time (s)
τ	Shear Stress (N/m^2)

Subscripts

sat	Saturation
sub	Subcooling
ji	Jet Inlet
vw	Departure
b	Bubble
w	Wall
sp	Single Phase
q	Quenching
e	Evaporative
stag	Stagnation
out	Outlet
int	Interfacial

Acknowledgements

My emotional and professional thanks go to my advisor, Dr.Doug Goering, Dean, College of Engineering and Mines, University of Alaska Fairbanks, who was instrumental in inspiring me to work on this project and passed on to me, a chunk of his knowledge on thermo-fluids. I owe a lot of gratitude to my committee members, Dr.Debendra Das, Dr. Jonah Lee and Dr. Cheng-Fu Chen who offered their valuable professional time and knowledge for this work.

My wife Jayashree and daughter Srilakshmi sacrificed a lot of pleasure in life to see me through the doctoral program. This is a good stage to acknowledge their sacrifices. The sacrifices made by my parents was invaluable. This work is dedicated to my father Prof.G. Ragunathan who taught me that the greatest things in life were achieved with perseverance, resilience and humility.

I want to gratefully acknowledge the financial assistance provided by the Center for Nanosensor Technology, the Office of Electronics Miniaturization, the UAF graduate school and the Mechanical Engineering department at various times during my doctoral degree. Finally, I owe everything to the Unseen Hand of the Providence who has guided me in life.

Chapter 1

Introduction

(1.1) Introduction

"Heat, like gravity, penetrates every substance of the universe; its rays occupy all parts of space. The object of our work is to set forth the mathematical laws which this element obeys. The theory of heat will hereafter form one of the most important branches of general physics." *Jean Baptiste Joseph Fourier, Analytical Theory of Heat.*

Fourier's categorical statement, as he likened heat to gravity while formulating his now-oft-used theory on conduction heat transfer, holds true to this day. The science of heat transfer continues to entice and enthrall the scientist and the engineer alike, presenting newer challenges every day. The latest in the line of these challenges is in the area of electronics cooling where increasing power densities coupled with shrinking sizes has led to excessive component heating and reliability issues, necessitating miniaturized cooling solutions that are drastically different from their conventional counterparts.

Even a cursory look at the history of electronics devices from the moment transistors were ingeniously conceived as viable alternatives to vacuum tubes tells us that there has been a strong drive toward miniaturization. The development of SSI, MSI, LSI and VLSI technologies all bear evidence of a gradual shift toward miniaturization (Ragunathan *et al.,* 2007) . Size reduction meant that more active electronic components could be assembled in a given space thus making them smaller and lighter. It, however, carried with it the onus of *heat dissipation* that only increased with the level of miniaturization.

Figure 1.1, for instance, shows the heat dissipation levels of different CMOS technology modules over the years (Ellsworth and Simons, 2005) .The increase in the heat dissipation levels is not limited to one particular organization (Ellsworth and Simons, 2005) . The design power for INTEL Itanium, for instance, is 110 W. Research is being done on increasing the power levels of stacked Chip Scale Packages to use them in active electronic circuitry (Ragunathan *et al.,* 2007) . Heat Fluxes of over

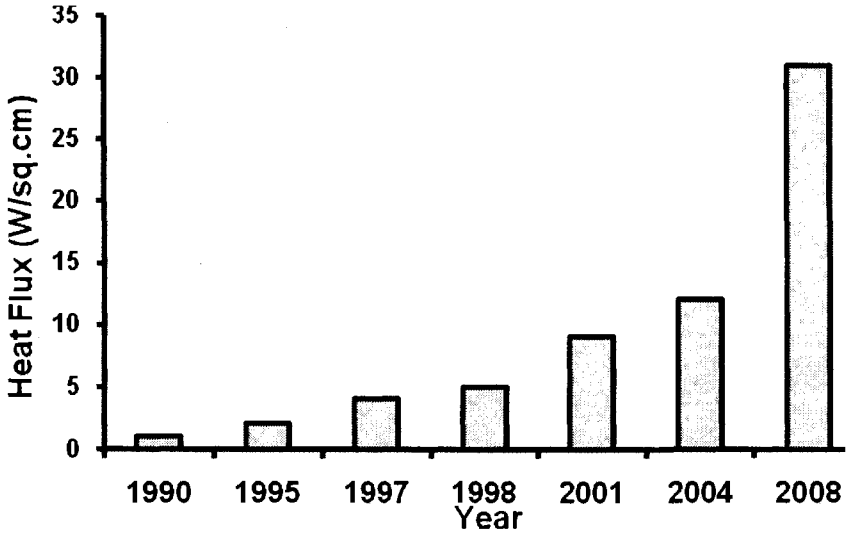

Figure 1.1: CMOS Technology Heat Dissipation Levels over the Years

150 W/cm^2 (comparable to heat flux values encountered in space-vehicle reentry) are being predicted in the next few years. In summary, electronic devices in the near future will dissipate an enormous amount of power such that conventional cooling mechanisms will no longer suffice to keep them at desirable operating temperatures.

The two critical effects of increased heat dissipation in an electronic device are as follows:

(1) ***Functional breakdown*** of the device – These may be due to several reasons such as burn-out, thermal stress-related fracture *et cetera.*

(2) ***Hot Spots*** within the device that elevate the temperature of the device relative to the surroundings. This effect is particularly undesirable in a military environment because the device is easily detected on account of its elevated temperatures in relation to its surroundings.

The afore-mentioned facts point to a fore-gone conclusion: A good cooling design *up-front* is an absolute necessity for the normal operation of an electronic device. The cooling design requirements vary from one electronic device to another. Some effort is made here to stress a few general cooling design requirements.

Until recently, cooling solutions for electronics revolved around using air as the coolant. Air cooling, unlike liquid cooling, is easy to design and operate in addition to the coolant being readily available. The heat transfer coefficient possible though, with air cooling, is limited to about 10-100 W/m^2K (Ellsworth and Simons, 2005) compared to liquid cooling offers a much higher heat transfer coefficient range in an impingement arrangement to about 200-1000 W/m^2K.

There has been a deluge of research activity, both academic and industrial, focusing on the development of a practical liquid cooling system design for high density electronics. The work on liquid cooling systems can broadly be categorized as follows:

(1) Liquid cooling using mini and microchannels: The work pioneered by Zohar (Zohar, 2003), Mudawar (Bowers and Mudawar, 1994) can be cited as examples in this category.

(2) Liquid Cooling using sprays, jets and mists: The works of Garimella (Garimella, 2000), Wang (Wang *et al.*, 2004) etc belong in this category.

(3) Two-Phase Heat Transfer devices: This is a very promising area of research. Research on boiling flows in microchannels, vapor chambers, micro heat pipes, thermpsyphons all belong in this category. The works of Wang (Wang *et al.*, 2004), Mudawar (Bowers and Mudawar, 1994) are some excellent examples.

Two–phase cooling systems, in addition to heat dissipation, offer some significant advantages over single-phase cooling systems. Two very significant advantages are:

(1) The temperatures of the surface dissipating heat to the cooling fluid stays uniform because latent heat dissipation is very high compared to sensible heat requiring minimal temperature gradient to transfer an enormous amount of heat. This aspect is particularly useful in a military environment requiring infra-red masking of the electronic device.

(2) Significantly lower pumping power compared to a single-phase system for the same level of heat dissipation. Two-phase cooling systems have the potential to exceed heat dissipation rates normally associated with turbulent flows.

The vision of the present work then is to make use of the significant advantages of both jet impingement and two-phase (boiling) flows, and to design a practical cooling system for dense electronic systems where space constraints coupled with high heat flux requirements poses a severe challenge. As mentioned above, since this work focuses on two aspects, namely, impinging micro-sized jets and two-phase flows (in micro-sized channels), it is imperative that a general discussion is given on these two very promising approaches in the paragraphs that follow.

(1.1.1) Jet Impingement

A schematic of the basic jet impingement problem is shown in Figure 1.2. In today's parlance, this configuration would be called an unconfined, free and unsubmerged planar or axisymmetric jet. The heat transfer for an axisymmetric jet differs slightly from that for a planar jet because the fluid flow pattern differs slightly. Almost all of the cases considered in this thesis are axisymmetric jets.

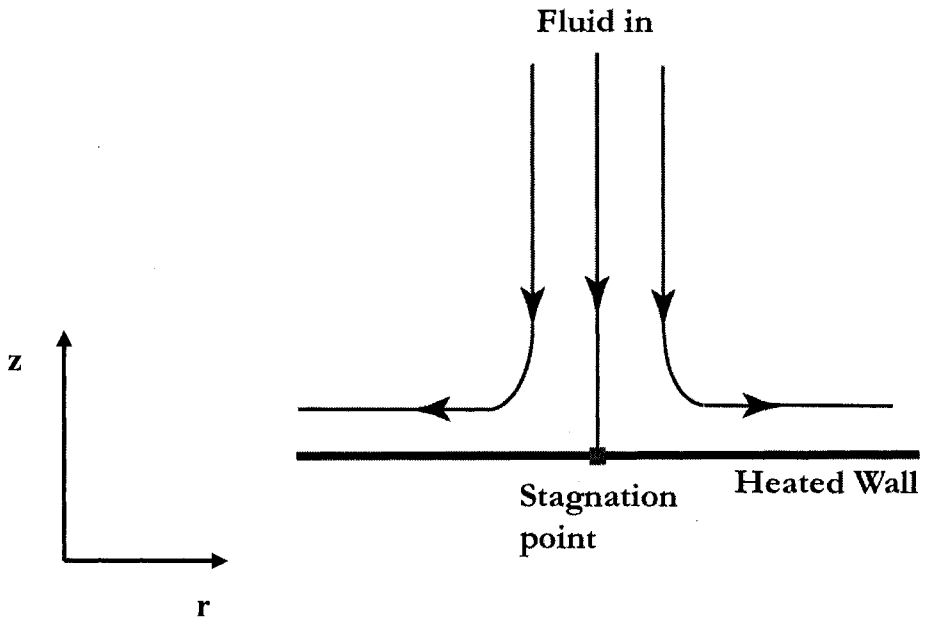

Figure 1.2: The Jet Impingement Problem.

As seen from Figure 1.2, the jet impinges (from a nozzle) on a wall which is at rest. The impingement on to a stationary wall decelerates the fluid to rest forming what is called a stagnation region. In jet impingement problems, the highest pressure region is the stagnation region. The pressure along the radial direction from the stagnation point decreases to ambient at some point downstream accelerating the flow along this direction. The hydrodynamic and thermal boundary layer thicknesses which represent a finite thermal resistance are theoretically zero at the stagnation point. Thus, very high Nusselt Numbers (heat transfer coefficients) are associated with the stagnation region.

The jet impingement problem (both planar and axisymmetric) belongs to a special class of problems in fluid dynamics called *similar flows*, elegantly summarized in White (White, 1991) and Batchelor (Batchelor, 1993). It follows that the analytical solution to the jet impingement problem is through the similarity variable technique where a group of independent variables are grouped together thus reducing the dimensions of the governing equation.

The reader is referred to White (White, 1991) for the analytical technique and the solution to this problem. Two important points that bear significant relevance to the problem under consideration are discussed here.

(1) As mentioned before, the boundary layer thickness is quite thin and the flow accelerates in the radial direction downstream of the stagnation point because of a favorable pressure gradient. The thickness of the stagnation layer is directly proportional to the square-root of the kinematic viscosity, a fluid property. The flow exhibits thin shear-layer behavior.

(2) The laminar Nusselt Number (dimensionless heat transfer coefficient) is directly proportional to the square-root of the Reynolds Number. The Reynolds analogy relating the ratio of the Stanton Number to the skin friction coefficient and the Prandtl Number provides us with a good estimate of the magnitude of heat transfer in the shear layer.

(1.1.2) Classification of Jets

Depending on the nature of the flow and the presence or absence of a wall confining the outflow region, jets are differentiated in a variety of ways. The different configurations are characterized by different hydrodynamic and heat transfer characteristics. Some of the prominent classifications of jets are given in the following paragraphs.

(1) Laminar and Turbulent Jets:

This is a deceptively straight-forward classification of jets based on the Reynolds Number. The Reynolds Number is usually determined based on the jet diameter and is given by the following expression:

$$\mathrm{Re}_d = \frac{V_{ji} d}{\nu} \tag{1.1}$$

It has to be borne in mind, though, that the onset of instability in jet impingement problems occurs at a relatively low Reynolds Number, 4 according to White (White, 1991). (The jet is always physically unstable and this physical instability manifests itself as a numerical instability which was experienced in all the simulation cases in this thesis). The transition of a laminar jet to a turbulent jet may occur anywhere, if transition is destined to occur, before it strikes the impingement surface or in the wall-jet region (radial outflow region). Turbulent jets are characterized by higher transport properties when compared to laminar jets. In a submerged jet configuration (explained in the next paragraph) turbulent jets entrain more fluid from the surroundings promoting thorough mixing. The transition Reynolds Number for jet impingement problems depends upon the configuration under consideration. The description that follows this paragraph further explains this aspect of jet stability.

(2) Free-surface Jets and Submerged Jets :

This is a more rigorous technical classification of jets. If a liquid jet impinges into a region containing the same liquid, it is called a submerged jet. In contrast, if a liquid jet issues into a gaseous environment (Webb and Ma, 1995) it is called a free-surface jet. Figure 1.3 shows a submerged jet and the different zones associated with it. The liquid issues out into a zone containing the same liquid which is stagnant.

As seen from the figure, a potential core is formed at the center of the jet where the velocity is equal to the inlet velocity. The jet velocity decreases in the radial direction outward radially from the potential core. This effect is because of the entrainment of the stagnant ambient fluid into the jet causing mixing which has a slightly deleterious effect on the stagnation heat transfer. Other

characteristics of submerged jets include absence of gravitational effects and the absence of hydraulic jumps as in free jets.

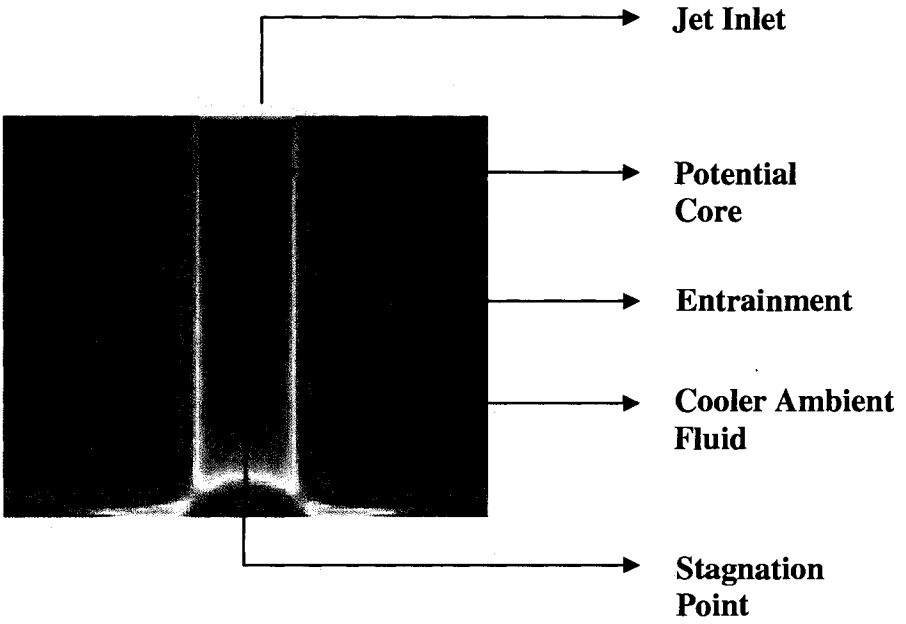

Figure 1.3: A Submerged Jet: Velocity Contour Plot.

Free-surface jets, in contrast, are characterized by the possible occurrence of a hydraulic jump down-stream of the stagnation point with an associated degradation in heat transfer. The roles of surface tension forces and gravitational forces cannot be neglected in a free-surface jet. Free-surface jets may also be subject to pre-impingement break-up and sputtering (Webb and Ma, 1995). Another distinction that can be made between free-surface jets and submerged jets, although it may be beyond the scope of this introductory explanation, is that the heat transfer coefficient for a submerged jet (and thus the Nusselt Number) depends strongly on the orifice-to-plate distance (z/d). In contrast, the heat-transfer coefficient for a free-surface jet is independent of z/d. The dependence on z/d for submerged jets is explained in detail in Chapter 3 of this thesis.

(1.1.3) Two-Phase Flow and Heat Transfer:

As mentioned before, another concept of relevance is introduced here. As the name indicates, two-phase flow refers to two distinct phases flowing concurrently. This may refer to cases where boiling and condensation are absent, for example, the flow of air bubbles with water. In this thesis, though, consideration is given only to two-phase flows which encompass boiling and condensation such as a mixture of a liquid and its own vapor flowing together. Though boiling is an everyday phenomenon in our lives; water and milk appear to boil easily, the physics of boiling is quite complicated. Ideally smooth surfaces do not promote boiling (Tong, 1975). The liquid has to be superheated to a temperature significantly higher than the saturation temperature to initiate boiling. This is called homogeneous nucleation. Heterogeneous nucleation, on the other hand, occurs more readily in practice because of the imperfections in the heated surface in the form of small cavities. These small cavities are the locations on the heated surface where vapor bubbles nucleate, grow to a certain maximum size and then depart when the forces tending to hold them (surface tension and gravity) are no longer dominant enough when compared to forces that tend to pull them off the surface (drag, lift and buoyancy). These sites are referred to as *nucleation sites* and this name is oft-repeated in this thesis. Nucleation site density, referred to as N in this work, the Number of nucleation sites in a given area of the heated surface, is strictly a surface property. Hsu (Hsu, 1962) brought out the importance of *active nucleation sites* in place of nucleation sites where the probability of a bubble growing to an equilibrium size and thus not collapsing, is very high. Most modern theories on boiling are based on Hsu's work on active nucleation sites and research has shown the dependence of active nucleation site density on the local superheat. Thus strictly a surface property, the nucleation site density, can be correlated to the local superheat which is dependent on the flow conditions and the heat transfer coefficient. This finding has made the modeling of flow boiling an easier task.

There are fundamentally two different types of boiling: Pool Boiling and Flow Boiling. A schematic of pool boiling is shown in Figure 1.4. Pool boiling occurs when a

pool of initially quiescent liquid is heated from below. Vapor bubbles are initiated at the active nucleation sites from where they grow to a size that is determined by a balance of gravitational, surface tension and buoyancy forces. After the bubbles detach from the wall, they move into the liquid (sub-cooled or saturated) where they collapse. Fresh liquid rushes in to fill in the void created by the departing bubble and the process continues until the bubble population at the heated surface becomes high enough to engulf the heated surface.

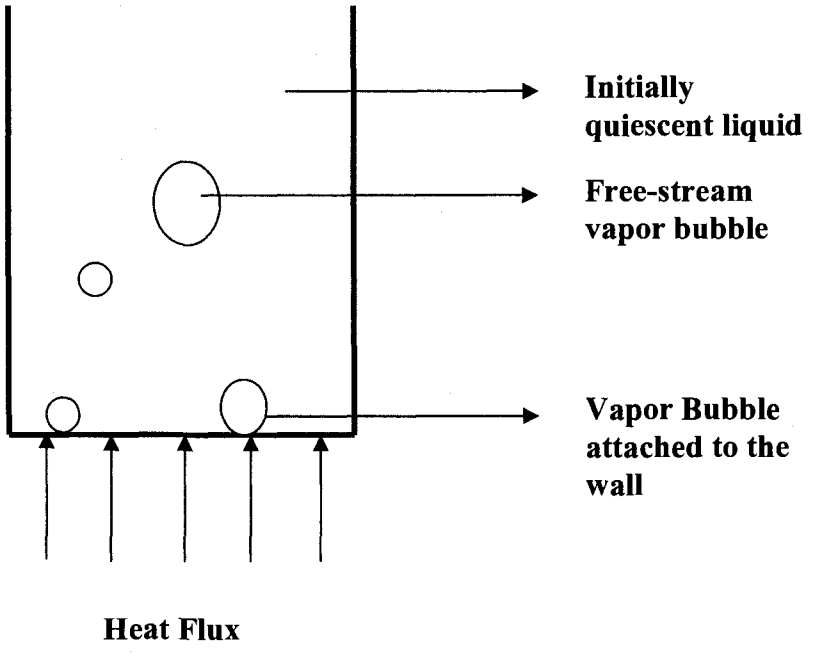

Figure 1.4: A Schematic of Pool Boiling.

Flow boiling is illustrated in Figure 1.5. The physics of flow boiling is similar to pool boiling but for the fact that in flow boiling, the bubble-ebullition process is primarily controlled by drag, lift and virtual mass forces because of the liquid flow. The bubble departure diameter is much smaller in flow boiling as compared to pool boiling.

Not surprisingly, it is not an easy task to simulate the boiling process because of the nature of forces involved and the highly non-linear physics of the problem. The energy equation which is de-coupled from the momentum equation for incompressible flows cannot be de-coupled for two-phase flows because the boiling process itself depends very much on the liquid flow. Added to this are another set of equations for vapor flow which again depend upon the equations for liquid flow and the interfacial terms that also exert some influence on the two-phase flow physics. One has to depend entirely on empirical correlations or flow regime mapping while attempting to model and study two-phase flow.

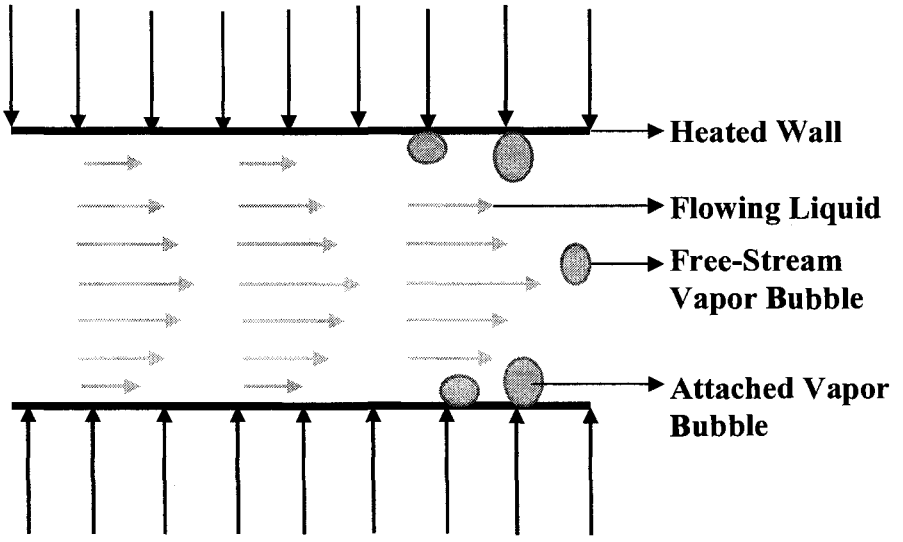

Figure 1.5: A Schematic of Flow Boiling.

Boiling flows in microchannels are reported to be drastically different from macrochannel boiling. One straight-forward difference is that the bubble size can grow only to the size of the channel walls (Zohar, 2003). This in turn, affects the flow regimes that are possible with the two-phase flow and thus the heat transfer that is possible. Recent research has also reported the dependence of the heat transfer coefficient (in nucleate boiling) on the inlet sub-cooling, something drastically different from macro-channel nucleate boiling regimes where the heat transfer coefficient is not very sensitive

to inlet sub-cooling. More details are discussed in the exhaustive literature review to follow.

(1.2) Thesis Objectives:

It is clear from the literature review presented that the focus of all past studies on jet impingement has been on larger size, turbulent, free-surface and confined jets for cooling in larger scale applications. There has been a lack of clear understanding of laminar microscale jets (100 μm) both in the single phase and boiling regimes. The flow dynamics and heat transfer characteristics both in single phase and boiling regimes at smaller scales are quite different from their macro counterparts. To be able to predict the physical processes associated with single and two-phase microjets by means of numerical simulation forms the main motivation for this thesis.

The objectives of this thesis are two-fold:

(1) CFD simulation of single phase microjet impingement for electronics cooling – To explore the effects of the jet Reynolds Number, Prandtl Number and nozzle-to-plate distances on the fluid flow patterns and heat transfer characteristics at varying power levels (heat fluxes) and to suggest optimized flow rates for optimal cooling of electronics.

(2) CFD simulation of boiling jet impingement for electronics cooling – To implement various models required for closure of two-phase flow and heat transfer equations and to suggest optimized flow rates and various two-phase flow parameters for effective cooling of electronics.

Chapter 1 presents a brief introduction and a review of the existing literature on jet impingement. Chapter 2 focuses on the details of the equations solved by the commercial CFD solver FLUENT, discretization methods, models used for closure and other solver details. Chapter 3 presents the results of the single phase microjet

impingement while Chapter 4 presents results of the boiling jet simulations. A summary of results and recommendations for future work are presented in Chapter 5.

Chapter 2

Literature Review

(2.1) Introduction

The literature review for this thesis, much like the entire thesis itself, is divided into three separate sections for easy understanding. They are:

(1) Single Phase confined jet impingement

(2) Boiling flow theories and models

(3) Two-Phase confined jet impingement

The most important and the most relevant technical literature encompassing these three areas from as early as the 1990s are described in detail. A brief discussion of the technical literature not directly related to the above three subject areas but holding some import regarding the physics of the problem being considered in this thesis, is also included in some places.

(2.2.1) Literature on Single Phase Confined Jet Impingement

Stevens and Webb (Stevens and Webb, 1991) experimentally measured and correlated local heat transfer coefficients for a range of jet Reynolds Numbers (4000 to 52000), nozzle diameters (2.2 to 8.9 mm) and nozzle-to-plate spacings. The Prandtl Number dependence was correlated using an exponent of 0.4 ($Nu \propto Pr^{0.4}$). They observed that the nozzle-to-plate spacing had a very minimal effect on the stagnation point Nusselt Number. No secondary peaks in the Nusselt Number were observed for the free jets (indicating absence of a potential core). A strong dependence of the stagnation Nusselt Number on the nozzle size was observed. The normalized Nusselt Number (ratio of the Nusselt Number to the Nusselt Number at the stagnation point) was observed to be

independent of the Reynolds Number up to an r/d (ratio of the radial distance to the nozzle diameter) of 2. Another interesting observation in this paper was that there was a constant Nusselt Number zone up to an r/d of 0.75. A sharp knee was observed in all the Nu/Nu_0 (ratio of the Nusselt Number to the Nusselt Number at the stagnation point) at different r/d values for different nozzle diameters beyond which a sharp dependence of the curves on the Reynolds Number was observed. A secondary peak in the Nusselt Number was also observed for smaller nozzles. Correlations were given for the local and average Nusselt Numbers. Hydraulic jumps characteristic of free-surface jets were observed and the locations of these jumps were given in terms of the Reynolds Number. These hydraulic jumps led to a sharp decrease in the local heat transfer coefficients.

Liu *et al.* (Liu *et al.,* 1991) dealt with the analytical and experimental investigations of stable, unsubmerged (free-surface), initially laminar single phase jets. Local Nusselt Number information was obtained from the stagnation point to a radial distance of up to 40 diameters. Transition to turbulence was observed in the film flow (wall jet region) after a certain radial distance downstream of the stagnation point beyond which a separate turbulent analysis was constructed. The effect of the Prandtl Number on the thermal boundary layer development and, hence, the heat transfer in the wall jet region was studied.

Ichimiya and Hosaka (Ichimiya and Hosaka, 1992) analyzed three confined slot jets experimentally for their impingement heat transfer characteristics in a confined arrangement. The parameters varied included the jet Reynolds Number (500 to 8000), nozzle-to-plate distance (0.5 to 3) and the dimensionless pitch (6-16). The flow field on the impinged surface was visualized using an oil film and the smoke insertion method. The fluid used for impingement was air. For laminar jets, apart from experiments, some numerical calculations (involving the finite difference method) were also done to study the local and average heat transfer characteristics. Experiments were conducted for both single jets and the jet array (3 jets). It was found both from experiments and numerical

solutions for single jets that the Nusselt Number peaked at the stagnation point and that the heat transfer in the outflow region resembled that of developed parallel flow in ducts. In this thesis, though, with water as the coolant, secondary Nusselt Number peaks were observed. This is discussed in Chapter 4 of this thesis. For multiple laminar jets, it was observed that the Nusselt Number was promoted locally and the position of the peak moved downstream. The average Nusselt Number was correlated in terms of the pitch between the nozzles, the Reynolds Number and the nozzle-to-plate distance.

Womac *et al* (Womac *et al.,* 1993) studied free surface jets and submerged jets and their heat transfer characteristics pertaining to impingement over small heat sources representing microelectronic chips experimentally. Data were obtained for a variety of flow conditions (jet inlet velocity, nozzle diameter) and nozzle-to-heater separation distances and the Nusselt Number was correlated in terms of these parameters. For submerged jets, it was observed that the Nusselt Number was very sensitive to the nozzle-to-heater distance unlike the free surface jets. This trend could be attributed to the potential core formation which is a distinguishing feature of submerged jets. It was also observed that beyond the fully turbulent Reynolds Number range of 4000, submerged jets showed a higher heat transfer coefficient than the free-surface jets. This finding was particularly important for this thesis because this thesis deals with submerged laminar jets for cooling electronics.

Elison and Webb (Ellison and Webb, 1994) through their pioneering experimental work on both free surface and submerged jets in the laminar, transitional and the turbulent zones showed that the Weber Number played a very important role in determining the heat transfer characteristics of free-surface jets while it played no role in submerged jets. Besides a very thorough description of *jet broadening* for free-surface jets it was shown for submerged jets that below the critical Reynolds Number of 2000, the data for all nozzle-to-plate distances collapsed into a single line suggesting a weak dependence of the stagnation Nusselt Number on the nozzle-to-plate distance. For both

free surface and submerged jets, the Nusselt Number was observed to correlate with $Re^{0.8}$ and $Re^{0.5}$ for laminar and turbulent zones respectively. A cursory mention is also made about the *knee* in the Nusselt Number plots versus r/d (radial distance from the stagnation point to the jet diameter) at an r/d value of 2. This aspect is discussed in detail in Chapter 4 of this thesis.

Garimella and Rice (Garimella and Rice, 1995) through their experiments on an turbulent, axisymmetric, submerged jet impinging on to a small square heat source in both confined and unconfined configurations argued that the heat transfer coefficient curves were found to follow a bell-shaped distribution being a maximum at the stagnation point and decreasing radially. The jet Reynolds Numbers used in the study ranged from 4000 to 23000, the non-dimensional nozzle-to-plate distances varied from 1 to 14 and the nozzle diameters used varied from 0.79 mm to 6.35 mm. For different non-dimensional nozzle-to-plate spacings, secondary peaks in the Nusselt Number were observed at an r/d (ratio of the radial distance from the stagnation point to the jet diameter) of 2. This particular observation was characteristic of all the single phase microjet impingement cases in this thesis. As the Reynolds Number was increased from 4000 to 23000, the magnitudes of the secondary peaks in the Nusselt Number were higher than what was observed at the stagnation point. Also, the location of the secondary peaks shifted away from the stagnation point radially as the Reynolds Number was increased. It was theorized that the recirculation patterns evident in a confined jet impingement arrangement was responsible for the secondary peak occurrence.

Fitzgerald and Garimella (Fitzgerald and Garimella, 1997) conducted experiments on normally impinging, submerged and confined turbulent jets on a flat plate. Laser Doppler Velocimetry was used to study the jet flow field. The fluid used was perfluorinated dielectric fluid (FC-77); the parameters varied were the usual nozzle-to-plate distance (2 to 4), the jet Reynolds Number (8500 to 23000) and nozzle diameters (3.18 mm and 6.35 mm). A relatively short nozzle was used in all the experiments which

gave rise to developing velocity profiles. The radial outflow region was characterized by a toroidal recirculation region depending on the Reynolds Number, the location of which moved radially outward from the stagnation point with increasing Reynolds Numbers and nozzle-to-plate spacings. Some qualitative observations of the turbulence levels associated with the nozzle and the centerline jet velocities were also made from the experimental observations. It was suggested that turbulence levels were more significant for the stagnation Nusselt Numbers than the jet velocities for the cases considered. At lower nozzle-to-plate spacings, the jet diameter alone was observed to affect the stagnation Nusselt Numbers. The radial velocities in the wall jet region, curiously, showed no dependence on the jet Reynolds Numbers. Decreasing nozzle-to-plate distances were shown to increase the magnitude of the peak velocity in the wall jet region. Increasing nozzle diameters were observed to reduce the magnitude of the peak velocity while moving its radial location nearer to the jet axis. Some of these observations, namely, the toroidal recirculation patterns and their displacement with respect to the jet Reynolds Number and Prandtl Number were observed in all of the simulation cases in this thesis.

Fitzgerald and Garimella (Fitzgerald and Garimella, 1997) also used these results to interpret heat transfer characteristics associated with turbulent jet impingement. It was observed that larger diameter nozzles were associated with higher stagnation heat transfer coefficients. The reason for this effect was attributed to the turbulence intensities being higher for larger diameter nozzles. It was widely believed prior to this work that the secondary peak in the Nusselt Number in the wall jet region was because of possible transition to turbulence. This paper theorized that the secondary peak occurrence was because of the boundary layer becoming fully turbulent rather than at the onset of transition. The higher heat transfer coefficients at higher Reynolds Numbers were attributed to the increases in the turbulence levels as the jet developed. Also, increasing nozzle-to-plate spacings caused a delay in the onset of transition and a decrease in the jet

turbulence levels in the wall jet region although increasing nozzle-to-plate distances resulted in higher stagnation heat transfer coefficients.

Morris and Garimella (Morris and Garimella, 1998) numerically investigated the flow fields and heat transfer in an axisymmetric, confined and submerged impinging jet for different orifice diameters (3.18 mm and 6.35 mm), orifice-to-target spacings (1 to 5) and turbulent jet Reynolds Numbers (8500 to 23000). The k-ε model based on the renormalization group theory (RNG) was used to compute the turbulent flow fields. The flow fields obtained with the computational analysis agreed well with the flow visualizations observed in an earlier paper with the exception of a secondary recirculation zone not being predicted by the computational model. The reattachment lengths and the pressure drops associated with the impinging jets were also predicted in this paper. The reattachment lengths were computed to be 0.80 and 0.81 diameters from the inlet for Reynolds Numbers 8500 and 23000 respectively. The length of the separated region was observed to be independent of the Reynolds Number for the turbulent flow rates used in this work. The work also featured the effects of the nozzle aspect ratio and shape on the overall fluid dynamic characteristics in the radial outflow region. Streamlines were presented for different flow configurations and empirical correlations were proposed over three different ranges of orifice aspect ratios.

Wheeler and Neti (Wheeler and Neti, 1999) used the finite control volume method to numerically solve for the flow field and heat transfer in a semi-confined impinging laminar slot jet. The problem was characterized using the Reynolds Number (50 to 500), slot width to the jet height and different thermal boundary conditions. The heat transfer characteristics in the stagnation region were found to be independent of the slot width to the jet height ratio as long as the jet impinged on the heated wall with the potential core intact. This is a very important result as far as this thesis was concerned. The z/d ratio in all the cases for the single phase jet impingement was kept under 5 in this thesis to ensure the existence of the potential core. Primary and secondary recirculation

zones were observed based on the jet Reynolds Number and the size ratio. These zones tended to move away from the stagnation region as the Reynolds Number and the size ratio increased. In addition, secondary peaks in the Nusselt Number were also witnessed. The numerical results obtained in this paper were compared to experimental results from previous work and the agreement was found to be good.

Li and Garimella (Li and Garimella, 2001) focused on the effect of the Prandtl Number on the local and average heat transfer coefficients in a turbulent, submerged and confined jet impingement configuration. Experiments were conducted on three different fluids water (Pr =7), FC-77 (Pr = 25) and air (Pr = 0.7) with varying Reynolds Numbers (4000 to 23000), nozzle diameters (1.59mm to 12.7mm) and nozzle-to-plate distances (1 to 5). Secondary peaks in the Nusselt Number along the radial direction away from the stagnation point were witnessed for all the cases. These secondary peaks were more pronounced for smaller nozzle-to-plate distances and higher Reynolds Numbers and tended to diminish for higher nozzle-to-plate distances. Fluids with lower Prandtl Numbers showed higher stagnation Nusselt Numbers at smaller nozzle diameters. The stagnation Nusselt Numbers were correlated in terms of the Reynolds Number and the Prandtl Number. Correlations for the average Nusselt Numbers included contributions from the area weighted average of the impingement region and the wall-jet region.

Some excellent reviews on the subject of single phase jet impingement heat transfer also exist, for instance, (Garimella, 2000, Lienhard V, 1995 and Martin, 1977).

(2.2.2) Literature Review on Two-Phase Flow Modeling in Microchannels

Hsu's seminal paper (Hsu, 1962) proposed the correlation between the range of active nucleation sites on a heated surface (a purely surface property) and the wall temperature or heat flux (thermal and flow properties). This work proposed that effective cavities (from where the vapor bubble embryo grows to and beyond the equilibrium size)

were those with finite waiting periods (the time required for the surrounding saturated liquid to progress to a superheated state and thus being able to transfer heat to the vapor bubble). The equations that Hsu developed based on the above-mentioned criterion predicted dependence of the maximum and minimum effective cavity sizes on subcooling, system pressure, physical properties and the thickness of the superheated liquid layer. Hsu assumed the shape of an incipient vapor bubble at the mouth of a nucleation site (cavity) to be a truncated sphere and successfully derived equations relating the critical, maximum and minimum bubble sizes with the wall superheat. He also introduced the concept of *preferred nucleation sites* based on the waiting time. With these equations, Hsu was able to relate some of the physically observed characteristics of nucleate boiling with his model successfully. The contributions of this paper to the CFD modeling of boiling phenomena were immense given the fact that almost all works that proposed semi-empirical formulae used the idea of active nucleation sites and related them to the local flow and thermal conditions.

Unal (Unal, 1976) introduced a heat transfer-controlled model for the maximum bubble radius, maximum bubble growth time and bubble growth rate. In fact, closure for the RPI model to be discussed later in this literature review, was achieved using these models. Unal assumed spherical and ellipsoidal bubbles growing on a thin layer of partially dry superheated liquid and used the energy balance equation to derive the equation for the maximum bubble diameter based on physical principles. Unal asserted in his paper that the equation he derived for the maximum bubble diameter covered a wide range of operating conditions, namely, system pressure 1 to 70 atm, heat fluxes of 0.47 to 10.64 MW/m^2, inlet liquid velocities of 0.08 to 9.15 m/s and inlet subcoolings of 3 to 86 K. Some of the closure terms required for the final expression for the bubble diameter were semi-empirical; a detailed explanation of this model can be found in Chapter 2 (3?) of this thesis. The final expression for the maximum bubble diameter was directly proportional to the system pressure and inversely proportional to the liquid velocity, a fact that can be physically visualized. The data obtained from subcooled flow boiling

experiments done at different pressures, heat flux values, inlet velocities were found to fit the model described above.

Del Valle and Kenning (Del Valle and Kenning, 1985) through their experiments on subcooled flow boiling of water at atmospheric pressure on a stainless steel surface studied the various parameters that affected subcooled flow boiling like the bubble diameter, bubble release frequency and the distribution of nucleation sites on the heated surface. They determined that the heat transfer coefficient which was supposed to be insensitive to the inlet subcooling in all the previous works, actually increased with increasing subcooling (possibly because of the single phase heat transfer dominating the other two mechanisms namely evaporation and quenching heat transfer) and with increasing wall thickness. Detailed flow regime maps were presented for different inlet conditions (inlet velocity and inlet subcooling). Bubbly flows were observed at 84 K subcooling, a transition from bubbly to slug flow was observed at 24 K. A simple heat transfer model was developed for the boiling process. This heat transfer model was divided into four distinct regions, each representing a different mechanism of heat transfer. They were (1) microlayer evaporation, (2) transient conduction (3) enhanced transient conduction in the overlapping areas of influence and (4) single phase convection heat transfer in the non-boiling areas. Semi-empirical equations were presented were each of these terms. It was observed that the heat transfer from the heated surface was primarily achieved through quenching (bubbles leaving the surface causing the colder liquid to rush in) supplemented by single phase convection and comparatively less microlayer evaporation. This work brought forth the conclusion that although new nucleation sites were activated at higher superheats, they tended to deactivate the sites formed at lower superheats. In many ways, this work was the forerunner to the heat flux partitioning theories to be discussed later in this thesis.

Kurul and Podowski's seminal work (Kurul and Podowski, 1990) contained the ingredients of what is widely known as "the RPI model". These models were originally

developed for application in the flow boiling problems encountered in the nuclear industry, but they have found use in a variety of other applications too. This study proposed partitioning of the heat flux at the heated wall into three components (1) single phase heat flux in the non-boiling areas of the heated wall, (2) evaporative heat flux in the boiling areas of the wall (governed by nucleation site density) and (3) quenching heat flux in the area vacated by the departing bubble (dependent on the nucleation site density and the bubble departure diameter). Further this work provided closure terms for bubble diameter at departure, bubble diameter in the freestream liquid, drag force, lift force, virtual mass force, nucleation site density, bubble departure frequency and the waiting period. This heat transfer model was verified with experiments in a vertical flow channel. The multi-dimensional nature of the subcooled boiling flows was brought out in this paper. More description of this model is given in Chapter 3.

Peng and Wang (Peng and Wang, 1993) through their pioneering experimental work on flow boiling and forced convection heat transfer inside mini-channels (600 x 700 μm) established some very important results. Firstly, it established that the boiling phenomena in small channels considered in this study were clearly different from the boiling phenomena associated with macrochannels. One of the differences that was in sharp contrast with macrochannels was the absence of a partial nucleate boiling regime and the initiation of a fully-developed nucleate boiling regime very early. The authors suggested that the lack of what they called "evaporating space" in microchannels prevented the formation and existence of vapor bubbles in the liquid. Evaporating space was defined as the minimum liquid bulk size at which bubbles could grow in a liquid bulk. Another difference was that steep increases in the heat flux values were observed for liquid single-phase convection. Secondly, the authors suggested that the Marangoni effect (capillarity) would be dominant as compared to the Reynolds Number in microchannels. Thirdly and very importantly, some of the data suggested that laminar flow and convection heat transfer may match or exceed heat transfer associated with turbulent flow in normal-sized channels. Fourthly, it was suggested that the nucleate

boiling process itself could be more intense in microchannels with the liquid velocity and sub-cooling having no obvious effect on the flow boiling.

Peng *et al* (Peng *et al.,* 1998) also introduced two concepts in a later paper, namely, evaporating space and fictitious boiling to explain the experimentally observed anomalies in the boiling characteristics inside microchannels. The evaporating space was defined as the minimum space required for boiling. Fictitious boiling occurred when the microchannel size was smaller than the evaporating space and it meant that, though the liquid had reached conventional nucleate boiling conditions, the conventional evaporation and bubble growth were replaced by highly superheated liquid or countless microbubbles. A dimensionless parameter was formulated using thermodynamic stability theory and Peng *et al.* related the nucleation characteristics to the applied heat flux, the thermal fluid properties and the microchannel hydraulic diameter. This work claimed that bubble nucleation was much harder to achieve in microchannels when compared to conventional-sized channels because of the lack of evaporating space. An expression for the superheat of nucleation was arrived at in this work. This work also showed that single phase liquids absorbed more energy in microchannels when compared to conventional-sized channels.

Bowers and Mudawar (Bowers and Mudawar, 1994) through their experiments characterized flow boiling in mini and micro-channels. Mini-channels (diameter 2.54 mm) and micro-channels (510 μm) were tested over a heated length of 1 cm using R-113 as the coolant. Measurements were taken for refrigerant flow rates from 19 to 95 mL/min, inlet sub-cooling from 10 to 32 °C with an inlet pressure of 1.38 bar (slightly above the atmospheric pressure) to study the effects of velocity and inlet sub-cooling on the critical heat flux. Correlations for the critical heat flux (CHF) and the overall pressure-drop were provided. Some key contributions of this work were:

i. Micro-channels provided a higher CHF as compared to mini-channels which is an excellent attribute as regards electronics cooling. This was because the

microchannel having a lower hydraulic diameter ensured a thinner thermal boundary layer when compared to a minichannel. However, this advantage was offset by the micro-channels requiring a higher pressure drop as compared to mini-channels, especially for higher heat fluxes and consequently, the microchannels unlike the minichannels experienced a decrease in the outlet temperatures with increasing heat flux values. The authors suggested that this fact made the mini-channels more practical than micro-channels in some applications.

ii. For the cases considered in this study, the effect of the inlet sub-cooling on the CHF was found to be minimal.

iii. One of the most important new findings of this study was that CHF was not triggered only by total dry-out at the exit but also by inlet conditions.

iv. A new pressure-drop model based on the homogeneous two-phase flow model was developed by the authors to study flow boiling in micro and minichannels. The gravitational component of the pressure drop was negligible in comparison with frictional and acceleration pressure drops. Also, an expression for the equilibrium quality was determined.

Jiang *et al* (Jiang *et al.,* 2001) used a transparent microchannel heat sink system made up of a microchannel array, microheater and an array of temperature sensors to study the flow boiling patterns within the microchannel arrays as a function of input power levels and flow rates while quantitatively measuring the temperature patterns within the device. Both pure single phase flow patterns, partially annular and stable annular flows were observed at different power levels. Their study also confirmed the already held view that boiling characteristics in microchannels were different than those in conventional-sized channels given that formation of active nucleation sites were difficult in microchannels. Their experimental results suggested that bubble formation and growth could be affected the microchannel shape and size. The boiling plateau (in a plot of wall heat flux versus ΔT_{sat}) which was present in conventional-sized channels and indicative of a bubbly flow regime, was absent in microchannels. For low heat fluxes

($q/q_{CHF} < 0.4$), local nucleation was observed with bubbles seen at a few nucleation sites. Nucleation of bubbles was intensified at higher heat flux levels and a local annular flow was observed with liquid droplets in a vapor core. However, this annular flow was short-lived with the nucleation sites disappearing with time. As the power level was increased further (q/q_{CHF} between 0.6 and 0.9), a stable annular flow was observed. The boiling plateau as observed in conventional-sized channels was absent in microchannels. This work led to some important results regarding the boiling flow patterns to be expected in microchannels. The flow pattern determined the heat transfer coefficient possible and the temperature distribution within the device.

Qu and Mudawar (Qu and Mudawar, 2002) through experiments, focused on predicting the incipient boiling heat flux (the heat flux just enough to create boiling) inside microchannels. 21 microchannels of rectangular cross-section (231 μm width and 713 μm depth) were fabricated and tests were done at various power levels with varying inlet liquid velocities and inlet temperatures (subcoolings). It was observed in this work that incipient boiling in microchannels marked an abrupt transition from liquid to two-phase slug flow which was not commonly encountered in macrochannels. Such abrupt transitions were found to be a characteristic of microchannel flows. A comprehensive model was then developed to predict incipient heat flux which accounted for some complexities such as bubble formation in the corner regions and the bubble engulfing the entire microchannel area at lower liquid velocities. (In the confined boiling jet problem that is a part of this thesis, the maximum bubble diameter predicted with the RPI model engulfed the microchannel area). In the model, the bubbles were treated as truncated spheres and a force balance with mechanical and thermal stability criteria on the bubbles yielded the maximum bubble diameter. Separate analytical expressions for the drag force and surface tension force were formulated for bottom wall, sidewall and corner bubbles. An expression for the maximum bubble diameter at departure was then formulated balancing the forces and also including thermal criteria (for the bubble to grow it must be engulfed in a superheated liquid) on the bubble. An analytical formulation for the

minimum liquid velocity at the outlet required to keep the maximum bubble radius within the confines of the microchannels was also completed.

Basu *et al* (Basu *et al.,* 2002) were able to predict two aspects of flow boiling that would prove essential for a later paper on heat flux partitioning at the heated wall, namely, the onset of nucleate boiling and the active nucleation site density. Although this work was originally done for flow in conventional-sized vertical conduits with direct application to the nuclear industry, some aspects of it could very well be applicable to flow boiling in microchannels. Experiments were done with varying mass fluxes, inlet subcoolings, heat fluxes and contact angles (by varying the levels of oxidation on the surface) for two types of test surfaces, namely, a flat plate and a set of rod bundles. The onset of nucleate boiling (ONB) was identified by both visual observations and the heat flux and temperature data (slope changes in the plot of q versus ΔT_{sat}). A new proposal for the identification of critical cavity sizes (to initiate nucleate boiling) was presented and the minimum wall superheat needed for ONB was calculated. It was further proposed that Hsu's criterion (discussed earlier in this chapter) diminished as the wettability of the surface increased. The active nucleation site density was also presented as a function of wall superheat and contact angle.

Warrier *et al* (Basu *et al.,* 2002) focused on formulating the interfacial heat transfer terms during subcooled flow boiling. Like the previous paper, this was concerned with flows that were prevalent in the nuclear industry but some of the theory could be very useful in formulating the interfacial heat transfer terms in micron-sized channels. All of the experiments done for this work were at low pressures (it is worth emphasizing that there was very little work that had been done at low pressures at that time). Again, the experiments were done at varying levels of mass flux, inlet liquid subcoolings, heat fluxes and contact angles while the pressure was maintained at atmospheric. The diameter of the vapor bubbles formed during the flow boiling process was measured as a function of time by filming the process using a camera. The condensation heat transfer

coefficient was then calculated based on this measured bubble diameter. A dimensionless bubble diameter was formulated using the modified Ranz-Marshall correlation and this was shown to be a function of the Reynolds Number based on the bubble diameter, the Prandtl Number based on the liquid properties, the Jakob Number and the Fourier Number. Based on this equation, a new correlation for the Nusselt Number was also formulated. The correlations formulated for condensation Nusselt Number and the bubble growth rates were compared with experiments and some important deviations were discussed.

Qu and Mudawar (Qu and Mudawar, 2003) studied instabilities that tended to trigger premature CHF in their experimental work on pressure drop characteristics in microchannels. An important instability that was identified in this paper was the mild parallel channel instability which caused the two phase flow to oscillate between slug flow and annular flow in the channel upstream while the flow remained predominantly annular downstream. Severe pressure oscillations were triggered by an increase in the heat flux which in turn produced a large quantity of vapor. The authors suggested that just throttling the fluid just ahead of the inlet alleviated the oscillations in pressure. It was conjectured and later proved that hydrodynamic instabilities actually affected the inlet and outlet pressures and greatly enhanced the pressure drop across the microchannels. Some of the older models for pressure drop showed the greatest possible MAE (Mean Average Error) and were deemed unsuitable for use in microchannel pressure drop modeling. A new model for pressure drop was developed to predict the pressure drop for the two-phase region. This model was based on the assumption that annular flow was the dominant flow mode. There were two liquid regions; one was the thin layer near the heated wall while the other was entrained in the vapor flow as slugs. This pressure drop model incorporated the effects of both the channel size and the coolant mass flux and was able to match the experimental results better.

Qu and Mudawar (Qu and Mudawar, 2003) studied flow boiling in rectangular microchannels experimentally and showed that the unique nature of flow boiling in rectangular microchannels included an abrupt transition to annular flow and the dominant heat transfer mechanism obviously corresponded to this type of flow. They also showed in this paper that the heat transfer actually decreased with increasing vapor quality because the liquid droplets were carried away from the wall to the inner vapor core. A mean heat transfer coefficient over the heated perimeter of the microchannel was calculated using the fin analysis method. Eleven previous correlations were compared with the experimental results obtained in this study and all of them were deemed unable to predict the correct trend of the heat transfer coefficient with increasing vapor quality.

Qu and Mudawar (Qu and Mudawar, 2003) then proposed an annular flow model for two-phase microchannel flow. The model incorporated some microchannel effects such as laminar liquid and vapor flow, smooth interfaces and droplet entrainment effects and was able to satisfactorily predict the decreasing trend of heat transfer coefficient with increasing vapor quality. The Weber Number was shown to be an important non-dimensional parameter characterizing the magnitude of entrainment of the liquid into the vapor core. The model was able to correctly predict some physical trends that were unique to microchannels.

Kumar *et al* (Kumar *et al.,* 2003) through experiments on bubbly wall heated flows at elevated pressures and formulated a model for the bubble departure diameter and the bubble diameter in the free-stream in terms of the liquid subcooling and the void fraction respectively. The dependence of these sizes on the Etovos Number was shown. The bubble frequency was observed to increase with an increase in system pressure which meant that bubbly flow could persist at high pressures at very high void fractions that were unique to high pressures. Bubble departure diameter measurements were made using a hot film anemometer. The bubble departure diameter thus measured was plotted against the liquid subcooling and a generalized correlation for the bubble departure

diameter in terms of the liquid subcooling was formulated. Drag and lift coefficients were formulated for multiple bubble interaction using single bubble formulations in an infinite liquid field. The lift coefficient was shown to increase with the Etovos Number and change sign beyond a certain "classical" average diameter.

Kandlikar (Kandlikar, 2004) introduced two new non-dimensional groups K1 and K2, based on mechanical considerations in his pioneering work on flow boiling in microchannels. The two non-dimensional groups were able to predict some very important flow and heat transfer characteristics in microchannels, the most important being the critical heat flux(CHF). The relevance of this work to this thesis lay in the fact that low Reynolds Number flows (such as those occurring in microchannels because of the small dimensions) had been addressed in this work while several of the past studies made no distinction between low (forces due to viscous shear tend to dominate) and high Reynolds Number flows. The dimensionless group K1 represented the ratio of the evaporation momentum force and the inertia force. Higher values of K1 actually indicated a reversed flow of the vapor (against the flow direction of the liquid). The second new dimensionless parameter K2 was defined as the ratio of the evaporation momentum force and the surface tension force and it had an important bearing on the CHF. The Weber Number and the Capillary Number, it was argued, were useful in determining the transition boundaries between different flow patterns. The rate of vapor generation once the bubbles nucleated was higher as the channel size became smaller and this eventually led to the reversed flow observed in parallel microchannels. In summary, in small channels with low Reynolds Numbers (about 300), the flow boiling cycle was similar to the ebullition cycle for nucleate boiling with bubbles nucleating and filling the entire microchannel. Some heat transfer correlations were also presented in the single phase and the two-phase regions.

Kumar *et al* (Kumar, 2004) implemented various empirical and mechanistic models developed in the literature for flow boiling in a thin geometry in a numerical

code. Some recommendations were made regarding the closure models for drag, lift, interfacial heat transfer and turbulence quantities using the ensemble-averaged approach developed by earlier researchers. This allowed writing the evaporative and condensation mass transfer terms from the heat transfer term which facilitated their implementation in a numerical code. The results from the numerical code were compared to experimental results from an earlier paper (Kumar *et al.,* 2003). This two-field modeling approach was found to give good results in the low void-fraction bubbly flow regime.

Zhang *et al* (Zhang *et al.,* 2005) in their experimental work dealt extensively with identifying and characterizing the mechanisms of boiling and other related processes in microchannels whose hydraulic diameters were greater than and lesser than 50 μm. The cooling fluid used was de-ionized water (lower surface tension) and uniform heat fluxes were provided in all experiments ensuring fully developed thermal boundary layers in all of them. The nucleation processes in these microchannels with different hydraulic diameter were recorded with a CCD camera. The boiling processes in these microchannels were marked by the absence of bubbly and slug/plug flow regimes. There were two distinct mechanisms by which bubble nucleation occurred in these microchannels depending on the hydraulic diameter – microchannels with hydraulic diameter larger than 100 μm exhibited typical nucleation (like in macrochannels) and microchannels with hydraulic diameter lesser than 50 μm exhibited eruption boiling. In larger microchannels where typical nucleation occurred, the flow was often annular (with a vapor core and a liquid annulus) which is beneficial for cooling applications. The eruption boiling process was marked with a mist flow regime that is deleterious for cooling applications. The authors attribute the eruption boiling process to the absence of effective nucleation sites in accordance with Hsu's criterion (Hsu, 1962) and suggest improving the surface conditions (notches) to avoid eruption boiling. The formation and departure of individual bubbles were accompanied by transient pressure fluctuations, the frequency of which was equal to the bubble departure frequency. The second part of the paper dealt with experiments on microchannels with surface improvements (notches).

The notches, as expected, improved the heat transfer rates by ensuring annular flow even in microchannels where the hydraulic diameters were lesser than 50 μm. Surface tension was observed to have a relatively weaker impact on the boiling process. The "evaporating space" concept proposed by Peng *et al* (Peng *et al.,* 1998). was not verified by this work. The authors recommended the "evaporating space" concept for smooth wall surfaces.

Basu *et al* (Basu *et al.,* 2005, Part 1) developed a theoretical model for wall heat flux partitioning in terms of the nucleation site density, bubble departure diameter and flow parameters that included liquid velocity, inlet subcooling, wall heat flux and system pressure. Experiments involving flow boiling under several pressures, mass fluxes, heat fluxes and contact angles were done to validate the model. The domain of interest (heated wall with the fluid flow) was divided into three regions based on the void distribution and separate heat transfer coefficients were formulated for each region since the mechanisms of heat transfer differed in these regions. The location of the onset of significant voids (OSV) was a very important demarcation point upstream and downstream of which were marked by different heat transfer coefficients, bubble growth and departure rates (sliding off the wall and lifting off). Upstream of the OSV (between the region of ONB and OSV), the bubble was found to be stable and downstream of the OSV, the bubble was found to grow and depart from the wall. The effect of the spacing size between the nucleation sites was also discussed.

Basu *et al* (Basu *et al.,* 2005, Part2) also applied the mechanistic model developed in the previous paper (discussed above) to several set of experimental data in this work and the agreement was found to be good. The essence of the mechanistic model as applied to any flow boiling scenario consisted of dividing the wall heat flux into a transient conduction component and a forced convection component which was also equal to the sum of the evaporative heat flux and the sensible heat flux. Once the geometry, mass flux, wall heat flux and the inlet liquid conditions (inlet liquid subcooling and velocity) were specified, it was possible to calculate the transient conduction heat

flux and the forced convection term using the model. This model was tested for different cases where the wall heat flux conditions and the inlet fluid conditions were varied (experiments by the authors) first. The onset of significant voids (OSV) was again a significant datum line upstream and downstream of which the wall superheats and hence the transient conduction terms and the forced convection terms varied. Downstream of the OSV, the wall superheat was high enough to cause the transient conduction component and hence the evaporative component to go up. The reverse of this trend was seen in the region upstream of the OSV. The model was also compared to other models in the literature and was found to give reasonably good results. The authors recommended usage of this model only for the vertical upflow configuration.

(2.2.3) Literature Review on Boiling Jet Impingement

Monde and Katto (Monde and Katto, 1978) through their experimental studies determined critical heat flux (correlated with the jet parameters) in an impingement system. Both pure water and R-113 were used as cooling fluids. Since this study dealt mostly with high heat fluxes (for CHF determination), fully developed nucleate boiling was prevalent in most of the cases which essentially meant that boiling and hence the heat transfer coefficients along the heated wall were insensitive to the flow conditions and the nozzle geometry. Some excellent photographs of water and R-113 boiling under different heat fluxes were provided in this paper. It was shown that the rate of liquid splashing was directly proportional to the heat flux at the heated wall. Experimental data for burn-out heat fluxes for both upward-facing and downward-facing heater surfaces were presented in this study. It was shown that surface tension was an important parameter affecting the burn-out heat flux (CHF). Experimental data were also collected for subcooled boiling. The degree of subcooling was varied; up to 30 °C for water and 16 °C for R-113. It was observed that for low wall superheats, the data deviated from classical correlations for nucleate boiling. At higher wall superheats, though, all of the data collapsed into the classical nucleate boiling curve for saturated boiling.

Bergles and Ma (Bergles and Ma, 1986) investigated the effects of the jet velocity, subcooling, flow direction and the surface condition on the characteristics of fully developed nucleate boiling experimentally . The liquid used in all the experiments was R-113. At high heat fluxes, it was observed that the plots of the heat fluxes versus the wall superheats (q'' versus ΔT_{sat}) merged into a common fully developed boiling asymptote. The superheat required to initiate boiling at low heat fluxes was reduced as the subcooling levels increased. Also, a pronounced temperature overshoot was observed for the saturated boiling case (zero liquid subcooling) in contrast to the subcooled case. The curves shifted toward the low wall superheat region for increasing heat fluxes. The nature of the surface was observed to affect the heat transfer characteristics as the curves showed significant differences when the experiments were repeated. Comparison of the experimental data for incipient boiling with the classical equations for incipient boiling fluxes brought out the fact that the active cavity sizes on the heated surface lay between 0.4–0.6 μm. It was recommended that most of the procedures developed for forced convection boiling inside tubes could be applied for jet impingement boiling.

Vader *et al* (Vader *et al.,* 1992) through their experimental study predicted boiling heat transfer from a heated surface to an impinging, planar free-surface jet of water. The nozzle dimensions used in the experiments were 10.2 mm x 105 mm (rectangular nozzle). The vapor in the flow field was identified with stop action photographic studies. The incipient boiling heat flux was approximately 0.5 MW/m^2, above which the heater surface was photographed to identify t nucleation and flow of vapor. For the cases investigated, it was both theorized and observed that the location of boiling incipience corresponded to the point of transition to turbulence (in the boundary layer). The region where liquid acceleration was prevalent (near the stagnation region), boiling was not observed because of the fact that acceleration tended to stabilize and maintain laminar flow. The critical Reynolds Number in the absence of boiling was similar to that of flat plate flow (since the problem under consideration is a free jet

without a confining top wall), 3.6 x 10^5. However, boiling tended to accelerate transition to turbulence: the critical Reynolds Number fell as low as 6.4 x 10^4 as the wall temperature rose above the saturation temperature (presence of boiling). In partial nucleate boiling, the wall temperatures downstream of the ONB were observed to reach a constant value. The heat transfer coefficients were correlated in terms of the heat fluxes, jet velocities and the inlet subcooling levels. Sensitivity to fluid velocity and temperature decreased as the boiling-induced mixing in the boundary layer was pronounced. Local temperature measurements were provided from the stagnation line to a downstream distance of about 14 jet widths.

Wolf *et al* (Wolf *et al.,* 1996) examined planar, free-surface jets of water experimentally. This work built upon the previous work of Vader *et al* (Vader *et al.,*1992) to study jet impingement boiling characteristics for heat fluxes ranging from incipience of boiling to the critical heat flux (CHF). The experimental results presented in this paper included the variation of the surface temperature at several locations downstream of the stagnation line (planar jet) and the surface temperature and the heat transfer coefficients at several heat fluxes. The results were presented as either q'' versus ΔT_{sat} (boiling regime) curves, q'' versus ΔT_f (defined differently in this paper as $T_w - T_f$) curves (single phase convection), or the heat transfer coefficient versus the heat flux levels (h versus q''). The plots of h versus ΔT_{sat} showed that the heat transfer coefficients obtained at a point downstream of the stagnation point (in this paper this location was at 90 mm from the stagnation point) at varying heat fluxes or wall superheats (ΔT_{sat}) showed a combination of heat transfer regimes; singe phase, partial nucleate boiling and fully-developed nucleate boiling, in that order, as the heat flux levels were increased. It was observed that at low velocities and at a ΔT_f of about 50 °C, the slope of the q'' versus ΔT_{sat} curve increased indicating the incipience of boiling. Partial nucleate boiling existed until a ΔT_f of about 80 °C (at this location) with the bulk flow conditions strongly affecting the nucleation, growth and departure conditions of the vapor bubbles. Beyond this ΔT_f, fully developed nucleate boiling conditions ensued with a sharper increase in the

slope of the q'' versus ΔT_{sat} curve. The convection coefficients in the partial nucleate boiling regime for low velocities increased monotonically by 35 percent when compared to the single phase convective coefficients. At higher velocities however, for partial nucleate boiling increased to about 20 percent and then stayed constant. This difference was attributed to the difference in the momentum of the free-stream in low and high velocity jets. As expected, the single phase and the partial nucleate boiling heat transfer coefficients exhibited a strong dependence on the bulk flow conditions in contrast to the fully developed nucleate boiling regime. The streamwise distance from the stagnation line was observed to influence the heat transfer coefficients only in the single phase and the partial nucleate boiling regimes. Partial nucleate boiling was observed only at locations farther downstream of the stagnation line and ceased to exist closer to the stagnation line. Correlations were developed for both q'' and h, valid for ΔT_{sat} between 23 and 51 °C.

It was predicted that, for the geometry considered in this paper, boiling incipience occurred at heat fluxes approximately equal to 0.75 MW/m^2 and at an axial location of about 30 mm from the stagnation point.

Hall *et al* (Hall *et al.,* 2001) obtained experimental results for boiling heat transfer occurring during quenching of a copper plate by a subcooled, circular, free jet. The surface of the copper plate was maintained at constant temperature in contrast with other work where a uniform heat flux was maintained. Heat flux distributions and boiling curves at various radial locations were presented for jet Reynolds Numbers between 11300 and 22600 (fully turbulent). Some excellent photographs depicting the impingement process as related to quenching were also presented as part of this paper. The experimental results showed three distinct boiling regimes; nucleate boiling near the impingement surface, nucleate boiling characterized by maximum heat flux and transition boiling. The data obtained for nucleate boiling were in good accord with the correlations developed from steady state boiling.

Zhou and Ma (Zhou and Ma, 2004) presented results from an experimental study on a submerged jet of R-113 impinging onto a heated plate 5 mm x 5 mm were presented. Although the focus of this paper was on determining the parameters that controlled boiling heat transfer from the heated surface in an impinging jet arrangement, results for natural convection, partially developed nucleate boiling, fully developed nucleate boiling and CHF (Critical Heat Flux) were also presented for completeness. The nozzle diameter (approximately equal to the jet diameter) used in all the boiling experiments was equal to 1.01 mm. Also, the large length-to-diameter ratio ensured fully developed conditions at the nozzle outlet. Plots of the heat flux (q) versus ΔT_{sat} (T_{wall} - T_{fluid}) and the heat transfer coefficient h versus ΔT_{sat} were presented and two sets of correlations were provided for fully developed nucleate boiling, each valid for different levels of the liquid subcooling, ΔT_{sub}

The increase in pressure at the stagnation point because of the deceleration of the jet to zero velocity was taken into account. One important finding of this study, at least for the cases investigated in this study, was that the high heat flux regime of the nucleate boiling curve was independent of the jet parameters like the jet velocity. This meant that the nucleate boiling regime could be correlated using pool boiling correlations. A new expression to predict partial nucleate boiling was also developed using a modified interpolation method.

Wang *et al* (Wang *et al.,* 2004) fabricated and analyzed micromachined jets and arrays of microjets for cooling a powered device representative of an active electronic chip. Both single phase and boiling jets were analyzed at various power levels and at various flow rates. The results indicated boiling inception at a heaf flux of around 10.5 W/cm^2. At radial distances far from the impingement point, the liquid flow rates were very low to promote only pool boiling. This was also seen in some of the numerical boiling experiments in this thesis. A simple numerical algorithm based on the finite difference method was developed for single phase impingement.

Wang *et al* (Wang *et al.,* 2004) also fabricated microjets (less than 100 μm in diameter) along with heater devices to study local heat transfer characteristics of an impinging confined jet. The experimental apparatus allowed visual access to observe the boiling process. Temperatures as functions of the radial distance from the stagnation point were experimentally determined and presented at different heat flux levels for two different jet diameters (50 μm and 70 μm). Preliminary visualizations of the boiling process were also presented as photographs. It was suggested that nucleate boiling was the dominant mode of heat transfer instead of stable film boiling for the parameters investigated.

(2.3) Summary of the Technical Literature

A thorough review of the literature reveals a plethora of experimental work and relatively fewer numerical works. This is especially true in the case of boiling heat transfer in channel and impingement configurations. This fact can be attributed to the complex nature of the boiling process and its strong dependence on material characteristics like surface roughness, the level of oxidation on the surface *et cetera,* parameters that cannot be easily simulated. The relation between the active nucleation site density on a heated wall and its local superheat due to Hsu (Hsu, 1962) paved the way for later researchers (Kurul and Podowski, 1990), (Peng *et al.,* 1998), for instance, to develop semi-empirical models and heat flux partitioning theories (Narumanchi *et al.,* 2006), (Kandlikar, 2004) for use in numerical simulations. To be able to simulate a boiling process is an onerous task (Dhir, 2006), but recent work (Narumanchi *et al.,* 2006) suggests that successful simulation of the boiling process is possible in the near future. This thesis is a humble attempt in that direction.

Simulating single phase laminar microjets presented a lot of technical features of jet impingement in a confined configuration in the laminar regime that provided very

valuable insight into the boiling jet impingement problem. Laminar microjets in a confined, submerged configuration exhibited fluid flow patterns that are normally evident in turbulent jets; primary and secondary recirculation zones leading to primary and secondary peaks in the Nusselt Number values obtained are particularly interesting and promising as far as electronics cooling is concerned. The simulation of single phase microjets are also expected to provide valuable insights for the effective design of arrays of microjets for practical electronics cooling systems.

To be able to use models in a simulation environment with confidence, especially when in their nascent stages, comparison and correlation to experimental data is vital. Boiling flows being a special class of two-phase flows have distinct flow regimes that affect heat transfer and fluid flow patterns. A lot of work has been done on flow regime mapping of flow boiling, especially in microchannels (Qu and Mudawar, 2003), (Peng *et al.,* 1998), (Zohar, 2003) and heat transfer models have been developed based on such flow pattern maps (0 and Mudawar, 2003). All of these data form important experimental evidence mainly for comparison purposes. The motivation for this thesis also arose from the incessant need for better cooling technologies especially for microelectronics where heat transfer aspects often limit their design. Liquid impingement cooling, both single phase and two-phase, has a lot of potential to achieve very high cooling rates (Lienhard V, 1995) for high-density microelectronics. Two-Phase cooling offers precise temperature control in addition to high heat flux removal (Wang *et al.,* 2004). Boiling Microjet impingement cooling has the potential to exploit both of these aspects (impingement cooling and two-phase cooling), the simulation of which is the aim of this work.

Chapter 3

Flow Boiling and Two-Phase Heat Transfer Model Development

(3.1) Introduction

This chapter is intended to serve as an introduction to the numerical modeling techniques used in FLUENT, a commercial CFD (Computational Fluid Dynamics) software package used for modeling both the single phase and the two-phase impingement problem in this thesis. FLUENT is based on the Finite Volume Method pioneered by Spalding; the finite volume method is discussed briefly in a section following this introduction. Besides offering several robust solver options, discretization schemes and visualization tools, FLUENT offers the possibility of interacting with the main solver though User Defined Functions (abbreviated as UDF). UDFs are used to enhance the functional prowess of the default solver by providing extra information for the solver; complex boundary condition profiles, additional source terms, reaction rates for chemically reacting flows, mass transfer rates and phase interaction laws for multiphase flows to mention a few. It is also possible to solve for additional conserved scalar quantities. UDFs are written in the C or C++ programming languages and are either compiled or interpreted by FLUENT. The boiling (two-phase) jet impingement problem is a flow, heat and mass transfer problem; the vapor mass is generated from the liquid mass by evaporation due the heat transfer from the wall. This evaporation rate depends on a host of different conditions, the liquid dynamics (affecting the heat transfer from the wall, the saturation conditions and the vapor bubble dynamics) and the nature of the heated surface (nucleation site density, roughness etc.) to name a few. Once a vapor bubble nucleates, grows and departs from the wall, it has its own momentum resulting from an interaction of forces acting on it; the drag force (which depends on the Reynolds Number), the buoyancy force, the virtual mass force (resulting from a difference between

the vapor and liquid densities) to mention a few. Heat transfer also occurs from the vapor bubble to the surrounding liquid (depending on the local subcooling) which may cause local condensation of the vapor adding to the liquid mass. It is clear from the above description that the actual process of subcooled flow boiling heat transfer is highly intricate and non-linear and that the solver needs a lot of information which may or may not be included by default. In fact, for the boiling jet impingement problem, a UDF was used to pass all of the information described above to the main solver. To summarize, this chapter is intended to describe in detail some of the methods used to simulate the single phase and the boiling jet problems in FLUENT; the models used, the solver parameters used and the UDF functionalities are described in some detail.

(3.2) The Finite Volume Method

The philosophy of any iterative numerical method to solve differential equations, be it the finite difference method, the finite element method or the spectral element method, is to convert a set of governing partial differential equations into a system of algebraic equations which are then solved iteratively or directly. The first step in the solution process is the approximation of the unknown variables or their gradients by means of functions that are then substituted into the set of governing differential equations through a process called *discretization.* The Finite difference techniques normally use truncated Taylor's series (at assumed node points) approximations to discretize the differential equations in contrast to the Finite Element techniques which use piecewise functions valid over elements and spectral methods that use truncated Fourier series or Chebyshev polynomials that are valid throughout the computational domain (Patankar, 1980). The Finite Volume Method is a special case of the finite difference method which will be described in some detail here.

The finite volume method comprises the division of the computational domain of interest into *finite control volumes* (areas in the case of two-dimensional domains) and

writing the governing equations (mostly for fluid flow and heat transfer) over all the finite control volumes as integral expressions. These integral expressions are then converted into algebraic equations (discretization) using finite-difference type approximations (Patankar, 1980). An iterative or a direct procedure is then employed to solve these algebraic equations.

The finite volume method of discretization is described below for a simple equation governing the conservation of a scalar quantity. This example is intended to illustrate the discretization method for finite volume schemes. A second order differential equation expressing the conservation of a property Φ (one-dimensional, steady) in simple cases is shown in (3.1).

$$\frac{\partial}{\partial x}(k\frac{\partial \phi}{\partial x})+S=0 \tag{3.1}$$

where Φ is a scalar or vector quantity, k is a material constant and S is the source term. Also, the computational domain (where this equation is satisfied) in the vicinity of one grid point P is shown is Figure 3.1 (Patankar, 1980).

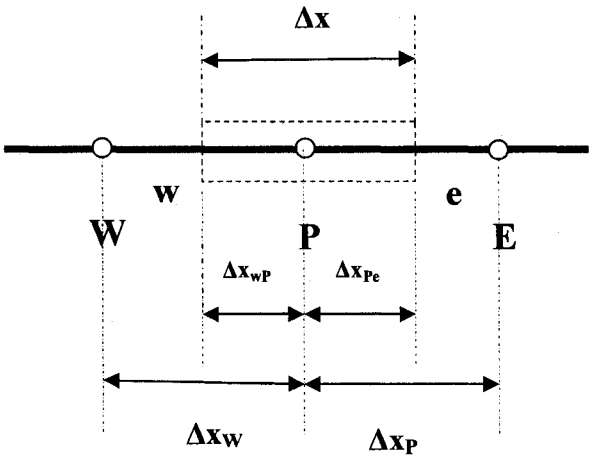

Figure 3.1: A Finite Control Volume.

In Figure 3.1, P is the grid point surrounding which, a control volume is constructed (dotted lines) with faces at w and e signifying "west" and "east" faces. W and E are neighboring grid points of P. The control volume size is Δx as shown. Equation (3.1) is then integrated over the control volume ΔV ($A\Delta x$, where A is the cross-sectional area of the control volume which is 1 in this case) resulting in equation

$$\int k\frac{\partial \phi}{\partial x} + \int S.dx = 0 \tag{3.2}$$

The k term (k may vary in a material) and the $d\Phi/dx$ terms at different points are then expressed from the interpolated values at adjacent points (interpolation could be linear or quadratic). The final equation can then be cast in a form shown in (3.3), a form that is applicable to all the equations governing fluid flow and heat transfer and is central to the finite volume method, Patankar (Patankar, 1980):

$$a_P\phi_P = a_W\phi_W + a_E\phi_E + S_u \tag{3.3}$$

where the coefficients a_P, a_W, a_E and the linear source term S_u are given by:

$$a_w = \frac{k_w}{\Delta x_{wP}} \tag{3.4}$$

$$a_e = \frac{k_e}{\Delta x_{eP}} \mathrm{a_e} \tag{3.5}$$

$$a_p = a_e + a_w + S_P \tag{3.6}$$

The non-linear source term is split into a sum of a linear part S_u and a non-linear part S_P which is seen in equations(3.4), (3.5) and(3.6). The coefficients accompanying the variable Φ at adjacent points P, E and W are a_p, a_e and a_w respectively and the particular form in equations and is derived from a central difference approximation of the gradient (grad) of Φ with additional assumptions of constant spacing between the finite control volumes and the control volume faces being located mid-way between the nodes. Again, the very simple equation considered is to illustrate the working principle of the finite volume method which, with modifications, is applicable to all problems involving fluid flow and heat transfer. An iterative procedure is then employed to solve for Φ_P.

Equation (3.1) is an example of a diffusion problem (heat conduction, for instance) where the central differencing approximation has been found to give reasonably accurate results without the added onus of divergence on coarse grids. The governing equations for fluid flow though (explained in the next section), contain non-linear convection terms (u d/dx (Φ)) which cannot be handled by the central differencing approximation due stability concerns that are succinctly summarized by Patankar. The remedy is to use an *upwind* approximation to model convection terms where the variable Φ at a control volume face is determined from the value at the point *upstream* of the face (depending on the flow direction). FLUENT provides the user with both first and second order upwind approximations for the convection terms in addition to other complex approximation schemes including the power law scheme, the QUICK scheme and the third order MUSCL scheme. All the cases that were considered for this thesis made use

of the second order upwind schemes. Excellent descriptions of the upwind methods are found in the literature (Patankar, 1980).

(3.3) Governing Equations for Fluid Flow and Heat Transfer

This section is devoted to a description of the mathematical equations governing fluid flow and heat transfer. The governing equations for both single phase flows and two-phase flows and heat transfer are given here along with a brief description of the terms in the equations. The governing equations for single phase fluid flow and heat transfer include those for conservation of mass, momentum and energy in a given control volume. Multi-phase (of which two-phase flow is a simplification) flows and heat transfer are governed by similar equations for individual phases but also carry with them interface interaction terms which define the effect of one phase the others and vice-versa. Boiling (and condensing) flows and heat transfer are a special class of multiphase flows where the vapor phase is initiated due to the evaporation and vaporization of the liquid (flowing in the case of flow boiling and static in the case of pool boiling) utilizing the heat from the wall. The vapor phase then has its own momentum (quantified by a separate momentum equation) and flows co-currently with the liquid exchanging energy and momentum. If the vapor phase is surrounded by sub-cooled liquid (at a lower temperature than the saturation temperature at the corresponding pressure), condensation occurs due to the heat transfer from the vapor thus reducing the mass of vapor flowing with the liquid. Thus the condensation and boiling rates, which are essentially a function of the heat transfer rates (which, in turn, depend on the liquid flow characteristics) become a source term in the continuity equation (mass conservation).

(3.3.1) Single Phase Flow and Heat Transfer

Single Phase flows and heat transfer are governed by the equations of continuity (conservation of mass), momentum and energy. Mathematically, they are expressed as (White, 1990):

$$\frac{\partial \rho}{\partial t} + div(\rho \vec{V}) = 0 \tag{3.7}$$

$$\rho \frac{DV}{Dt} = \rho g + div(\overline{\overline{\tau_{ij}}}) \tag{3.8}$$

$$\rho \frac{Dh}{Dt} = \frac{Dp}{Dt} + div(k \text{ grad.T}) + \Phi = 0 \tag{3.9}$$

where the upper-case D/Dt represents the material or the substantial derivative (D/Dt = ∂/∂t + div). The symbols in this equation are all described in the list of symbols at the beginning of this thesis.

Equations (3.7), (3.8) and (3.9) represent the governing equations for the most general case of fluid flow and heat transfer without any assumptions about compressibility or stress-strain behavior. Obviously, these equations can be simplified for use for Newtonian, incompressible fluids which are of interest here in this thesis. For incompressible, unsteady, two-dimensional flow and heat transfer, these equations become

$$div(\vec{V}) = 0 \tag{3.10}$$

$$\rho \frac{D\vec{V}}{Dt} = \rho g + div(\bar{\bar{\tau}}_{ij}) \tag{3.11}$$

$$\rho \frac{Dh}{Dt} = \frac{Dp}{Dt} + div(k \text{ grad.T}) + \Phi \tag{3.12}$$

(3.3.2) Multiphase Flow and Heat Transfer

For multi-phase flows, a variety of modeling techniques are available but a vast majority of them fall under two broad categories: Averaged equations representing both phases (equations for the mixture) and separate equations for each individual phase. FLUENT offers three distinct approaches for multiphase flow modeling and they are

(1) The Volume of Fluid Method (VOF)

(2) The Mixture Model

(3) The Eulerian model.

The first two models described before are variations of the averaged approach where the phases are represented by a single equation which accounts for all the phases concerned. The Eulerian multiphase model supports separate equations for each individual phase in the problem with the mass, momentum and energy equations containing interaction terms between the phases. Since the Eulerian multiphase model was used in the flow boiling problem that model alone is described in some detail here. For a complete description of all the models available, the reader is referred to FLUENT's online documentation on multi-phase flow modeling.

The equations representing the conservation of mass, momentum and energy for an arbitrary (q'th phase) in a multiphase problem are given by equations (3.13), (3.14) and (3.15) respectively as in the next page. Some of the terms in the conservation

equations are self-explanatory. The term α_q which represents the volume fraction of the q'th phase has been multiplied to all of the terms in the equation to account for the fact that the equations cease to exist when the volume fraction goes to zero. The interaction terms are evident in all of the equations in the right hand side of the equations, have a subscript of pq (meaning interaction between phase p and q) and for convenience have been grouped as C-I (for continuity interaction), M-I (Momentum Interaction) and E-I (Energy Interaction) in this work. The term in equation represents the rate of addition of mass from phase p to q and vice versa. The term Sq in represents a source term that can be added through a user-defined function if needed. In the boiling microjet problem, for instance, the evaporative and condensing mass were evaluated from the heat transfer from the wall by the Ranz-Marshall correlation as will be explained later. The M-I terms in equation carry a lot of import particularly in a flow boiling problem. The $\vec{R}_{pq}$ term in represents the interphase force (the drag force), the $\vec{F}_q$ term an external body force, the $\vec{F}_{lift,q}$ term the lift force and the $\vec{F}_{vm,q}$ term which represents a virtual mass force which assumes significance when the ratio of the densities of the phases involved is large.

Equation of Continuity for Phase q

$$\partial/\partial t(\alpha_q \rho_q) + \nabla.(\alpha_q \rho_q \vec{v}_q) = \underbrace{\sum_{p=1}^{n} \dot{m}_{pq} - \dot{m}_{qp}}_{\text{C-I}} + S_q \qquad (3.13)$$

Momentum Equation for Phase q

$$\partial/\partial t(\alpha_q \vec{v}_q) + \nabla.(\alpha_q \rho_q \vec{v}_q \vec{v}_q) = -\alpha_q \nabla p + \nabla.\bar{\bar{\tau}}_q + \alpha_q \rho_q \vec{g} +$$

$$\underbrace{\sum_{p=1}^{n} \vec{R}_{pq} + \dot{m}_{pq}\vec{v}_{pq} - \dot{m}_{qp}\vec{v}_{qp}}_{\text{M-I}} + \vec{F}_q + \vec{F}_{lift,q} + \vec{F}_{vm,q} \qquad (3.14)$$

Energy Equation for Phase q

$$\partial/\partial t(\alpha_q \rho_q h_q) + \nabla.(\alpha_q \rho_q \vec{v}_q h_q) = -\alpha_q \partial p/\partial t + \bar{\bar{\tau}}_q + \nabla \bar{u}_q - \nabla.\vec{q}_q + S_q + \underbrace{\sum_{p=1}^{n} Q_{pq} + \dot{m}_{pq} h_{pq} - \dot{m}_{qp} h_{qp}}_{\text{E-I}} \tag{3.15}$$

The M-I term refers to momentum interaction and the E-I refers to energy interaction. The $\vec{R}_{pq}$ term is an interphase force term (drag, for example) and is important as it needs to be closed for the solution of the governing equations for two-phase flow and heat transfer. FLUENT offers a default closure relation for this drag force term depending on whether the interface is solid-liquid or fluid-fluid. The Schiller-Naumann drag relation which is applicable for laminar a spherical liquid-vapor interface was chosen for the boiling microjet problem. Recently, there has been a surge of research activity in terms of experimentally determining drag coefficients for two-phase flow, especially for such flows in microchannels. A comparative study of other drag laws and their influence on the two-phase flow physics is suggested as future work. Using the Schiller-Naumann drag relation the following expressions can be employed to determine $\vec{R}_{pq}$:

$$\sum_{p=1}^{n} \vec{R}_{pq} = \sum_{p=1}^{n} K_{pq}(\vec{v}_p - \vec{v}_q) \tag{3.16}$$

$$K_{pq} = \frac{\alpha_q \alpha_p \rho_p}{\tau_p} f \tag{3.17}$$

$$f = \frac{C_d . Re}{24} \tag{3.18}$$

$$C_d = \begin{cases} (1 + 0.15 Re^{0.687})/Re & Re \leq 1000 \\ 0.44 & Re \succ 1000 \end{cases} \tag{3.19}$$

With regard to the energy equation, all of the heat flux from the wall is assumed to go into the liquid phase (meaning there is no vapor superheating); a source term to this effect (derived from the wall heat flux) is supplied as a source term to the liquid energy equation. The vapor energy equation is not solved and its temperature is fixed. These are the basic terms that are input into the mass, momentum and energy equations of the liquid and the vapor phases to provide complete closure. The simulation of boiling flows is achieved using a heat flux partitioning technique which is described in detail in the next section. The wall heat is assumed to go only to the liquid phase which is a valid assumption in the nucleate boiling range.

(3.4) Heat Flux Partitioning: The Modified RPI Model

In the recent years, there has been significant progress in the numerical simulation of flow boiling using heat flux partitioning theories pioneered by Kurul and Podowski (Kurul and Podowski, 1990). Heat flux partitioning, in essence, is the apportioning of the wall heat flux into different components: single phase heat flux, quenching heat flux and the evaporative heat flux. To facilitate this partitioning, the wall area is also split into different parts accordingly. Based on the active nucleation site density, the bubble departure frequency, the bubble departure diameter, and the wall area occupied by the boiling sites is determined first. Once a vapor bubble nucleates grows to its maximum size and departs from the wall, colder liquid rushes in to occupy the area previously occupied by the nucleating bubble. The heat transfer rate to this colder fluid is different from the purely single phase heat transfer to a relatively warmer fluid and is accounted for by the quenching heat flux. The unsteady nature of the flow boiling physics is also accounted for in the heat flux partitioning model. The semi-empirical model developed by Kurul and Podowski (Kurul and Podowski, 1990) is called the RPI (Renssealer Polytechnic Institute) model and is currently being used in successfully simulating many flow boiling problems of interest.

The RPI model, in general, provides semi-empirical closure relations for the mass (evaporation and condensation terms), interfacial heat flux (as a combination of the single phase, quenching and the evaporative heat fluxes), momentum (turbulent drag, lift and virtual mass effect) along with other turbulence quantities. It is worth noting here that the RPI model was originally conceived for flow boiling problems in the nuclear industry which were predominantly turbulent. In contrast, the confined microjet impingement problem considered in this thesis features flows at very small scales that have minimal turbulence effects and are subject to laminar drag. The drag term in the original RPI model had to be modified to account for this laminar drag behavior. The Schiller-Naumann drag law offered as a default drag law in FLUENT was used in place of the

turbulent drag term offered by the RPI model. Potentially, a lot of work in future could be directed towards experimentation with the drag laws to be used for flow boiling in microchannels. In addition to the modification of the drag law, the lift term and the virtual mass term were neglected because they had very little effect on the flow physics for the geometry considered. The lift terms assume significance in highly turbulent flows, especially when there is a strong wake behind the vapor bubble (Narumanchi *et al.*, 2006). With the liquid velocities being small in the areas of vapor generation for all the cases considered in this thesis, the lift term was considered negligible. The gravity term, though was enabled which took into account, the effects of buoyancy. Besides the lift term, the virtual mass force term was also neglected as it was found to have a negligible effect on the heat transfer as is described in Chapter 5 in this thesis.

The closure terms for the two-phase flow and heat transfer problems for this thesis are shown in equations (3.20) through. The interphase heat transfer terms are given by the Ranz-Marshall correlation (Ranz and Marshall, 1952) which is valid for laminar flows. The bubble size at departure and the bubble size in the free-stream are from the RPI model.

The RPI model, in essence, partitions the heat flux "arriving" at the wall into the single phase, quenching and evaporative heat fluxes as shown in equations (3.20), (3.21) and (3.22) respectively

$$q_{sp} = h_{sp}(T_w - T_{f,\infty})(1 - \Omega) \tag{3.20}$$

$$q_q = 2\pi^{-0.5}\Omega(fk_l\rho_l C_{pl})^{0.5}\,(T_w - T_l) \tag{3.21}$$

$$q_e = \frac{\pi}{6} d_{vw}{}^3 fn\rho_v L\,. \tag{3.22}$$

The individual terms in the equations carry their meanings as defined in the nomenclature. Ω is the area of the wall occupied by the active nucleation sites, h_{sp} is the single phase heat transfer coefficient given by the Ranz-Marshall correlation, f is the bubble release frequency, d_{vw} is the bubble departure diameter and n is the nucleation site density expressed in terms of the wall superheat:

$$\Omega = \min (0.25 \pi d^2_{vw} n\eta, 1.0) \tag{3.23}$$

$$\eta = 4.8 \exp(-Ja / 80) \tag{3.24}$$

$$h_{inter} = \frac{Nu.k_l}{d_v} \tag{3.25}$$

$$Nu = 2.0 + 0.6 \mathrm{Re}_b^{0.5} \mathrm{Pr}_l^{0.3} \tag{3.26}$$

$$f = \sqrt{\frac{4g(\rho_l - \rho_v)}{3 d_{vw} \rho_l}} \tag{3.27}$$

$$d_{vw} = 0.0000242 P^{0.709} .a.(b\theta)^{-0.5} \tag{3.28}$$

$$a = \frac{(T_w - T_{sat})}{2} \frac{1}{\rho_v} \sqrt{\frac{\rho_s C_{ps} k_s}{\pi}} \tag{3.29}$$

$$b = \frac{1}{2(1 - \frac{\rho_v}{\rho_l})} MAX\left((T_{sat} - T_l), \frac{q_w}{0.0065 \ \rho_l C_{pl} U_l} \right) \tag{3.30}$$

$$\theta = MAX(\frac{U_l}{0.61}, 1.0) \tag{3.31}$$

$$n = (200(T_w - T_{sat}))^{1.80}. \tag{3.32}$$

$$A_{\text{int}} = 6 * \alpha_{sv} \frac{(1-\alpha_v)}{d_v(1-\alpha_{sv})} \tag{3.33}$$

$$\alpha_{sv} = \min(\alpha_v, 0.25) \tag{3.34}$$

The interphase mass transfer (liquid to vapor) is calculated from these expressions as

$$m_{l-v} = \frac{h_{\text{int}} A_{\text{int}} (T_l - T_{sat})}{L + C_p (T_l - T_{sat})} \tag{3.35}$$

and the energy into the liquid required to form this mass of vapor is calculated as

$$Q_{lv} = m_{l-v} * L \tag{3.36}$$

(3.20) through (3.34) represent a form of the original RPI model modified for laminar sub-cooled flow boiling. In particular, the turbulence quantities have been left out of the original RPI model as they should be for laminar flow, the drag coefficient has been modified to accommodate the default Schiller-Nauman drag model, the lift and the virtual mass terms were neglected as their effects were found to be insignificant through some test cases that were run. All the test cases for this thesis as well as all the evaporative impingement cases for Chapter 5 utilized a UDF that incorporated the above-mentioned equations. The original source code for turbulent multiphase flows came from FLUENT and it was modified to fit laminar flows in this thesis. In some cases, experimental results were available and in such cases the simulation results from this thesis were compared to the experimental results available from the literature. The qualitative agreement was found to be generally good. This is discussed in some detail in Chapter 4 of this thesis.

(3.5) Modeling of Flow Boiling and Heat Transfer in Microchannels

The past literature concerning boiling and condensation, in particular those works concerned with attempts to numerically model the problem (of boiling and condensation) have all hinted at the enormity of the task. The models developed were by no means universal being strictly applicable only to specific geometries and problems of interest. The difficulties encountered in modeling flow boiling are further enhanced by microchannel effects which are summarized in Chapter 1 of this thesis. Of particular importance to all microchannel flows is the Knudsen Number which quantifies the magnitude of slip encountered at the wall due to fluid flow. Fortunately, for the geometries considered in this thesis and for the fluid (water) used, the Knudsen Numbers turned out to be quite low which meant that the no-slip boundary condition enforced on the wall was valid.

Some significant questions arose with the simulation results of the single, single-phase liquid microjet impingement. With the diameter and hence the impinging area of the jet remaining small compared to the heated area, the effective heat transfer was confined to a very small portion of the impinging microjet. This unfortunate fact is particularly deleterious to high power devices and a single phase single microjet is of limited use to cool such applications. The solutions to this problem can be found by either modifying the surface conditions (Dhir, 2006) or by employing boiling microjets.

Another significant problem that occurred during the simulation of the boiling microjet in a confined arrangement was that the bubble diameter at departure exceeded the channel height. Thus the departure diameter given by (3.28) had values more than 200 μm (channel heights used in this thesis) during the course of the simulation which led to unrealistic heat transfer rates and eventually to divergence of the equations. In fact, a solution to this problem was found from the technical literature. Yitzhak Zohar very elegantly discusses this issue in his treatise on microchannel boiling (Zohar, 2003). In his

boiling experiments inside microchannels once the vapor bubbles reached the height of the channel and are constrained from growing any further, they tended to spread out in a horizontal direction and assumed an ellipsoidal shape for a limited time after which they are pushed out by the oncoming liquid flow rapidly. In our simulations, some remedy to the problem mentioned above was achieved by artificially limiting the bubble size to the height of the channel. This might have potentially led to some inaccuracies at higher heat fluxes and the magnitudes of these inaccuracies have to be quantified through experiments. One possible situation where the bubble departure diameter assumption may be invalid is when the two or more bubbles coalesce and cloud the heat transfer surface. This would cause instabilities especially at high heat fluxes. A thorough analysis is suggested for future research.

(3.6) Conclusions

The aim of this chapter was to introduce the mathematical equations that were used to solve all of the problems considered in this thesis. In particular, modifications were made to the original RPI model suitable for the laminar flow boiling situations of interest. A brief discussion about the limitations of the current two-phase flow model is also given. This subject is further discussed in detail in Chapter 5.

Chapter 4

Numerical Simulation of Laminar, Single Phase, Axisymmetric, Submerged, Confined Liquid Microjet Impingement: Flow Field and Heat Transfer Characteristics

(4.1) Abstract

In this chapter, numerical simulation results for the flow fields and heat transfer characteristics in a laminar, confined microjet (76 μm in diameter) impingement arrangement are presented. The parameters varied included the jet Reynolds Number (300 to 1500), the fluid Prandtl Number (0.7, 3.5, 7 and 23) and the ratio of the nozzle-to-plate distance to the jet diameter (1.2, 2.6 and 4). Primary and secondary recirculation zones were observed in the stagnation region and the radial outflow region which had a significant impact on the local Nusselt Number distribution on the heated surface. A secondary peak in the Nusselt Number distribution was observed at the reattachment point at higher Prandtl Numbers. With increases in the jet Reynolds Number, the center of the secondary recirculation zone is observed to move away from the stagnation region radially and also towards the top confining wall causing the secondary peaks in the local Nusselt Number to be displaced in the radial direction while increasing in magnitude. Increasing Prandtl Numbers are observed to increase the magnitude of the secondary peaks in the local Nusselt Number and to displace them radially towards the stagnation point. Increasing ratios of nozzle-to-plate distances to the nozzle diameters are observed to push the secondary recirculation zone and the secondary Nusselt Number peak radially outward from the stagnation zone. Secondary peaks in the Nusselt Number were observed only for higher nozzle-to-plate distances. With decreasing Prandtl Numbers, the secondary peaks diminish in magnitude and are practically absent for low Prandtl Numbers. The fluid flow patterns and heat transfer characteristics in the single phase liquid impingement are envisioned to provide significant insight into the boiling microjet impingement problem which is the current focus of research of the authors.

(4.2) Introduction and Literature Review

Impinging liquid jets, conventionally used in the cooling of turbine blades, metallurgical applications such as quenching, *et cetera*, have recently begun to find applications in high density electronics cooling. This may chiefly be attributed to the fact that they provide excellent boundary layer and heat transfer characteristics and their potential for directed hot spot cooling (Wang *et al.,* 2004). Garimella (Garimella, 2000) provides an elegant description of the fluid flow and heat transfer characteristics pertaining to several such jet configurations. The current trend in electronics design is toward miniaturization in tune with Moore's law and this means increased heat flux densities that are expected to match those of a nuclear reactor within the next decade (Goodson, 2003, Ellsworth and Simons, 2005). Since the electronic package size also includes that of the heat sink, it is imperative that the size of the heat sink matches that of the electronic circuitry itself to achieve overall miniaturization.

A tremendous amount of technical work has been completed on a variety of impinging jet configurations, see (Fitzgerald and Garimella, 1997, Di Marco *et al.,* 1994, Elison and Webb, 1994, Ichimiya and Hosaka, 1992, and Stevens and Webb, 1991) for instance, and comprehensive reviews are available. To summarize the technical literature corresponding to axisymmetric, submerged, impinging jets in a confined configuration, since such configurations in the microscales are the focus of this thesis, they exhibit primary and secondary vortical structures (recirculation zones) the location and strength of which vary according to the Reynolds Number (Fitzgerald and Garimella, 1997). They were also theorized to have a very significant effect on the Nusselt Number peaks. A large proportion of the literature has been devoted to turbulent jets barring a few on laminar planar jets, such as (Wheeler and Neti, 1999) and (Elison and Webb, 1994), which focus on laminar jet impingement on a conventional scale. Smaller systems demand smaller flow rates and miniaturized flow paths which necessitate a systematic

flow-field and heat transfer study on laminar jet impingement. Recently, Wang *et al* (Wang *et al.,* 2004) published results on the heat transfer characteristics of microjets with flow rates small enough to ensure laminar behavior. Their experimental studies presented temperature plots of a miniaturized microjet impingement arrangement although it did not present any detailed flow field structures. The focus of this work is to explore the fluid flow and heat transfer characteristics of single phase microjets (less than 100 μm in diameter) using a commercial CFD code.

(4.3) Problem Description

An axisymmetric, submerged and confined jet was considered in this study. Figure 4.1 depicts a liquid jet of diameter d issuing into the problem domain and impinging onto a heated plate. A solid region representing an Integrated Chip (IC) is also included in the problem domain. The length and thickness of the solid block (in the radial direction in a two-dimensional view) are kept constant at 1.12 cm and 300 μm respectively; these values represent standard IC industry design parameters. Moreover, these values were chosen for a comparative study with Wang (Wang *et al.,* 2004). The distance between the top confining plate and the heated wall is denoted by z and is varied in the simulations reported in this paper to study the effect of z/d on the heat transfer characteristics of the microjet. The jet Reynolds Number is varied by varying the jet inlet velocity. The conjugate heat transfer problem involving the conduction in the solid block and convection in the fluid domain is then solved numerically using a commercial CFD code based on the Finite Volume Method.

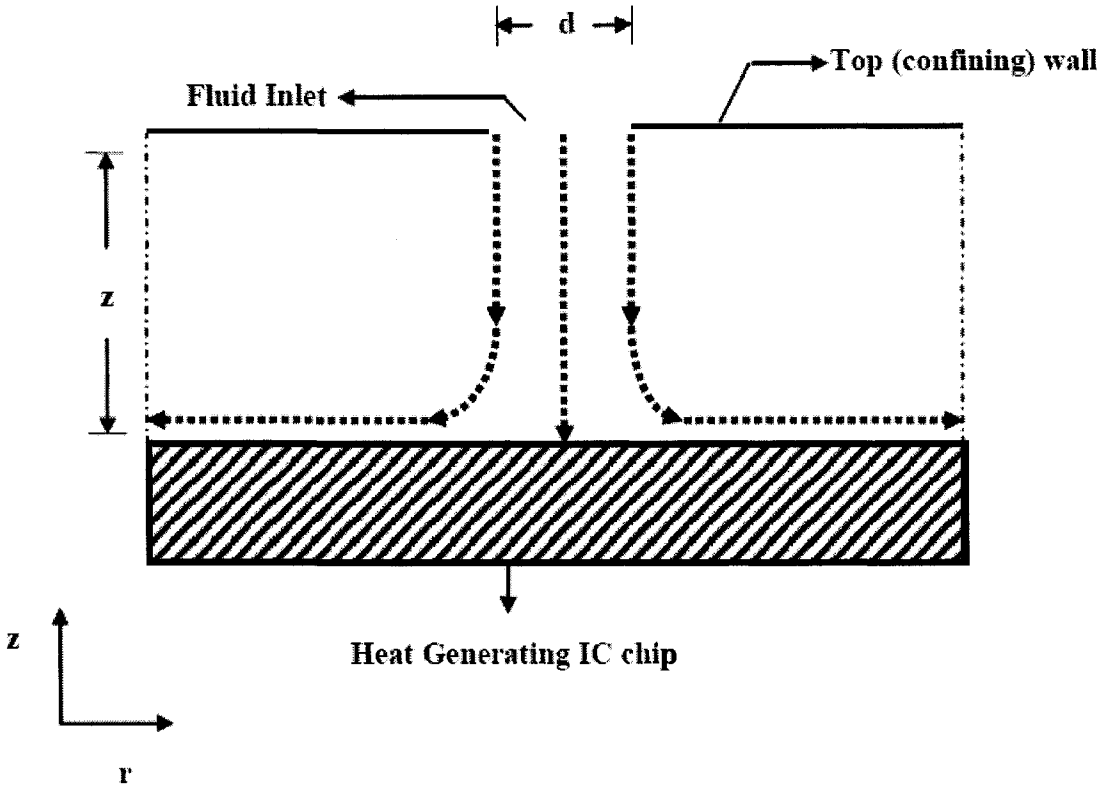

Figure 4.1: Schematic of the Single Phase Microjet Impingement Problem.

(4.4) Solution Procedure

The governing differential equations for the microjet impingement problem considered in this paper are the equations of continuity (mass conservation), momentum and energy described in equations (3.10), (3.11) and (3.12) for the fluid zone and the energy equation in the solid region with a solid-liquid interface.

A schematic of the numerical model with the boundary conditions is presented in Figure 4.2. The problem was approximated as an axisymmetric (two-dimensional) model. Only a radial slice of the problem domain as shown in Figure 4.1 was modeled, taking into

account the symmetry of the problem. Zero heat flux boundary conditions were prescribed for the top confining walls, the side walls and the bottom wall of the heated chip as the heat loss through these surfaces was expected to be a minimum. The chip wall in contact with the fluid (the chip top wall) was assigned a coupled boundary condition (heat flux balance due to convection and conduction). The radial fluid outlets were dealt with using fixed pressure (at atmospheric pressure) conditions on both the faces as indicated in Figure 4.2. The residual monitors were set at 1e-06 for the pressure and the momentum terms and 1e-08 for the energy equation. These stringent residual limits were deemed necessary after it was observed that less stringent residual limits produced velocity and temperature fields that were significantly different (and erroneous) from those for their more stringent counterparts.

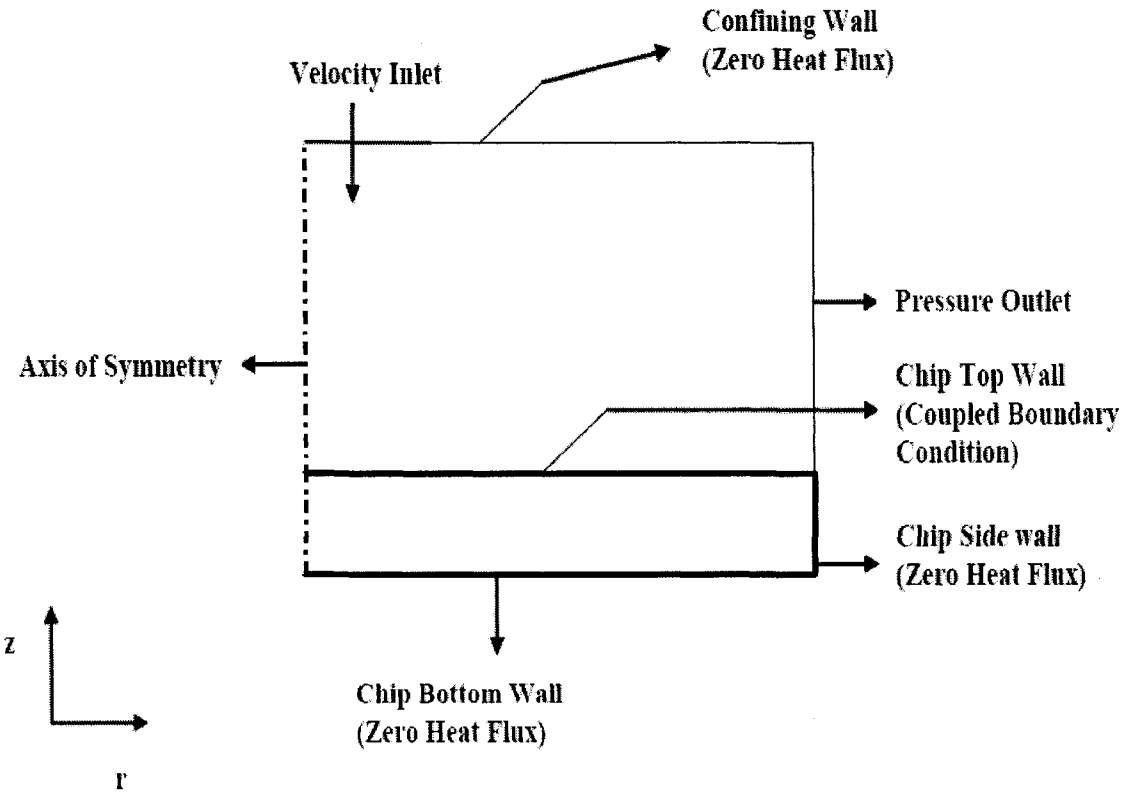

Figure 4.2: Computational Model Description.

(4.5) Meshing Considerations and Grid Resolution Study

The problem presented some unique flow physics of interest which necessitated careful arrangement of the cell volumes in areas of interest. Some areas of interest were identified as being critical to the physics of the problem both from the existing literature on impinging jets as well as from the authors' test runs for the problem. The three critical regions of interest are (1) the region near the velocity inlet where the jet issues into a region containing the same fluid at rest, (2) the stagnation region where the axial velocity reduces to zero and pressure rises to a maximum, and (3) the primary and secondary recirculation zones due to the confined arrangement depending on the jet Reynolds Number. Testing was done to ensure mesh independence of the results obtained. The general meshing strategy adopted for the problem is shown in Figure 4.3. An expanding grid (more nodes in the vicinity of the stagnation region and expanding downstream) is made use of in the radial direction. In the axial direction, as shown in Figure 4.3, a two-way expanding mesh which ensured more nodes near the nozzle inlet, the top confining wall and the top chip wall and fewer nodes in the center of the fluid domain was used.

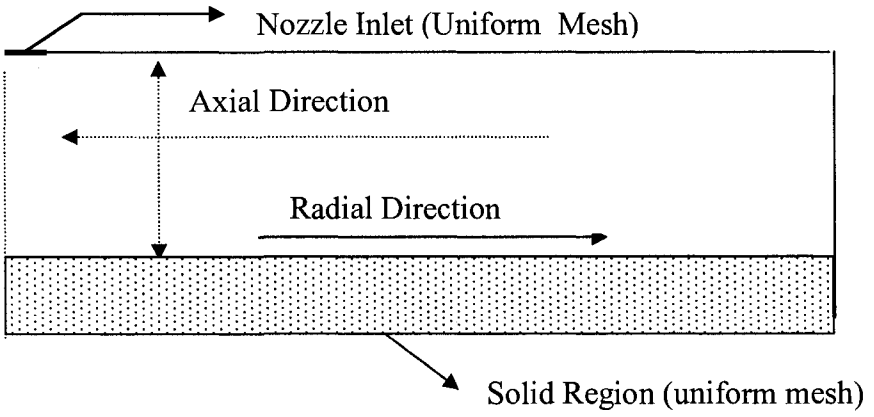

Figure 4.3: Meshing Considerations.

A thorough mesh refinement analysis was done with mesh sizes increasing from coarse (about 9000 quadrilateral cells) to fine (about 15000 cells) for a Reynolds Number of 1500, z/d of 2.5 and a Prandtl Number of 7. Invariance of the velocity and temperature fields with increasing mesh sizes ensured grid independence of all the results obtained.

(4.6) Validation Study

A validation study was done by comparing some of the results obtained in this study to the results obtained by Wang *et al* (Wang *et al.,* 2004). The comparison is shown in Figure 4.4. The jet diameter used for this validation study was 76 μm, a jet velocity of 7.35 m/s which translated into a jet Reynolds Number of 550 and two power levels 4.3 W (43000W/m^2) and 6.7 W (67000 W/m^2).

The temperature along the radial direction r in the direction of the jet outflow is shown in Figure 4.4. As seen from Figure 4.4, the numerical results obtained in this paper are in excellent accord with the experimental results from Wang *et al.* which motivates further use of CFD for parametric study.

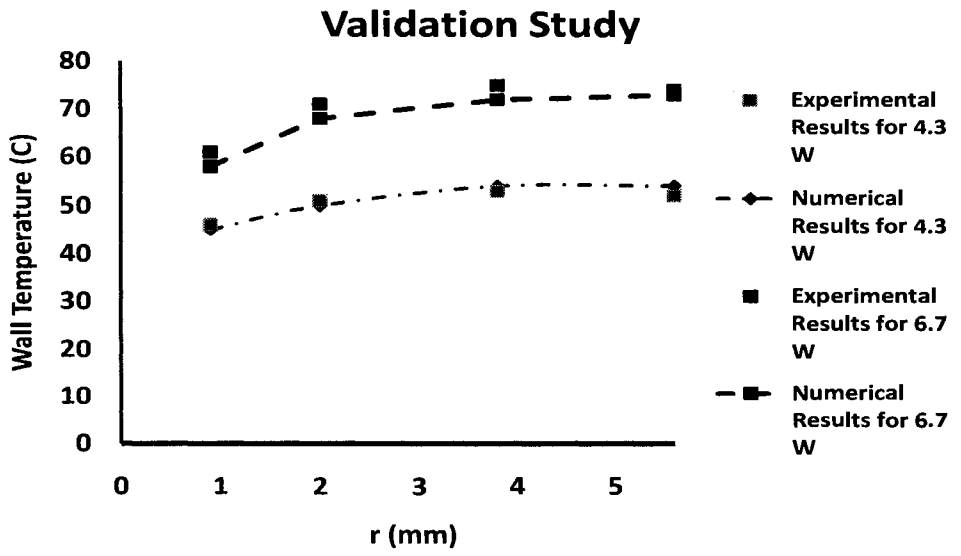

Figure 4.4: Single Phase Microjet Validation Study

(4.7) Parametric Study

A parametric study was then done to examine the effects of the jet Reynolds Number, the fluid Prandtl Number and the dimensionless ratio of the nozzle-to-plate distance to the jet diameter on the heat transfer characteristics of the microjet. The jet Reynolds Number and the fluid Prandtl Numbers are given by (4.1) and (4.2) respectively.

$$\mathrm{Re}_d = \frac{V_{ji}\, d}{\nu} \tag{4.1}$$

$$\mathrm{Pr} = \frac{\nu}{\alpha}. \tag{4.2}$$

Table 4.1 lists all of the cases that were considered for this work. Care was taken to ensure that all the cases considered were laminar in flow behavior and that the potential core of the jet always struck the impingement surface ($z/d < 6$). As mentioned before in this thesis, when z/d is greater than 6 for a submerged, confined jet, the potential core does not strike the surface. Consequently, z/d values of 1, 2.5 and 4 were considered for this study.

Table 4.1 : Cases Considered for Single Phase Microjet Parametric Study

Case	Re_j	Pr	z/d
1	300	7	2.6
2	550	7	2.6
3	700	7	2.6
4	900	7	2.6
5	1100	7	2.6
6	550	0.7	2.6
7	550	3.5	2.6
8	550	24	2.6
9	550	7	1.2
10	550	7	4

(4.8) Results and Discussion

A series of stream function plots are shown in Figures 3.6 and 3.7 that illustrate the dependence of the flow characteristics on the Reynolds Number and the z/d ratio. The heat transfer characteristics are explained through local Nusselt Number plots at dimensionless distances r/d in Figure 4.5 through Figure 4.9. The Nusselt Number was calculated using the expressions:

$$Nu = \frac{h\ z}{k_l} \tag{4.3}$$

$$h = \frac{q_w}{(T_w - T_{bf})}. \tag{4.4}$$

(4.8.1) Stream Function Plots

Figure 4.5 shows the stream function plots for a series of jet Reynolds Numbers (300,500, 700, 900 and 1100). Regions of interest here are the primary and secondary recirculation zones which were observed in the literature mostly for turbulent jet impingement problems. At a Reynolds Number of 300, a primary recirculation zone is observed near the stagnation region with the secondary recirculation zone, albeit weak when compared to those at higher Reynolds Numbers, a little farther away from the stagnation region. When the jet Reynolds Number is increased to 500, the primary recirculation zone is observed to move radially away from the stagnation region while also increasing in magnitude. The secondary recirculation zone is pushed radially away from the stagnation region and rises to the top-confining wall. Consequently, the reattachment point located after the secondary recirculation zone is also displaced as the Reynolds Number increases. The location of the reattachment point has a direct bearing on the location of the secondary Nusselt Number peak that will be explained in a later section. Figures 4.5 (c), (d) and (e) reveal the same trend of the primary and the secondary recirculation zones being displaced from the stagnation region in the radial direction and the secondary recirculation zone also moving toward the top confining wall in the axial direction. At a jet Reynolds Number of 1100 (Figure 4.5 (e)), the secondary recirculation zone almost reaches the top confining wall.

Figure 4.6 shows the effect of the z/d ratio on the flow structure. The effect of the z/d ratio is very interesting from a fluid dynamical point of view. It is obvious that as the

z/d value increases, the primary and the secondary re-circulation zones move farther away from the stagnation region. For confined jet arrangements, a z/d value of 6 is suggested in the literature (Garimella, 2000) as the limit beyond which the potential core no longer strikes the surface. For laminar flows, this attribute has a deleterious effect as the heat transfer in the stagnation region deteriorates as z/d increases. Our simulations though suggest that as z/d increases, the primary and the secondary recirculation zones are pushed out and in essence, there is appreciable fluid velocity near the outlet consequently increasing the average heat transfer otherwise impossible with single microjets cooling a large heated area.

(4.8.2) Nusselt Number Plots

(4.8.2.1) Effect of the Jet Reynolds Number On The Local Nusselt Number Distribution

Figure 4.7 shows plots of the local Nusselt Number versus r/d for Reynolds Numbers of 300, 500, 700, 900 and 1100 (the Prandtl Number and z/d ratio remaining constant at 7 and 4 respectively). Secondary peaks are observed in all the Nusselt Number plots (the primary peaks are at the stagnation zone) which closely correspond to the reattachment point in the wake of the secondary recirculation zone. It can also be observed that the secondary peaks in the Nusselt Number increase in magnitude and shift radially away from the stagnation point consistent with the shift of the secondary recirculation zone at higher Reynolds Numbers. Thus the effect of increasing jet Reynolds Numbers is to push the streamlines farther from the stagnation point in the radial direction. Increasing Reynolds Numbers are also observed to cause the secondary recirculation zones to increase in magnitude and move radially outward. At a Reynolds Number of about 1000, the secondary recirculation zone almost reached the top-confining plate. All of these effects are observed in conventional-sized turbulent jets (Garimella, 2000).

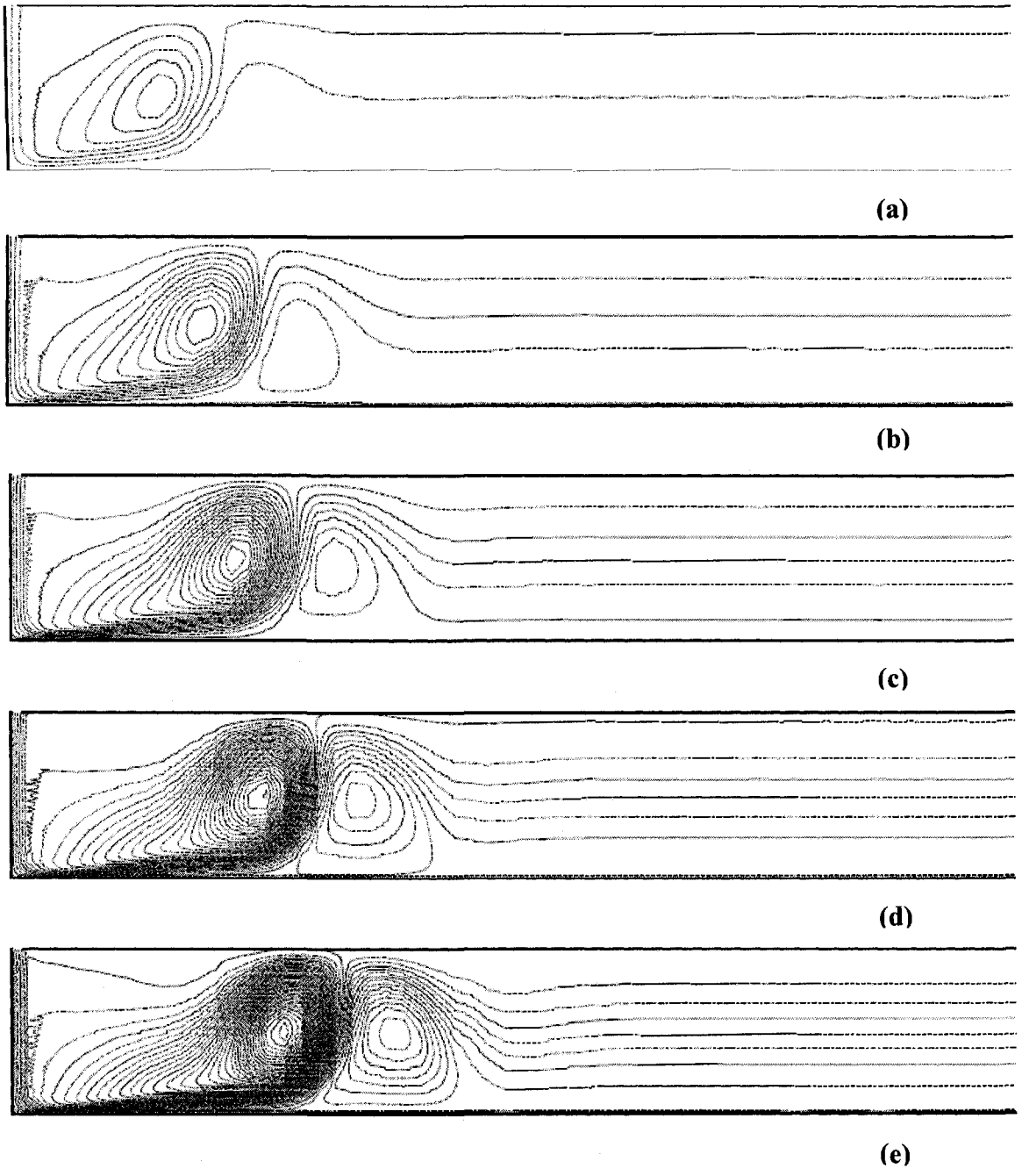

Figure 4.5: Stream Function Plots for (a) $Re_d = 300$, (b) $Re_d = 500$, (c) $Re_d = 700$, (d) $Re_d = 900$ and (e) $Re_d = 1100$, with $z/d = 4$ and $Pr_f = 7$.

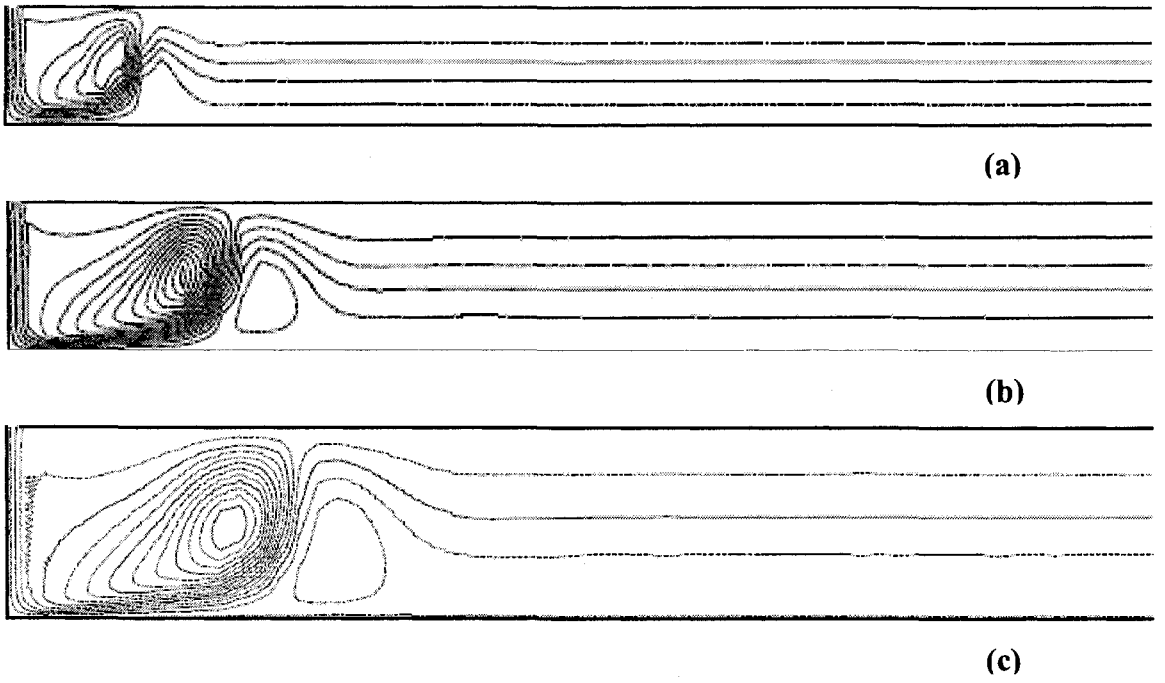

Figure 4.6: Stream Function Plots for (a) z/d = 1.2, (b) z/d = 2.6 and (c) z/d = 4 Re_d = 500 and Pr_f = 7.

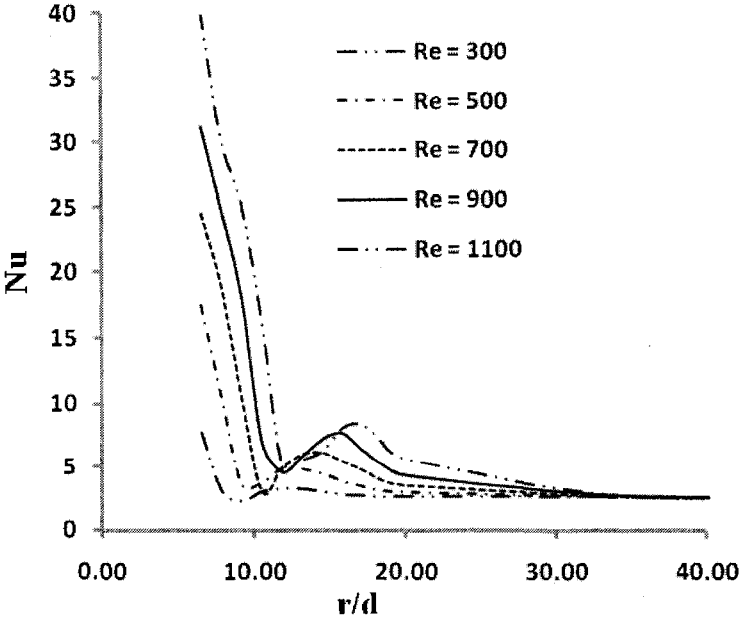

Figure 4.7: Local Nusselt Number Plots as a function of Reynolds Number.

(4.8.2.2) Effect of the Prandtl Number on the Local Nusselt Number Distribution

Figure 4.8 shows the effect of the Prandtl Number on the local Nusselt Number distribution. Four Prandtl Numbers were investigated in this work, 0.7, 3.5, 7 and 24, respectively. It can clearly be seen that increasing Prandtl Numbers lead to an increase in the magnitude of the secondary Nusselt Number peaks and also a slight shift toward the stagnation zone. Lower Prandtl Numbers have very weak secondary Nusselt Number peaks as was witnessed with air impingement in earlier work (Wheeler and Neti, 1999). The Prandtl Numbers chosen for this work, with the exception of Pr 3.5, represent potential cooling fluids used in the electronics industry (Air – Pr = 0.7, Water – Pr = 7, and FC-77 Pr = 24).

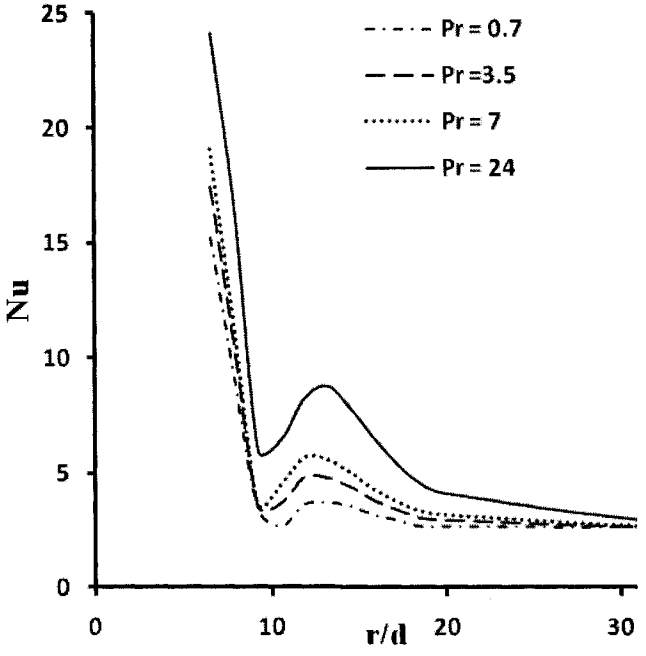

Figure 4.8 : Effect of the Prandtl Number on the Local Nusselt Number Distribution.

(4.8.2.3) Effect of z/d on the local Nusselt Number Distribution

Figure 4.9 is an interesting plot showing the dependence of the local Nusselt Number on the z/d ratio. Three z/d ratios were chosen for this work 1.2, 2.6 and 4 at a fixed jet Reynolds Number of 550 and a Prandtl Number of 7. Secondary Nusselt Number peaks were observed for all three cases. As z/d values increase, the secondary Nusselt Number peak is shifted away from the stagnation zone. However, the magnitude of these peaks does not increase drastically and actually show a slight decrease with increases in z/d. A lot of work is currently being done with lower z/d values than what is mentioned in this paper to completely understand the effects of decreasing z/d values on microjet impingement. Also, as mentioned before, the higher z/d cases show a lot of interesting results that are beneficial for heat transfer with single microjets. Further, the stream-function plots and the Nusselt Number plots are of great benefit in the design of boiling microjet impingement cooling systems.

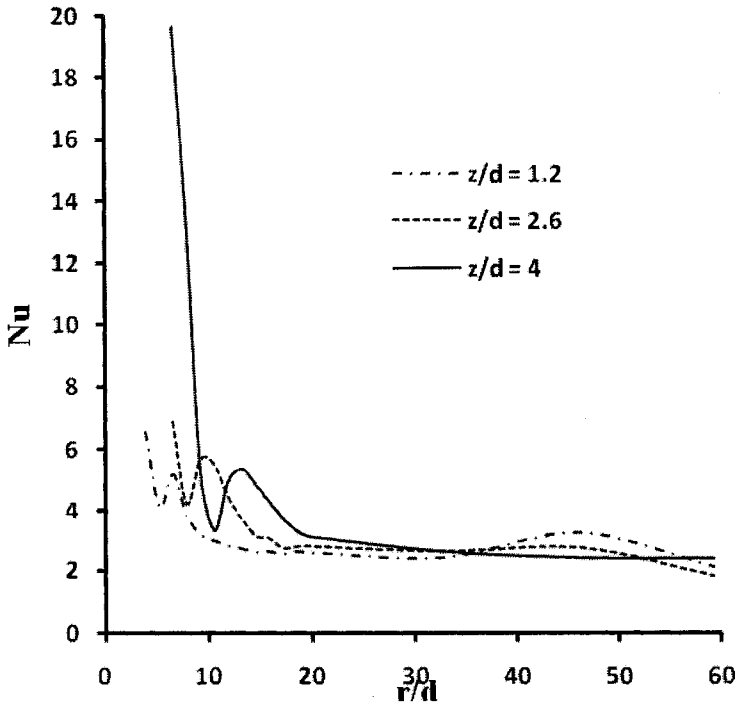

Figure 4.9 : z/d Effect on the Local Nusselt Number Distribution.

(4.9) Conclusions

Single phase microjet impingement cooling was analyzed numerically and a parametric study was carried out. The parameters investigated were the jet Reynolds Number, the Prandtl Number and the nozzle-to-heated plate (z/d) ratio. The effect of increasing Reynolds Numbers and z/d ratios was to push the secondary recirculation zones farther downstream of the stagnation point. Secondary peaks in the Nusselt Number were observed very close to the stagnation zone for low z/d. The effect of decreasing Prandtl Numbers is to suppress the occurrence of the secondary peak in the Nusselt Number. Higher z/d values in combination with an optimum laminar Reynolds Number and fluid Prandtl Number holds a lot of promise for single microjet cooling of large heated areas. Secondary recirculation zones and associated secondary Nusselt number peaks cause an increase effective area for heat transfer. This work on single phase, confined, laminar microjet impingement is envisioned to provide valuable insights into the design of boiling microjet impingement systems.

Chapter 5

Two-Phase Flow Model Testing and Validation

(5.1) Introduction

The aim of this chapter is to describe the validation methodology used to test the modified Renssealer Polytechnic Institute (RPI) model to simulate the boiling microjet impingement problem. Since the problem was simulated using a commercial CFD code in conjunction with User Defined Functions (UDF), a brief description of the UDF is also presented. The UDF in conjunction with the main solver is first applied to a case of microchannel flow boiling which represents a case of boundary layer boiling, and then to several different boiling jet scenarios; the results from these simulations are presented, and in some cases compared, to the existing experimental evidence from the literature. The grid size and the time-step size resolution are also described in some detail. The various terms of the component momentum equations are described and a rationale is provided for their usage and a description is provided for the relative contribution of each term.

(5.2) Structure of the UDF in the context of the Eulerian Multiphase Model

The UDF listed in the Appendix A1 is written for the Eulerian Multiphase model offered by FLUENT. This model treats individual phases as interpenetrating continua and has individual mass, momentum and energy equations for each phase with only the pressure shared between the phases. All properties are calculated on a per-cell basis with an average volume fraction for individual phases in each cell and it is not possible to track the evolution of the shape of the phases involved. For instance, in this work, a cell-averaged volume fraction of each phase involved (liquid and vapor) is available as output from FLUENT but the evolution of the individual vapor bubble shape is out of the scope

of the Eulerian Multiphase model. If the individual bubble shape is of interest, the Volume of Fluid method whose surface tracking algorithm is based on the Level-Set method is to be used. Since this work focuses on the effective implementation of the heat flux partitioning along the heated wall, the Eulerian multiphase model, which was best suited for such purposes, was used. This work does not place any special emphasis on tracking individual vapor bubbles although some inferences were drawn from the vapor phase fraction contour plots obtained from FLUENT.

The UDF is written to accomplish the interphase mass, momentum and energy transfer through the RPI model. To get a clearer idea of how the modified RPI model is implemented via a UDF, the reader is referred to equations (3.13) through (3.32). These equations are phasic governing equations along with the closure (interaction) terms for mass, momentum and energy. Also included are expressions for the single phase, the quenching and the evaporative heat fluxes. At this point, it would also be better to remind the reader that the wall heat flux is assumed to go completely into the liquid phase (no superheating of the vapor occurs). This is implemented in FLUENT through the UDF, and the equations, in such a way that a control volume cell attached to the wall can receive heat only if it has a non-zero liquid fraction. If the cell is filled with only vapor, the vapor momentum (through the forces acting on it) has to transport it into the neighboring cells. To satisfy continuity on a per-cell basis, the vacant portion of the cell has to be filled with surrounding liquid (which has its own momentum and temperature values). This liquid filling in the cell volumes attached to the heated wall after being vacated by the departing vapor bubble, in a sense, mimics the quenching mechanism of flow boiling heat transfer

The entire program listing for the UDF is given in appendix A1. As mentioned before, UDFs for the commercial CFD code are written in the C programming language.

The heat and mass transfer interaction between the liquid and the vapor (evaporation and condensation) is handled by the DEFINE_MASS_TRANSFER macro

in the UDF (Appendix A1). The Ranz-Marshall correlation given by (3.26) is implemented here and the evaporation-condensation mass exchange between the vapor and the liquid is calculated based on the heat transfer coefficient given by this model.

The heat flux partitioning is achieved through the use of the DEFINE_HEAT_FLUX macro. The DEFINE_HEAT_FLUX macro is used to modify the heat arriving at the wall by modifying its coefficient values. The coefficient values are referred to as c0, c1 and c2 and these values are modified to implement the three different partitions of heat transfer described in this thesis. These are highlighted by bold characters in the Appendix. The single phase, the quenching and the evaporative heat flux equations implemented in the UDF are from (3.20) through (3.22).

The source term for the liquid energy equation is implemented through the DEFINE_SOURCE macro. Problem parameters like the active nucleation site density, area of the wall occupied by the boiling sites, bubble diameter at departure, and bubble diameter in the free stream are all included in the calculation of the various boiling parameters in the UDF.

The drag coefficient is from the FLUENT main solver itself. FLUENT calculates the drag force on the vapor bubbles using equations (3.16) through (3.19) and this term is implemented as the interphase momentum transfer.

Table 5.1 shows the various macros used in the UDF and the equations in this thesis they refer to.

Table 5.1: Macros used in Appendix A1

Macro	Description	Equation(s) in Thesis
DEFINE_MASS_TRANSFER	Inter-phase mass transfer through Ranz-Marshall correlation	(3.35)
DEFINE_HEAT_TRANSFER	Heat flux partitioning into single phase, quenching and evaporative heat fluxes	(3.20), (3.21) and (3.22).
DEFINE_SOURCE	Energy to the liquid to form vapor	(3.36)
Other Functions (real type)	To calculate the bubble departure diameter, interfacial area, boiling site density,	(3.28), (3.32) and (3.33)

Also, as mentioned before, the effective area occupied by the boiling sites, Ω, given by (3.23), is the critical parameter that apportions the area of any given wall-attached cell into different areas applicable to single phase cooling, cooling due to quenching, and/or evaporation. The evaporative heat flux does not contain the Ω term. The maximum value the Ω term can take is 1. All the heat flux terms are included as default but the single phase component ceases to exist if Ω is 1 in which case the entire cell is allocated to the quenching heat flux and the evaporative heat flux until the complete cell is filled with vapor. Also, from equation (3.22), it can be seen that there is evaporative heat flux only if the wall temperature exceeds the saturation temperature at the local pressure, which is again realistic from a physical point of view. The evaporative and the quenching heat flux components are also built in with the nucleation site density which determines the cells along the heated wall on which the different heat transfer components are initiated and the bubble departure frequency which really determines the duration for which these components act on a particular cell. The bubble departure frequency in essence imparts an unsteady (time-dependent) component to the problem, which is again very close to reality but requires an unsteady solver to resolve the unsteady component. This also necessitates appropriate time-step size resolution as described in the next section.

(5.3) Time-Step Size Resolution

The need for proper time-step size resolution in a numerical procedure is essential, especially in cases where the physical process is inherently unsteady. As explained in Chapter 1 and in the previous paragraph, the bubbles nucleating along the heated wall at the active nucleation sites depart from the wall when the forces acting on them tend to overcome the forces holding them together. This process is inherently unsteady and the time spent by the nucleating vapor bubble at the heated wall is governed by the bubble departure frequency which in turn depends upon the liquid and vapor densities and the local flow conditions through the bubble diameter at departure (equation (3.28)

Equation (3.27) is reproduced here for brevity:

$$f = \sqrt{\frac{4g(\rho_l - \rho_v)}{3 d_{vw}\ \rho_l}}. \tag{3.27}$$

The vapor density ρ_v being small compared to the liquid density equation 3.27 reduces to the form shown below (equation 5.1) for most cases:

$$f = \sqrt{\frac{4g}{3 d_{vw}}}. \tag{5.1}$$

At high heat fluxes with the liquid velocity being a constant, based on equation and also based on physical intuition (more nucleation sites are activated at higher heat fluxes and the frequency of bubble generation increases), the bubble departure diameter d_{vw} term is lower, causing the frequency term to be higher compared to the other extreme when the heat flux is low and the bubble departure diameter is higher. The UDF is written in such a way that the bubble departure diameter can reach a maximum of the flow channel height (200 μm for all cases in this thesis). Based on this maximum diameter (200 μm), the bubble departure frequency is calculated to be 256 Hz. The corresponding time period is

then about 4 ms. This is the minimum time period for the bubble ebullition cycle for all cases in this thesis.

At the other end of the spectrum, namely, at lower heat fluxes the bubble departure diameter is higher and the frequency of bubble generation is lower. The corresponding time period for the bubble ebullition cycle is higher in this case. For time-step resolution reasons, it is only required that the time-step size chosen resolves the smallest time period of any cycle which is encountered in the former case. So, for all the cases considered in this thesis, the smallest time scale is about 4 ms. The highest time step size chosen for the cases considered in this thesis was 1e-05 s (for lower heat flux values) and the lowest time step size used was 1e-07 s which was sufficient to resolve the unsteady bubble ebullition processes based on the arguments above. The convergence was observed to be very stable for the above-mentioned time-step sizes and any increase in the time-step size rendered the solution process unstable and the solution eventually diverged. This is an area which has a lot of potential for future work.

The unsteady bubble ebullition process also implies that the different components of the heat flux (single phase, quenching and evaporative) are a function of time, and this was observed in all the cases considered in this thesis. Also, the vapor volume fractions inside the computational domains were time-dependent. Figure 5.1 and Figure 5.2 show snapshots of vapor volume fraction at different physical times that correspond to a case where the jet inlet velocity was 7.35 m/s, the applied wall heat flux was 125000 W/m^2 and the inlet subcooling was 77 °C. Figure 5.2 portrays the bubble ebulltion process in much more detail than Figure 5.1which is meant especially for a description of the time-averaging method used in this thesis. The bubble ebullition process as observed in Figure 5.2 is described in some detail in a section to follow.

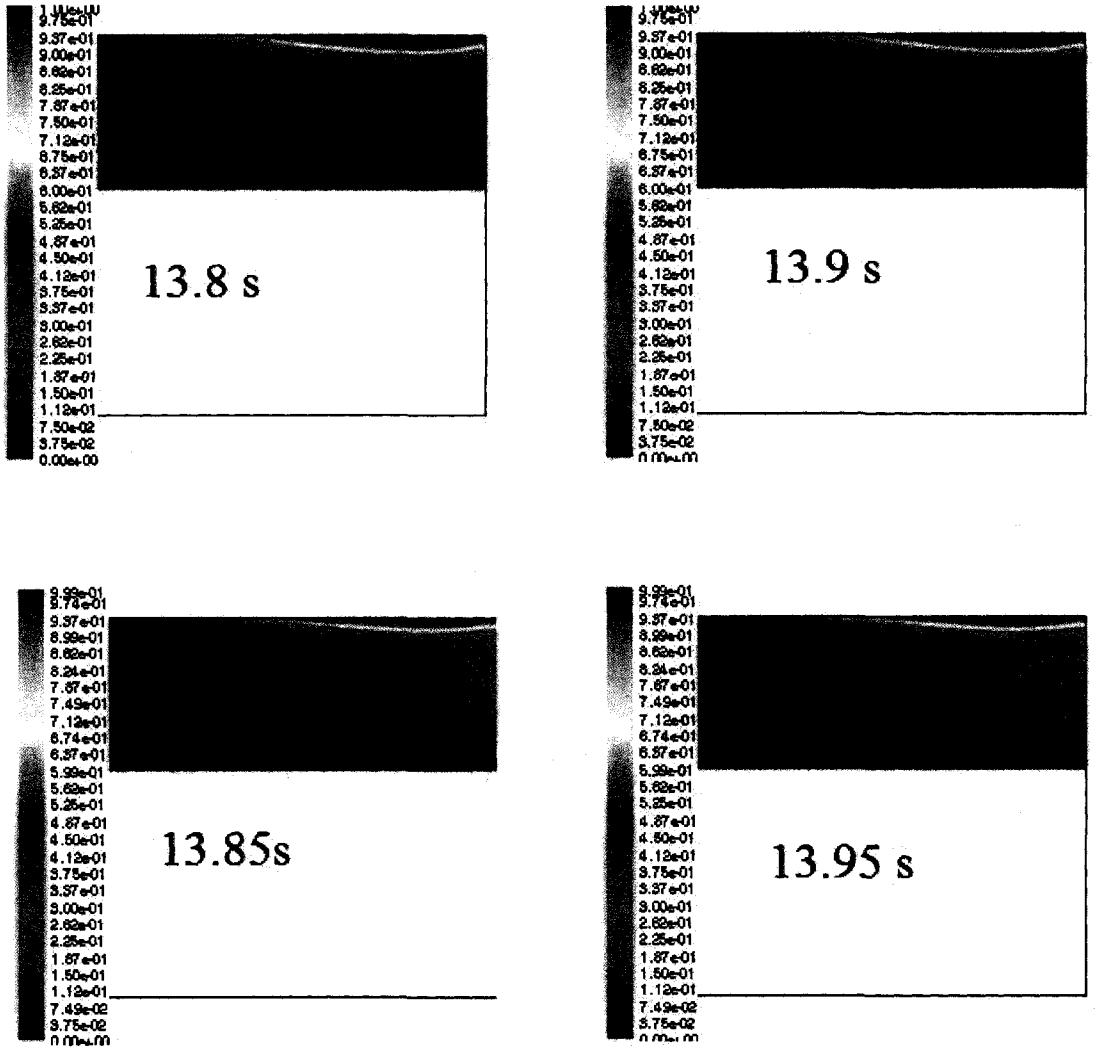

Figure 5.1: Time Snapshots of Vapor Volume Fraction ($q = 125$ kW/m^2, $Re_d = 550$, $\Delta T_{sub} = 77$ °C).

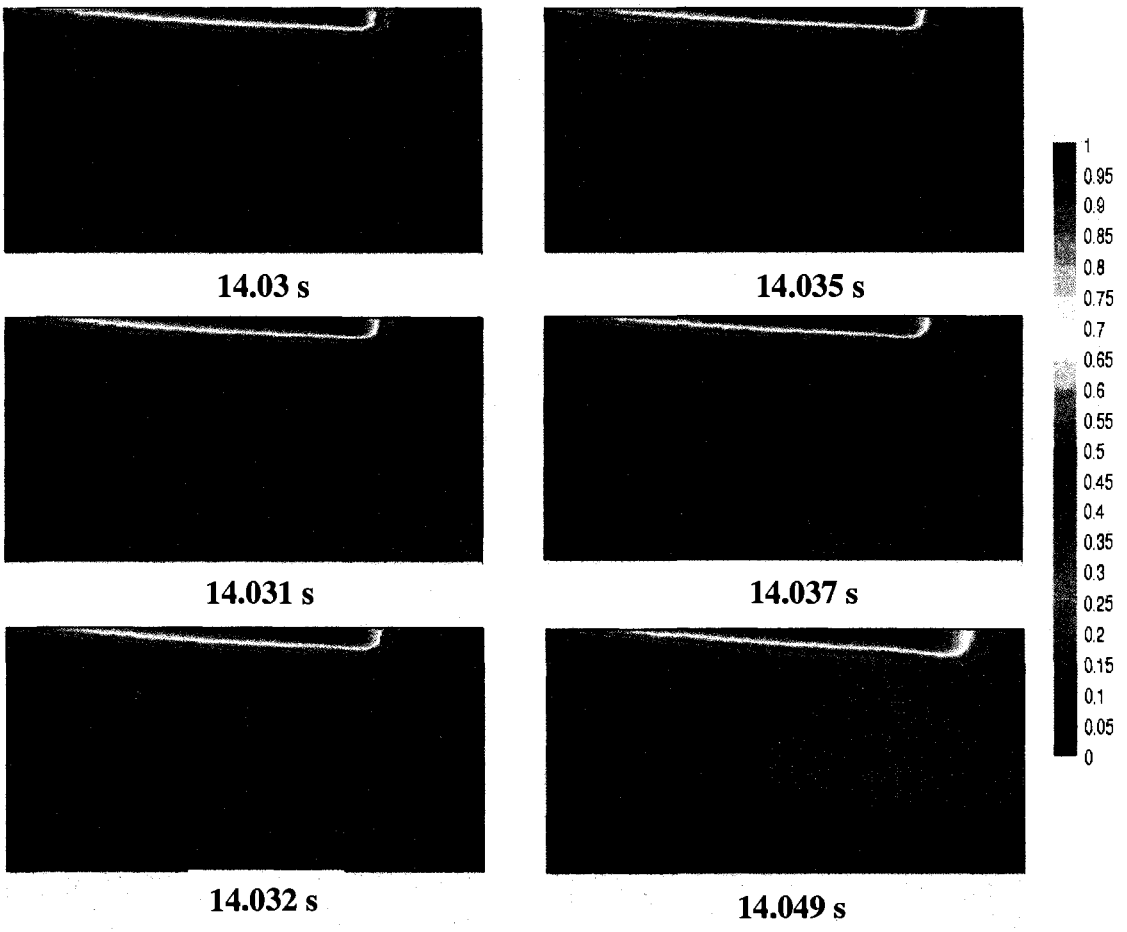

Figure 5.2: Time Snapshots of Vapor Volume Fraction ($q = 125$ kW/m^2, $Re_d = 550$, $\Delta T_{sub} = 77$ °C).

A typical vapor bubble ebullition process is shown in Figure 5.2. As the wall temperature rises above saturation due to the heating of the solid element, vapor bubbles are generated. When the forces holding bubble to the wall can no longer balance the forces pulling the bubble apart (liquid drag and the buoyancy force), the bubbles depart from the wall and acquire momentum. Figure 5.2 depicts the vapor volume fraction contours near the domain outlet (the wall temperature rises above the saturation temperature at this location). The vapor bubbles rise to the top wall because in the absence of considerable liquid velocity (near the outlet) the buoyancy force dominates the liquid drag force resembling a pool boiling scenario (this observation is consistent with experimental results from Wang *et al,* 2004). This is witnessed at 14.03 s (Figure 5.2). The continuous

bubble growth process is witnessed from 14.031 s through 14.049 s in Figure 5.2. The vapor front that departs from the heated wall (indicated by the light blue shade in the contour plots) rises to the top while also expanding in size. At 14.037 s, the vapor front from the bottom (heated) wall merges with the vapor front near the top wall. Interestingly, the merged vapor front now moves with an increased velocity to the outlet. We attribute this observation to the fact that the merger of the two vapor fronts causes a disturbance in the local liquid velocities causing an increased liquid drag on the vapor. A detailed analysis would throw more light on the micro-processes that occur for these boiling scenarios. This is a potential area for future research in this area.

Another interesting fact was witnessed in the simulations in this thesis, especially for cases where the heat flux was low and the degree of subcooling was high (Cases 1 through 4, as explained in Chapter 6). There was significant reversal of the vapor flow into the computational domain from the outlet. These observations were also made by Kandlikar (Kandlikar, 2004) in his studies of flow boiling in microchannels. He attributed this flow reversal to the inherent fluid flow instabilities occurring in flow boiling.

Figure 5.1 summarizes the time-dependent ebullition process maximum and minimum that repeats over time. This fact helped establish a basis for a time-averaging technique that is explained in the following section.

(5.4) Time-Averaging

The unsteady process of flow nucleate boiling as encountered in an axisymmetric microjet impingement problem yields unsteady heat transfer components (the single phase, the quenching and the evaporative heat flux components) that oscillate over time. The frequency of this cycle depends on the local flow conditions (through the bubble departure diameter) as evident from (3.28). The physics of the problem being very complicated, especially for high heat fluxes and low subcooling levels, the local flow conditions change with time and so does the bubble departure frequency. Never-the-less,

maxima and minima exist for the heat flux components which are the key to establishing a method for time-averaging the results. For this thesis, such maxima and minima in the heat flux component values along with vapor fraction contour plots were studied in coming up with time-averaged results for heat flux components and temperature plots.

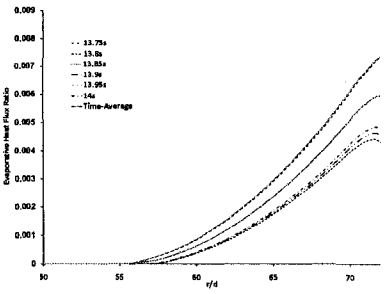

Figure 5.3: Time Averaging Applied to Evaporative Heat Flux Component.

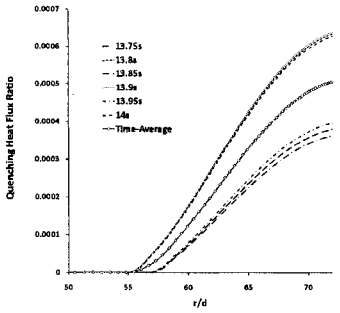

Figure 5.4: Time Averaging Applied to Quenching Heat Flux Component.

Figure 5.3 and Figure 5.4 show the time-averaging process applied to a particular case corresponding to Figure 5.1. As explained before, for higher heat flux values and lower sub-cooling levels, the frequency of the bubble ebullition process becomes higher and the time-period for these cycles becomes lower. In each case though, there is a maximum and a minimum value of the quenching and evaporative heat flux distributions over time; they repeat in a near-cyclic fashion. Several such cycles are identified and a simple average over time is computed. All of the results presented in Chapter 5 are time-averaged using the method above.

(5.5) Treatment of the Virtual Mass Force Term

There is considerable debate in the technical literature over the use of the virtual mass force term in boiling simulations. The virtual mass force term assumes significance when the dispersed phase in a two-phase model accelerates considerably with respect to the primary phase. The effects of the virtual mass force were investigated for two boiling scenarios in this thesis (one for low heat flux value and one for a higher heat flux value). The differences in the evaporative heat flux ratio when the virtual mass force term is enabled in the numerical solver and not enabled are shown in Figure 5.5 and Figure 5.6 .

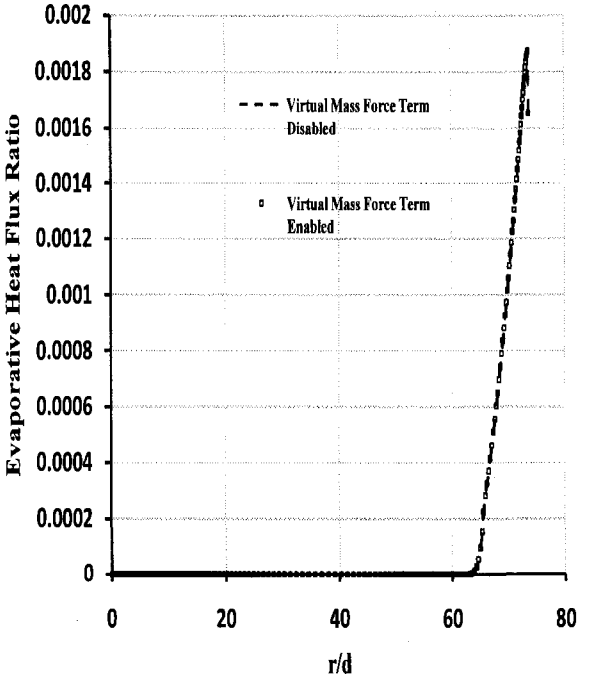

Figure 5.5: Effect of the Virtual Mass Force Term: q = 10.8 kW/m^2, Re_{ji} = 550, ΔT_{sub} = 77 K.

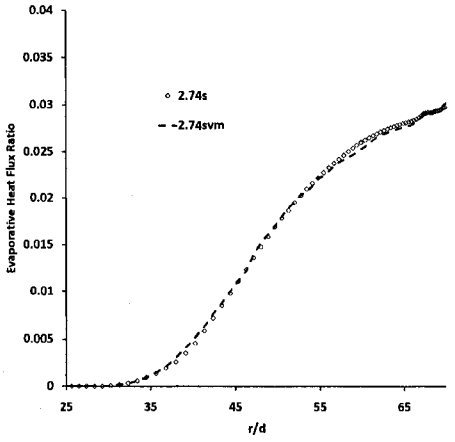

Figure 5.6: Effect of the Virtual Mass Force Term, $q = 20\ kW/m^2$, $Re_{ji} = 550$, $\Delta T_{sub} = 77\ K$.

From Figure 5.5 and Figure 5.6, it was deemed reasonable to neglect the virtual mass force term for all the simulations considered in this thesis.

(5.6) Model Validation

To provide confidence in our boiling simulations, a validation study was carried out by comparing some of our numerical results with experimental results from (Wang *et al.,* 2004). Wang *et al.,* considered several configurations of microjets, single and multiple in both single phase and boiling regimes. We compared some of our boiling, single microjet results to the experimental results from the above-mentioned work. They presented temperature measurements averaged along the heated wall for different levels of heat flux. The comparison of the numerical results obtained in this study with the experimental results is shown in Figure 5.8. The modified RPI model was used to simulate the boiling single jet impingement problem with conditions the same as in their paper.

The problem domain and the parameters for the validation are shown in Figure 5.7. The heat generating IC chip (1cm x 1cm area), represented as a solid region, is provided with inputs of varying power levels above the power threshold that is needed to initiate boiling (10.8 W observed in the present simulations, consistent with what was seen in Wang et al.). At a power level of 10.8 W (heat flux of 108000 W/m^2), vapor generation is observed in the region downstream of the stagnation point very near the outlet boundary. The vapor generation rate increases as the heat input levels are increased, as expected, and the vapor front is observed to move inward from the outlet region toward the stagnation point. The percentage deviation from the experimental results in each of these simulations is shown in Table 5.2.

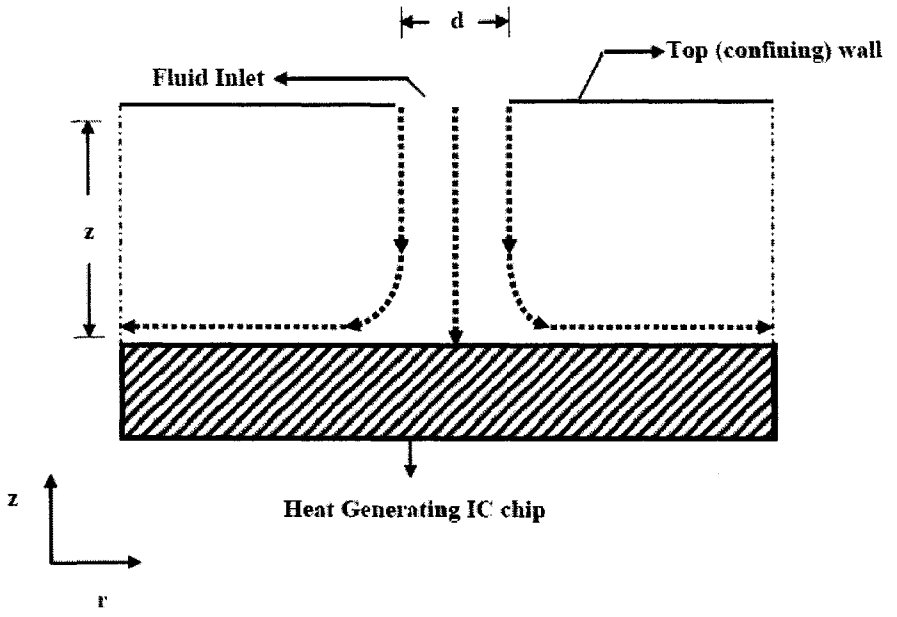

Figure 5.7: Domain for Validation Study. z = 200 μm, d = 76 μm.

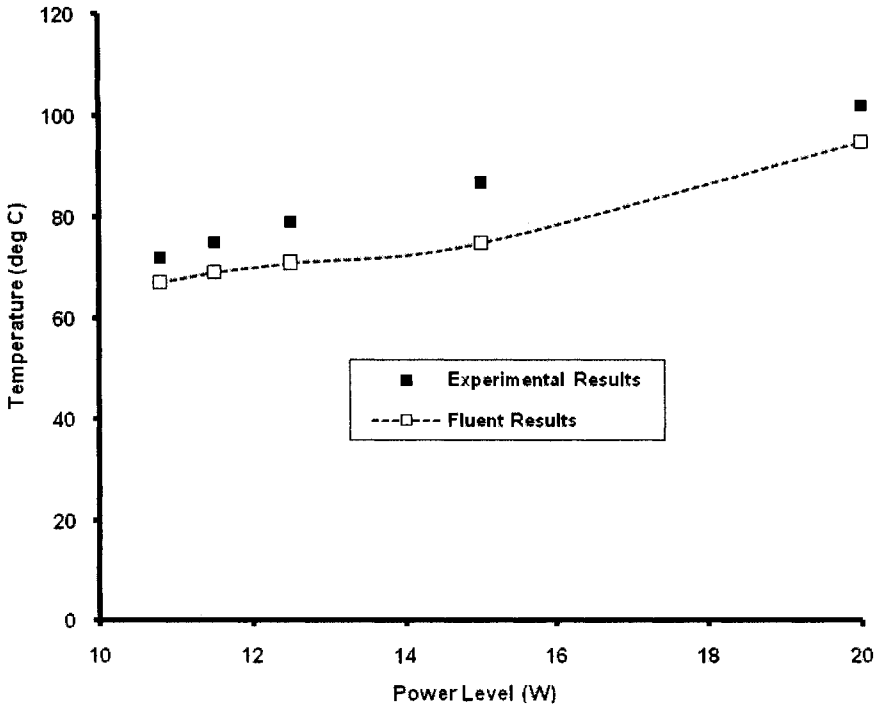

Figure 5.8 Validation Study Results (Validation with Wang *et al.*, 2004).

Thus, for the cases investigated in this study, the maximum deviation from the experimental results due to Wang *et al.* is 13 % with an RMS deviation of 10%. Considering the complexity of the two-phase problem, this deviation is deemed acceptable. Further, Wang *et al.* note that for all of the cases considered in their studies of single microjets, a physical dryout point (Critical Heat Flux) was reached when the average exit vapor fraction reached 0.3. For a few higher heat flux cases in this work and a few cases not reported in this work, this observation manifested as increases in the wall temperature and numerical instabilities when the average exit vapor fraction reached a value of 0.35. These observations added a lot of confidence to our boiling simulations using the modified RPI model.

Table 5.2: Percentage Deviation of Numerical Results from Experimental Results (Wang *et al.*, 2004).

Power Level (W)	**Percentage Deviation from Experimental Results**
10.8	7
11.5	8
12.5	10
15	13
20	7

(5.7) Global Energy Balance:

An additional verification check for different cases involving the global energy balance equation (for the entire domain) was also carried out. The procedure and the global energy equations are as follows:

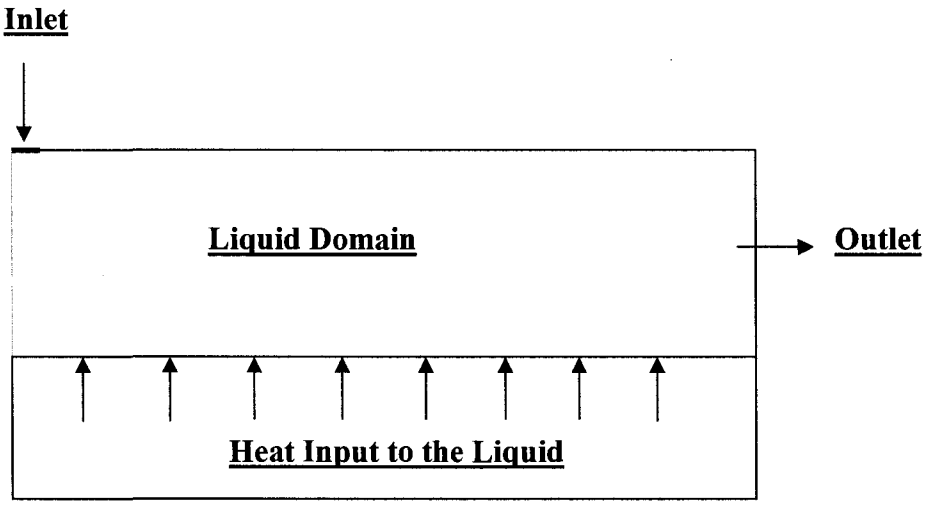

Figure 5.9: Problem Domain for Global Energy Balance.

The axisymmetric problem shown in Figure 5.9 has one inlet and one outlet for the fluid to enter and exit respectively. The heat input to the liquid volume comes from the solid as shown. Writing a simple global energy balance equation for this set-up, we have,

$$\left[\alpha_{li}\,\mathrm{m}_{li}h_{li} + q_w A_w - (\alpha_{lo}\,\mathrm{m}_{lo}h_{lo} + \alpha_{vo}\,\mathrm{m}_{vo}h_{vo})\right] = \frac{dE}{dt} \tag{5.2}$$

Flux In

Wall Heat

Flux Out (Liquid Vapor Mixture)

Rate of Energy Stored in the Control Volume

The unit of all the terms in this equation is W (Flux of Energy). The last term on the right hand side, namely the energy storage term is a differential (involving two finite time steps) and the whole equation can be written in finite difference notation as shown below.

$$\alpha_{li}\,\mathrm{m}_{li}h_{li} + q_w A_w - (\alpha_{lo}\,\mathrm{m}_{lo}h_{lo} + \alpha_{vo}\,\mathrm{m}_{vo}h_{vo}) = \frac{E_2 - E_1}{\Delta t} \tag{5.3}$$

$$E_1 + \left[\alpha_{li}\,\mathrm{m}_{li}h_{li} + q_w A_w - (\alpha_{lo}\,\mathrm{m}_{lo}h_{lo} + \alpha_{vo}\,\mathrm{m}_{vo}h_{vo})\right]\Delta t = E_2$$

Equation (5.3) expresses the relation between the energy (in Joules) stored at two different time steps spaced by Δt (where Δt is the finite time-step size). The overall energy balance check involves verifying that this equation is satisfied with values for the terms determined from the numerical results. All the terms in (5.3) were determined for a few adjacent time steps (for each case at least 4 time-steps were chosen each separated by the time-step size).

The following tools in FLUENT were used to calculate each of the quantities appearing in (5.3).

Flow Rate

The $\alpha \dot{m} h$ terms in the LHS of (5.3) involve a flow rate of enthalpy of the liquid and the vapor phases at both the inlet and the outlet. The flow rate utility (essentially a surface integral) was used to estimate these terms at the inlet and the outlet. The Flow Rate integral in FLUENT computes fluxes of any given quantity across any surface. For example, the flux of the quantity $\alpha_l h_l$ is computed as a flow rate given by (5.4).

$$\dot{m}\alpha_l h_l = \int(\alpha_l h_l \rho_l \vec{v}_l).dA_i = \sum_{j=1}^{n} \alpha_{lj} h_{lj} \rho_j \vec{v}_{lj}.\vec{A}_j \tag{5.4}$$

Integral

The total heat into the liquid domain over the wall area A is computed using the Integral tool in FLUENT defined by:

$$Q_w = \int q.dA = \sum_{j=1}^{n} q_j A_j . \tag{5.5}$$

Mass Integral

The total energy stored (mh) in each phase (liquid and vapor) in the fluid domain at each time step is calculated from the mass integral expression given in (5.6).

$$E1 = (m_l h_l + m_v h_v)_{CV} = \int h_l \rho_l .dV + \int h_v \rho_v .dV = \sum_{j=1}^{n} h_{lj} \rho_{lj} V_{lj} + \sum_{j=1}^{n} h_{vj} \rho_{vj} V_{vj} \tag{5.6}$$

Using these three integral tools to calculate the terms in (5.3), cases 2, 3 and 6 were chosen for the energy balance analysis (at random). The energy balance analysis is summarized in Table 5.3. E_2 has two values: one coming from equation (5.3) and one directly from the numerical prediction (at a later time step than when E1 is calculated). From Table 5.3 , it is clear that the global energy conservation equation is satisfied to within 5 significant digits (the difference between the E_2 values from FLUENT match those from Equation 5.3 to within 5 significant digits). With the energy residual limit set to 1e-05, this is the level of agreement that is expected. This global energy balance agreement also instilled some confidence in the numerical procedure.

Table 5.3: Global Energy Balance Check

Case	Flux In (W)	Flux Out (W)	Energy Stored at time t1 E1(J)	Energy Stored at time t1+Δt, E2 (J)	
				Predicted from (5.3)	FLUENT prediction
2	10.641280	9.001016	7.841304	7.841320	7.841316
3	11.321218	5.110829	7.806440	7.806502	7.806498
6	15.347767	2.506264	6.203129	6.203256	6.203241

(5.8) Summary and Conclusion:

The main aim of this chapter was to provide a description of how the RPI model was implemented within the Eulerian multiphase model of FLUENT. The bubble departure frequency and its role in determining the unsteady nature of the boiling process and hence on the associated time-step size resolution for the problem is discussed. The influence of the virtual mass force term is also explained in some detail.

Armed with the confidence in the UDF based on the validation study we conducted and in the modified RPI model, a parametric study of boiling microjet impingement was undertaken. This is explained in detail in Chapter 6.

Chapter 6

Numerical Simulation of Boiling Microjet Impingement for Electronics Cooling

(6.1) Introduction

This work presents numerical simulation results for boiling microjet impingement in a confined arrangement. The RPI (Renssealer Polytechnic Institute) model (Kurul and Podowski, 1990) for subcooled boiling flows was modified to account for laminar flow boiling in a confined, axisymmetric microjet impingement arrangement. The method was first validated with experimental results from the literature and then extended to study the effects of liquid subcooling, microjet Reynolds Number based on the nozzle inlet, and heat flux levels. The simulation results were in good agreement with results from comparable experiments in the literature. The average wall temperature increases as the applied wall heat flux is increased. The slopes of the temperature curves in the radial direction flatten out at a certain value that depends upon the heat flux value. The vapor front once generated begins to move inward toward the stagnation region as the heat flux is increased. The change in the quenching and the evaporative components with respect to increasing heat fluxes is at first slow but an order of magnitude rise is seen after the level of subcooling is decreased. For the cases considered in this study, the single phase heat transfer component dominates the other two modes of heat transfer. The quenching heat transfer component occupies the next spot followed by the evaporative heat transfer coefficient. Lower inlet subcooling levels are associated with flatter temperature profiles than those with higher subcooling levels. In effect, lower inlet subcooling levels are associated with lower streamwise ΔT values. In a confined microjet impingement arrangement, the liquid velocity profile has considerable impact on the vapor bubble nucleation, vapor drag and the bubble departure diameter. Lower levels of subcooling are associated with boiling inception and more vigorous boiling in the vicinity of the stagnation zone rather than those with higher levels of subcooling. The degree of

subcooling may emerge as the single largest factor controlling the lateral temperature rise in a chip cooled by a single, confined impinging microjet.

(6.2) Literature Review

A combination of jet impingement and boiling heat transfer, both attractive heat transfer mechanisms with small changes in temperature, is being deemed as the best alternative to conventional methods of electronics cooling as rising heat flux levels demand both effective heat removal and precise temperature control. There has been a lot of work on boiling jet impingement, both experimental and theoretical, some of which is discussed in Section 4.2. The ability to numerically model two-phase flows (of which flow boiling is a special subject) has been an area of very dedicated research over the last several decades. Numerical modeling of flow boiling, however, has always been very difficult because of the complicated physics of phase change involved with it. Recent advances in heat flux partitioning theories (Kurul and Podowski, 1990) have helped produce a lot of progress and success in simulating flow boiling and condensation (Wolf *et al.,* 1996). Several studies have emerged in the recent literature all based on the RPI model developed by Kurul and Powdowski. Flow boiling in microchannels presents another formidable challenge as presented very eloquently by Kandlikar (Kandlikar, 2004). Confined jet impingement featuring a top wall to confine the jet outflow from the stagnation point and also featuring boiling either at the stagnation point or further downstream is of great research interest to industry and the academia alike. This is particularly true when the nozzle diameter and the distance between the jet inlet and the heated plate are much smaller (few hundreds of microns) than conventional nozzles (few millimeters). Because of the complicated nature of the physics involved with the boiling processes, the vast majority of research done on boiling flows including those on boiling jets has been experimental. Very recently, heat flux partitioning theories pioneered by Kurul and Powdowski have led to a surge of interest in simulating flow boiling in high pressure applications such as those encountered in nuclear reactors. Some work (Stevens

and Webb, 1991) has also been published on turbulent boiling jets applied to automotive electronics cooling. The focus of this paper is to numerically simulate a boiling microjet (less than 100 μm in diameter) in an axisymmetric, confined arrangement (the distance between the top confining plate and the bottom heated wall is kept at 200 μm). Because of the dimensions used in the models, modifications had to be made to the RPI model which was originally meant for turbulent flow boiling. The modified model was implemented in a commercial CFD code (FLUENT v.6.2.16) via a user-defined function in conjunction with the Eulerian multiphase model to simulate boiling flows in a confined microjet impingement arrangement.

(6.3) Problem Definition

The problem under consideration in this paper is shown in Figure 6.1.

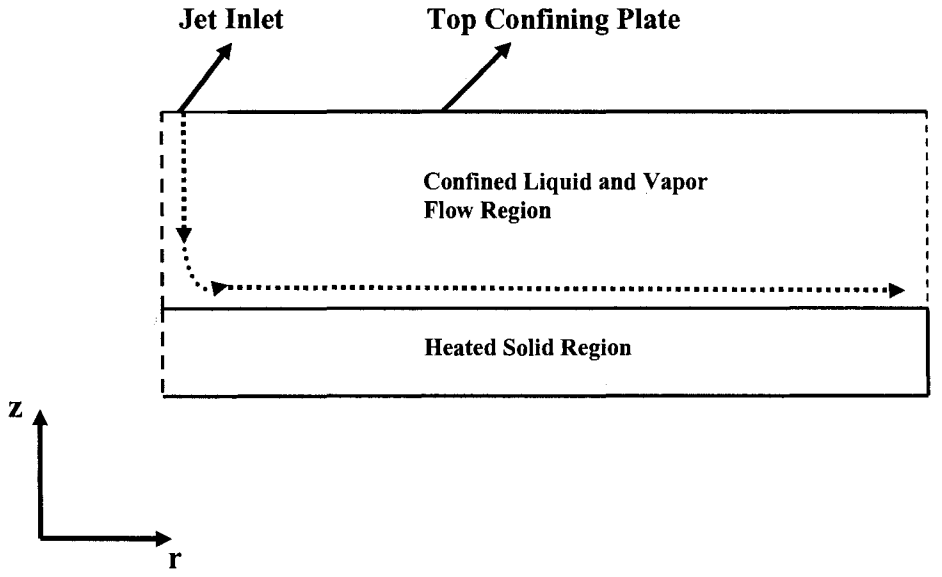

Figure 6.1: Problem Definition.

As mentioned before, an axisymmetric jet configuration is considered in this paper with r and z representing the radial and axial coordinates, respectively. The jet inlet diameter considered was 75 μm and the z/d distance was maintained at 200 μm. This z/d ratio ensured that the heated wall was always within the potential core of the jet to maximize heat transfer. The jet inlet velocities considered in this paper were carefully chosen to ensure laminar flow conditions throughout the domain of interest. The solid region shown in the figure represented an active integrated circuit chip which generates heat. The solution of the governing equations along with the appropriate boundary conditions provided the velocity field, the temperature field and the phase fractions of each of the two phases involved.

(6.4) Governing Equations and Solution Methodology

The Eulerian multiphase model in FLUENT was used to model the boiling microjet impingement problem. The governing equations for the Eulerian multiphase model, the closure terms and the boundary conditions along with the closure relations are described in equations (3.13) through (3.32)

(6.5) Computational Domain and Grid Resolution Study

In general, in an impingement problem, the regions of interest are the stagnation region where the velocity is a minimum and the pressure rises to a maximum, the region near the nozzle inlet, and the boundary layer regions near the wall-bounded flow. The process of boiling downstream of the stagnation point further complicates the physics of the problem. Unlike a single phase jet impingement problem where the velocity downstream of the stagnation point reduces in the radial direction, thus needing only a coarse mesh, in a boiling jet problem the nucleating vapor bubbles necessitate a fine mesh in the region downstream of the stagnation point. This makes the grid resolution study an arduous task but it suffices to say that a general methodology was adopted to ascertain reasonable grid independence for all the results obtained in this paper. The

general meshing strategy and the boundary conditions used are demonstrated in Figure 6.2. Only a radial slice of the domain was modeled making use of the symmetry of the problem with respect to the jet centerline.

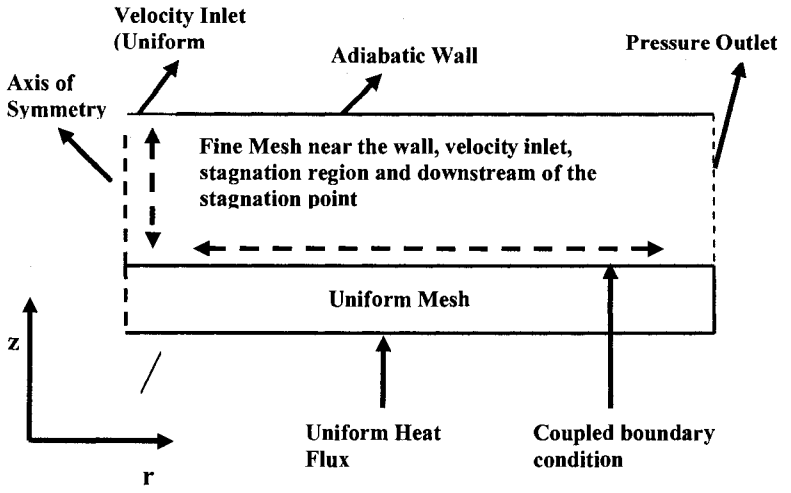

Figure 6.2: Computational Model and Grid Resolution Study.

Three different mesh sizes were used for the grid resolution study, a coarse mesh containing about 6000 cells, a fine mesh containing about 13000 cells and a finer mesh containing about 17000 cells. The parameters tested for grid independence were the liquid stream function plots, wall temperatures along the solid wall and the vapor volume fraction and velocity. Experience from the results of the single phase microjets also provided very valuable insights into efficient meshing of the computational domain. The fine mesh containing 13000 cells provided results comparable to the finer mesh and was thus adopted in the rest of the simulations carried out in this study.

(6.6) Parametric Study

Once a reasonable amount of confidence was established with the validation study described in section 5.6, a parametric study was done on the single boiling microjet to study the effects of the inlet Reynolds Number, applied wall heat flux and the inlet subcooling level on the boiling heat transfer performance in an impingement arrangement. The parameters investigated are defined in equations (6.1) and (6.2)

$$\mathrm{Re}_{ji} = \frac{V_{ji}\, d}{\nu} \tag{6.1}$$

$$\Delta T_{sub} = T_{sat} - T_{ji}\,. \tag{6.2}$$

The details of the parametric study are given in Table 6.1

(6.7) Numerical Solver Details

The second order upwind discretization scheme with a phase-coupled SIMPLE pressure-velocity coupling algorithm was chosen for all the numerical studies for this boiling problem. As mentioned before, the Eulerian multiphase model was used for the problem. The Eulerian multiphase model accommodates separate governing equations for each of the phases being modeled. Only the pressure term is shared between the phases. All of the heat energy from the wall was assumed to go into the liquid phase (no superheating of the vapor) and thus the temperature of the vapor phase was fixed at saturation. Consequently, the equations that were solved by FLUENT were the liquid and vapor momentum equations, the liquid and vapor continuity equations, and the energy equation for the liquid. A particular problem that cropped up during the simulation of the boiling problem was that the vapor bubble size predicted by equation (3.28) was larger than the size of the channel (because of the confined jet arrangement this was physically unrealistic) causing the solution to diverge. To avoid this physically untenable situation,

the maximum bubble size was restricted to that of the channel height. The two-way interaction between the main solver and equations (3.13) through (3.32) by means of a user-defined function written in the C programming language. As mentioned before, the lift terms and the virtual mass terms in the Eulerian model were not included. The results presented for this work include the radial temperature distribution along the heated wall and the quenching and the evaporative heat flux ratios for each case considered in the parametric study. The study concludes with a description of the effects of the jet inlet Reynolds Number, applied wall heat flux, and the inlet subcooling level on the temperature distribution and the evaporative and the quenching heat transfer coefficients.

(6.8) Results and Discussion

Figure 6.3 through Figure 6.13 portray the effects of the inlet Reynolds Number, wall heat flux and the inlet subcooling on the wall temperature, vapor generation, vapor momentum and general heat transfer characteristics of the single, confined microjet impingement problem under consideration for this work. Changes in all of these parameters are expected to alter the bubble ebullition process and are also interrelated. An increase in Reynolds Number, for instance would tend to exert more drag on the vapor bubble leading to lower bubble departure diameter and possibly intense bubble activity near the wall. The wall heat flux should be sufficiently high enough and the local liquid velocity should be sufficiently low enough to support this intense bubble motion. The absence of either could mean an altered bubble ebullition cycle. The effects of the degree of subcooling are also intuitive in this regard. A lower subcooling level (high fluid inlet temperature), for example, would help evaporate more liquid because of the reduction in sensible heat required to raise the fluid temperature to the saturation point.

Table 6.1: Boiling Microjet Impingement Problem – Parametric Study

Case No	Heat Flux (kW/m^2)	Jet Inlet Reynolds Number	Inlet Subcooling (°C)
(1)	108	550	77
(2)	115	550	77
(3)	125	550	77
(4)	150	550	77
(5)	200	550	77
(6)	108	550	43
(7)	115	550	43
(8)	125	550	60
(9)	125	550	30
(10)	150	550	50
(11)	150	837	50
(12)	150	1100	50

(6.8.1) Effect of Increasing Heat Flux on Boiling Jet Impingement

Figure 6.3 shows the effect of increasing heat flux on the temperature profiles. In general (as is to be expected), as heat flux increases, the volume of vapor generated increases and the growing vapor front moves radially inward from the outlet region (towards the stagnation zone). Figure 6.3 is a plot of the time-averaged wall temperatures at different heat flux levels. It is observed that as the heat flux increases (meaning increased power generation in the solid region representing the active electronic chip), the temperature levels along the radial direction are observed to increase, but the slope of each of these lines varies. The profiles begin to flatten out as the heat flux increases indicative of more vapor mass being generated (and thus greater quenching and evaporative heat transfer components). The region at which these plots flatten out also are pushed inward toward the stagnation zone at higher heat fluxes. For increased heat fluxes at the wall, the radial location at which vapor nucleation is initiated on the heated wall moves inward toward the stagnation zone. This fact is reflected in the temperature profiles flattening out in the vicinity of the stagnation zone. Also, liquid velocities, being higher near the stagnation zone and eventually dying out near the outlet, exert more drag on the vapor generated near the stagnation zone as compared to that being generated near the outlet. This aspect is reflected in Figure 6.4 and Figure 6.5. They show the evolution of the quenching and the boiling heat flux ratios as the heat flux increases from 10.8 to 20 W/cm^2. It was observed for most of the cases considered in this study that the evaporative heat flux dominates the quenching heat flux component. The quenching and the boiling heat flux operate in unison (in the same region) and are significantly smaller than the single phase component. The comparatively lower values of the evaporative and the quenching heat fluxes are consistent with trends seen in previous work (Narumanchi *et al.*, 2006). The predominant mode of heat transfer in almost all cases considered in this thesis is the single phase heat transfer accounting for about 97 percent of the total heat transfer. This is because of the very high energy required for boiling (latent heat) and also due to the fact that it is inherently difficult to create active nucleation sites.

Figure 6.4 portrays some very interesting results. For relatively low heat fluxes, (Cases 1, 2 and 3), the initiation of the quenching component is at an r/d of 55 to 65. For Cases 4 and 5, though, the initiation of quenching (because of the initiation of boiling) is at r/d ratios of 35 and 25, respectively, which is very advantageous for an electronics cooling system incorporating a two-phase impingement heat transfer mechanism. Ideally, nucleate boiling should commence in the vicinity of the stagnation point although this is very rarely observed in practice. The quenching heat flux ratio (ratio of the quenching component to the total heat transfer) increases from very low values for Cases 1, 2 and 3 to 0.0015 for Case 4 and 0.0012 for Case 5. Thus we observe an increase of one to two orders of magnitude in the quenching heat flux component as the heat flux increases from 12.5 W/cm^2 to 15 W/cm^2 and from 15 W/cm^2 to 20 W/cm^2. This is an indication that at higher heat fluxes, the quenching component and the evaporative component might become comparable to the single phase heat transfer component which, again, is very advantageous for electronics cooling since boiling heat transfer is associated with very high heat flux removal rates with low gradients in temperature. Also, for higher heat fluxes, the quenching and the evaporative heat flux ratios appear to taper off towards the exit. This is because at higher heat fluxes, boiling and hence the associated quenching are initiated radially closer to the stagnation point the cooler liquid possibly travels around the vapor phase resulting in higher single phase heat transfer towards the outlet plane. In contrast, for the lower heat flux cases, the evaporative and the quenching heat flux components are initiated much closer toward the outlet which explains the behavior seen in Figure 6.3, Figure 6.4 and Figure 6.5. The behavior of Case 5 is also different from Case 3 or Case 4 because for Case 5, the heat flux rate (200000 W/m^2) is high enough to cause vapor generation from an r/d ratio of 28 and all the way toward the jet outlet. This is reflected in the orders of magnitude rise in the evaporative and the quenching heat flux components for Case 5 when compared to the other cases.

These results offer significant insight into the design of two-phase cooling systems. From the observations for Cases 3 and 4, it appears that the vapor bubbles nucleating at the wall may act as turbulators or boundary layer trippers enhancing the heat transfer rate in the wake of these sites.

Overall, the effect of increasing wall heat flux can be summarized as follows:

(1) The average wall temperature increases as the applied wall heat flux is increased. The slopes of the temperature curves in the radial direction flatten out at increased heat fluxes indicating increased boiling. As the heat flux increases, the flattening in the temperature plots occurs more in the vicinity of the stagnation region.

(2) The change in the quenching and the evaporative components with respect to increasing heat fluxes is slow at first for relatively low values of heat flux, but an order of magnitude to two orders of magnitude rise is seen after a certain point.

(3) For the cases considered in this study, the single phase heat transfer component dominates the other two modes of heat transfer. The evaporative heat transfer component occupies the next spot followed by the quenching heat transfer coefficient. This is a markedly different observation than those found in the technical literature of flow boiling in microchannels.

Figure 6.5 shows plots of the evaporative heat flux ratio versus varying wall heat fluxes. As mentioned before, the single phase heat flux component dominates the other two components of heat transfer. It is observed that the evaporative heat flux ratio is an order of magnitude higher than the quenching heat flux ratio for Cases 1 through 5. This is a markedly different result from the results observed in the microchannel literature where the quenching heat flux dominates the evaporative heat flux. The only possible reason that could be attributed to this change is the relatively low liquid Reynolds Number for the cases considered in this thesis in comparison with the higher Reynolds Numbers used in other works. Higher Reynolds Numbers, meaning higher liquid

velocities and increased liquid drag on the vapor, cause the vapor bubbles to depart at lower diameters and also increase the frequency of bubble generation. Consequently, more liquid fills in more frequently in the places vacated by the departing vapor bubbles resulting in increased quenching heat transfer. Lower Reynolds Numbers have the opposite effect which was observed in most cases in this thesis. An order of magnitude increase in the evaporative heat flux component is observed though, when the wall heat flux is increased from 10.8 W/cm^2 to 20 W/cm^2 , a fact that is encouraging for heat dissipation from, say, 100 W/cm^2 electronic chips.

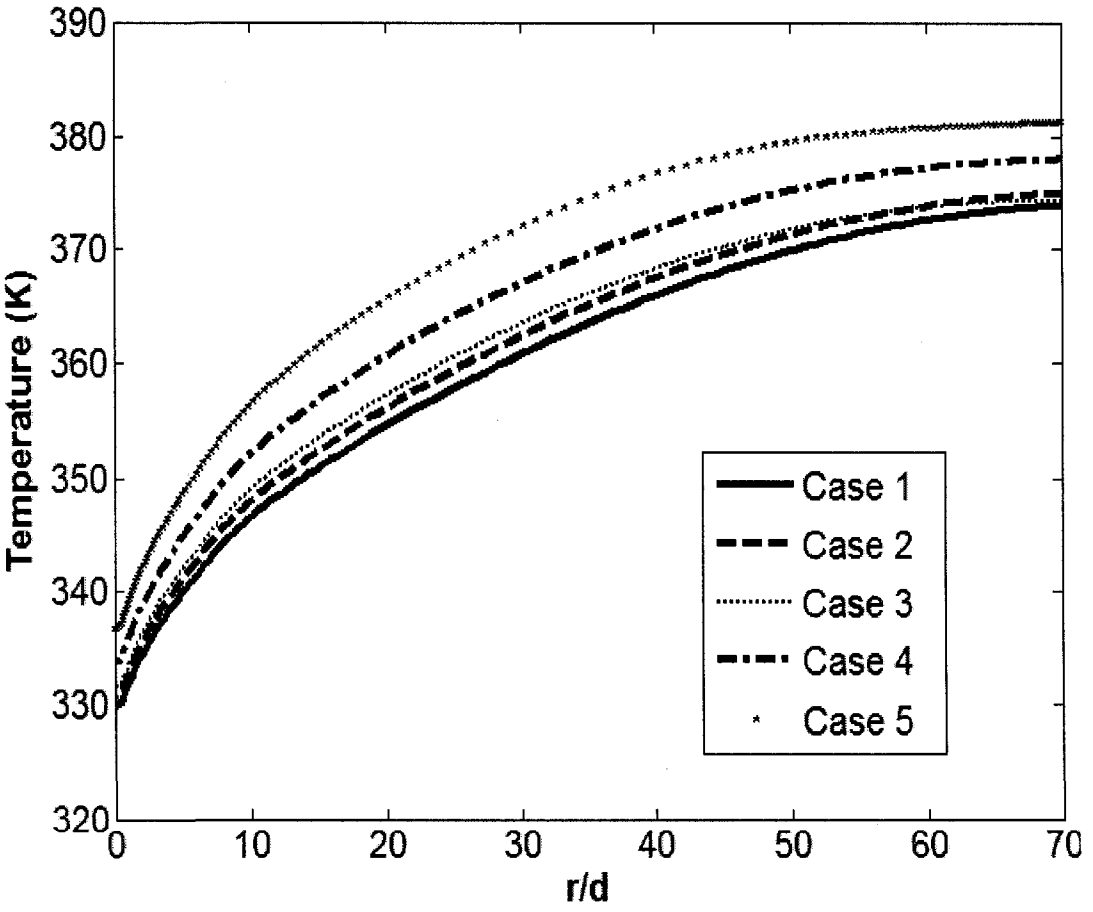

Figure 6.3: Temperature Plots for Increasing Heat Fluxes.

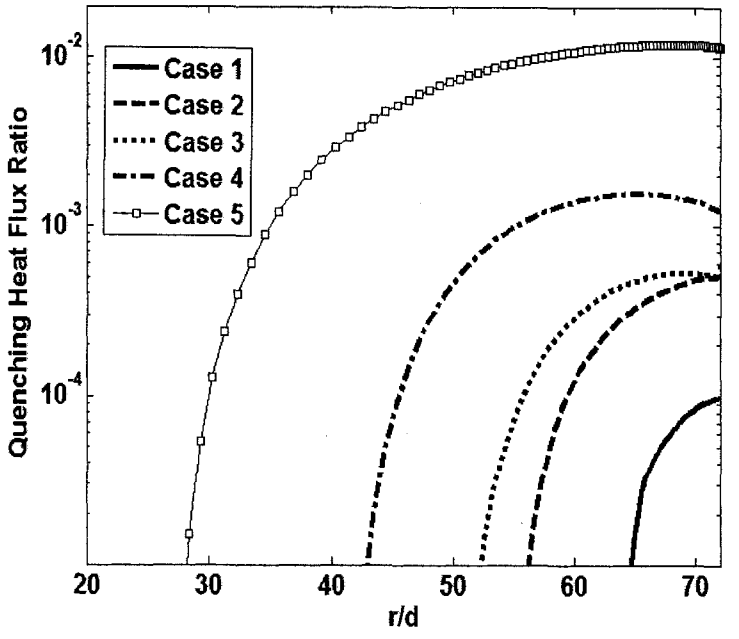

Figure 6.4: Quenching Heat Flux Ratio as a function of varying heat flux.

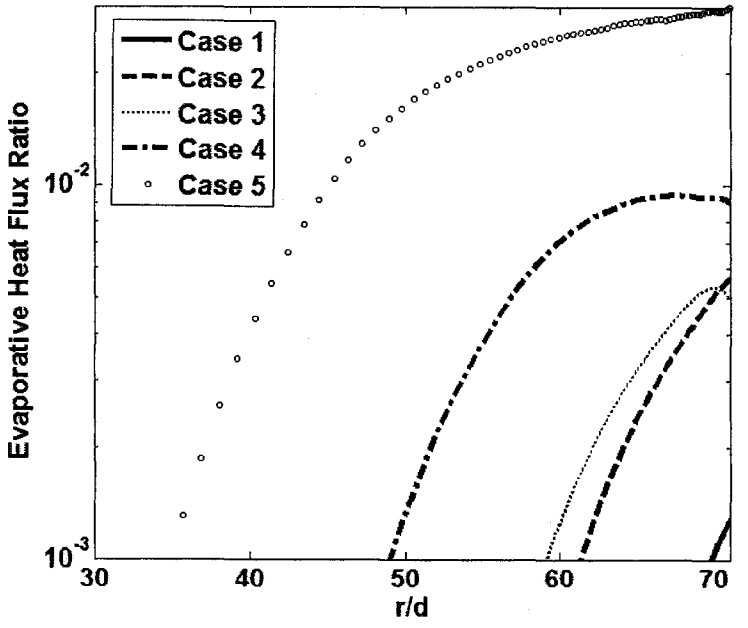

Figure 6.5: Evaporative Heat Flux Ratio versus varying Heat Fluxes.

(6.8.2) Effect of the Inlet Sub-Cooling on the Boiling Jet Impingement

The cases considered to study the effects of the inlet subcooling on the boiling microjet impingement are Case 1 vs Case 6, Case 2 vs Case 7 and Cases 3, 8 and 9. The wall temperatures along the radial direction are plotted for these cases in Figure 6.6 accompanied by the boiling and the quenching heat flux ratio plots in Figure 6.7 through Figure 6.10, respectively. The temperature plots in Figure 6.6 reveal interesting details. A comparison between the plots for Case 1 and Case 6 where the heat flux is 10.8 W/cm^2 and the inlet Reynolds Number is 550 and the inlet subcooling is lowered from 77 °C (Case1) to 43 °C (Case 6) shows that the slope of the plot for Case 6 is much flatter than that for Case 1. This means that the same degree of cooling could be achieved with a much lower ΔT when the inlet subcooling is reduced. These trends are also realized for comparisons between Case 2 and Case 7 and those for Case 3 and Cases 8 and 9. This is because of the fact that at lower subcooling levels, boiling inception takes place nearer the stagnation region along the radial direction than those with higher subcooling levels. Ideally, a cooling system incorporating boiling should have as low a ΔT as possible and the degree of subcooling may emerge as the single biggest factor that controls the temperature gradients in a boiling microjet impingement cooling system. Figure 6.7 through Figure 6.10 show the evolution of the evaporative and the quenching heat flux ratios as the degree of subcooling is varied. It is clear from these plots that as the degree of subcooling is lowered, boiling (and hence quenching) becomes more pronounced and is also realized much closer to the stagnation region.

This observation is particularly desirable for a single boiling microjet because the liquid velocities are larger in the vicinity of the stagnation region which causes a pronounced drag on the vapor bubbles leading to a decrease in bubble departure diameter which, in turn, leads to sustained nucleate boiling. A comparison between Cases 3,8 and 9 shows that boiling is initiated at an r/d of 0.1 for Case 9 (Inlet subcooling of 30 °C) in

contrast to an r/d of 0.5 for Case 8 (Inlet subcooling of 60 °C) and around 0.85 for Case 3 (Inlet Subcooling of 77 °C). Also observed is the tremendous increase (10 times) in the quenching and the evaporative heat flux ratios for Case 9 in comparison with Cases 3 and 8. This may be attributed to the afore-mentioned effect of increased drag on the vapor bubbles by the liquid. The liquid flow patterns in the confined jet region and the local liquid velocities affect the location at which boiling and quenching are initiated and thus the results from a single phase analysis may provide considerable inputs for the design of a boiling jet cooling system.

The effects of Inlet subcooling then may be summarized as follows:

(1) Lower subcooling levels are associated with flatter temperature profiles than those with higher subcooling levels. In effect, lower subcooling levels are associated with lower streamwise ΔT values.

(2) In a confined microjet impingement arrangement, the liquid velocity profile has considerable effects on the vapor bubble nucleation, vapor drag and the bubble departure diameter. Lower levels of subcooling are associated with boiling inception and more vigorous boiling in the vicinity of the stagnation zone rather than those with higher levels of subcooling.

The degree of subcooling may emerge as the single largest factor controlling the lateral temperature rise in a chip cooled by a single, confined impinging microjet

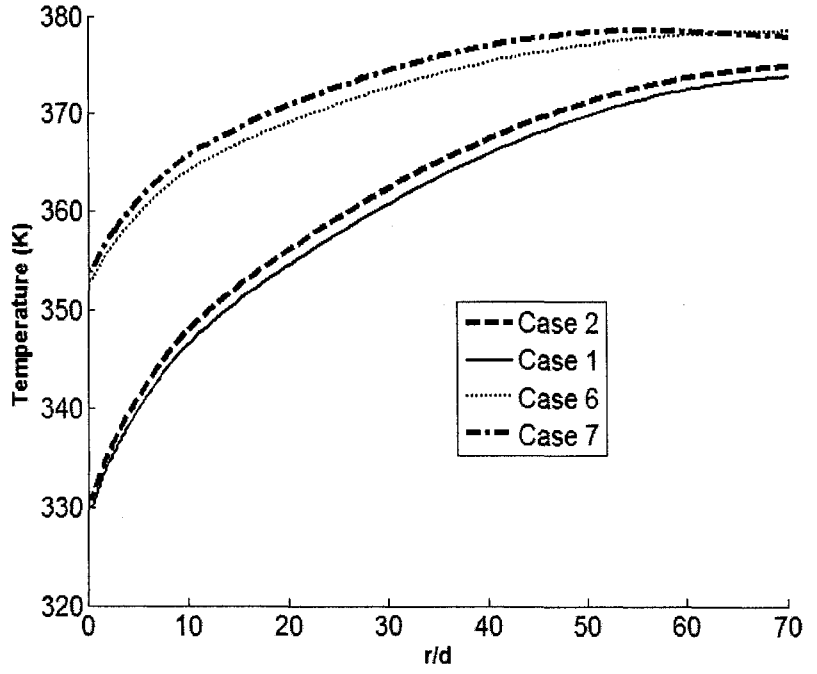

(a)

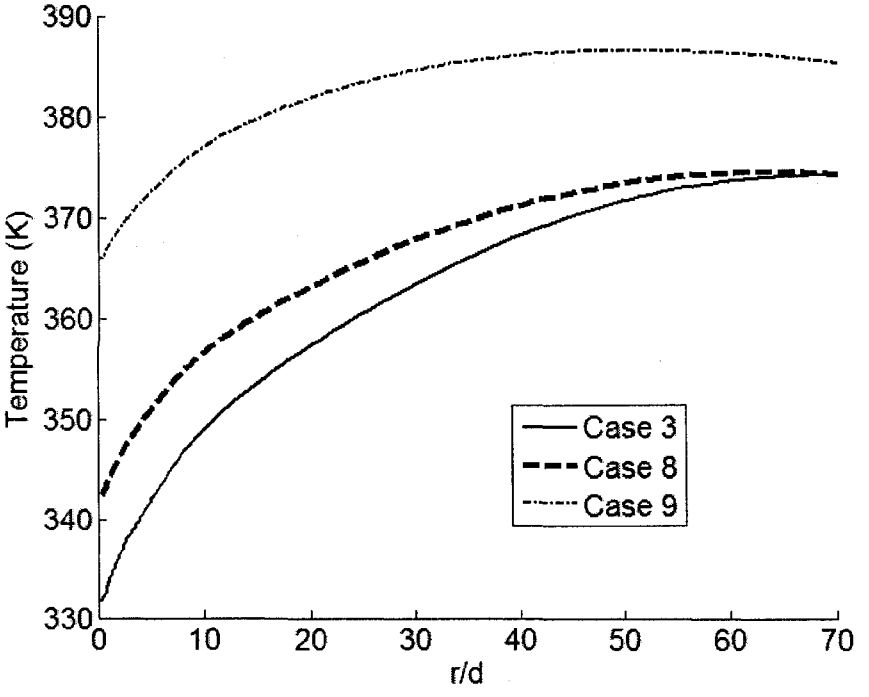

(b)

Figure 6.6: (a) and (b): Effect of Inlet Subcooling on the Temperature Distribution.

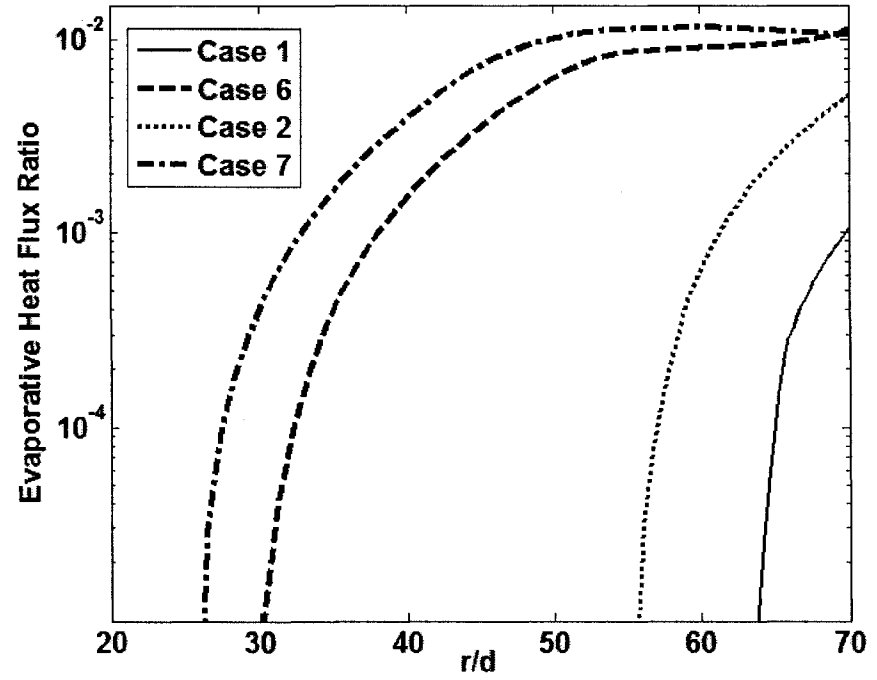

Figure 6.7: Evaporative Heat Flux Ratio Dependence on Inlet Subcooling – Part 1.

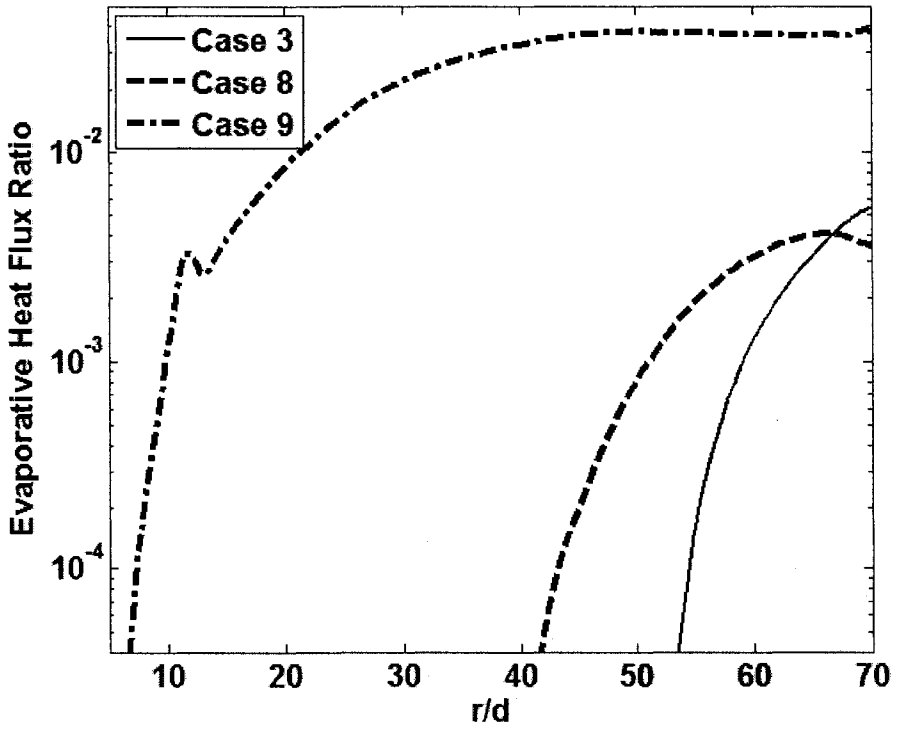

Figure 6.8: Evaporative Heat Flux Ratio Dependence on Inlet Subcooling – Part 2.

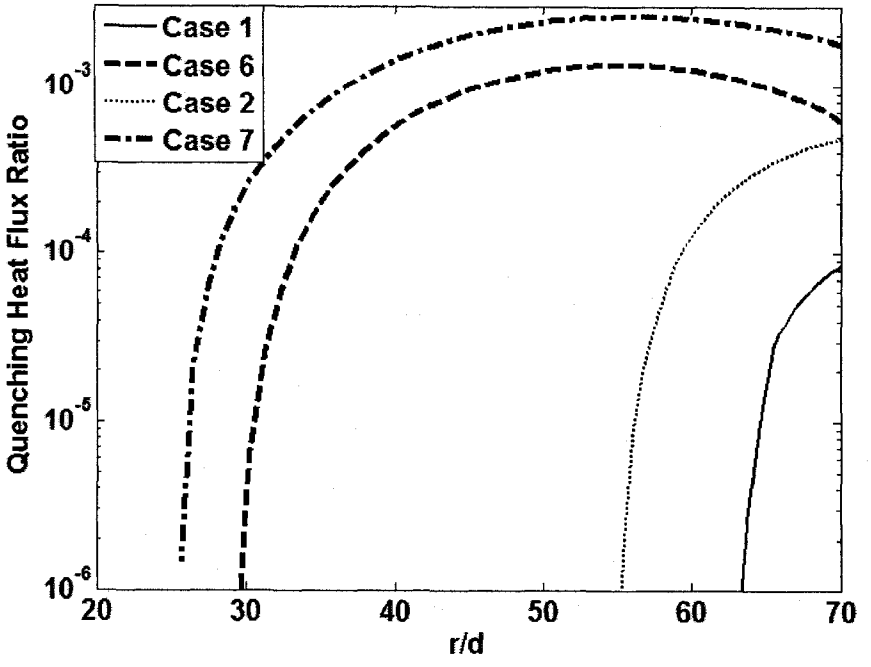

Figure 6.9: Effect of Inlet Subcooling on the Quenching Heat Flux Ratio – Part 1.

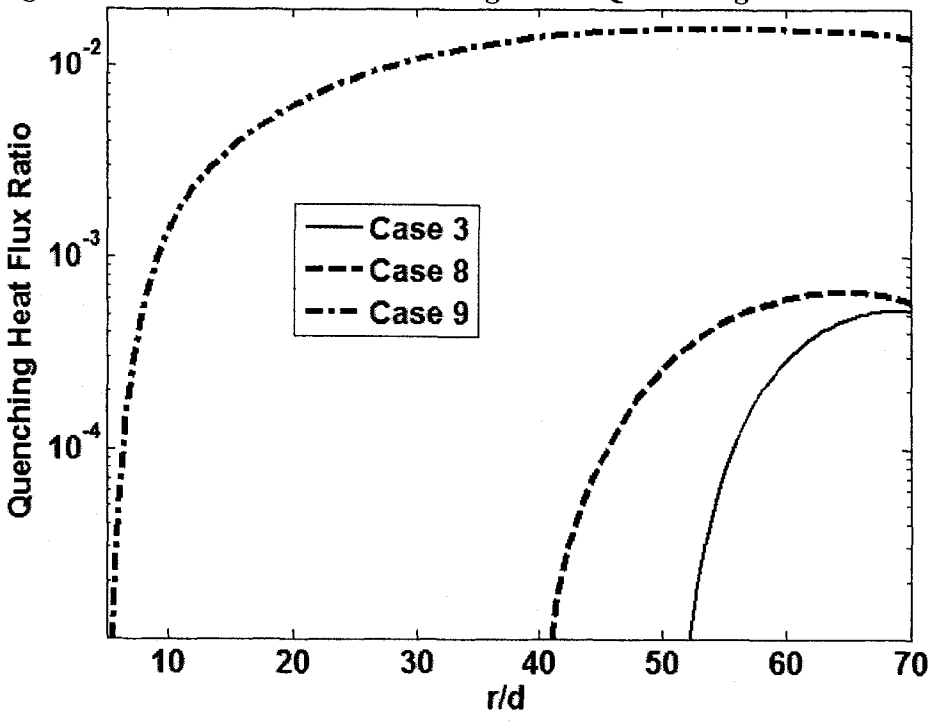

Figure 6.10: Effect of Inlet Subcooling on the Quenching Heat Flux Ratio – Part 2.

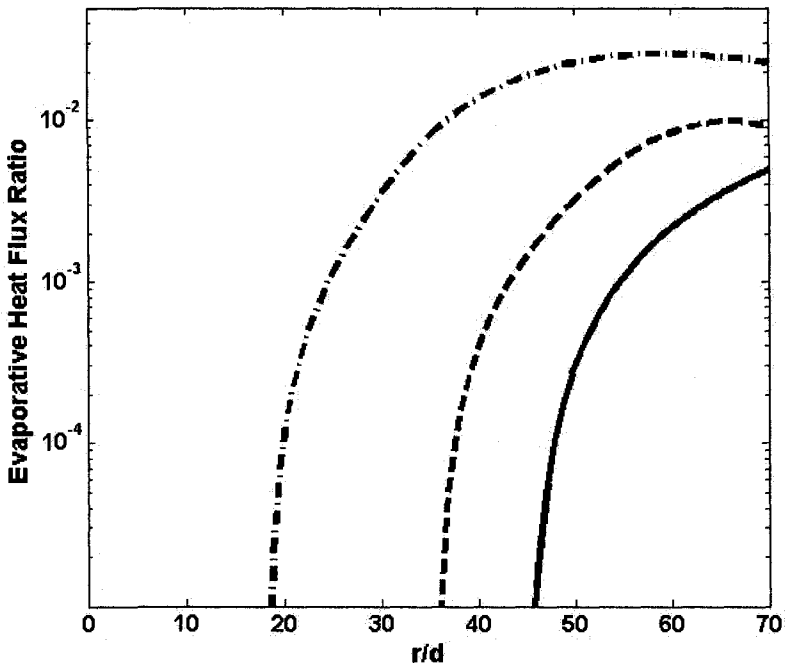

Figure 6.12: Effect of the Reynolds Number on the Evaporative Heat Flux Ratio.

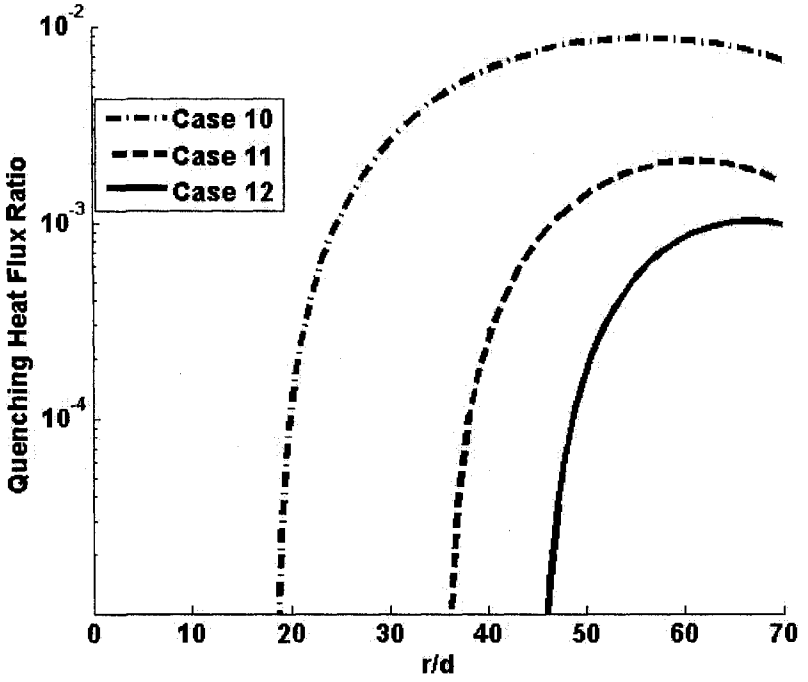

Figure 6.13: Effect of the Inlet Reynolds Number on the Quenching Heat Flux Ratio.

Shown in Figure 6.11 are plots of the temperature versus the inlet jet Reynolds Number with the heat flux fixed at 150 kW/m^2 and the inlet subcooling level at 50 ° C. Some interesting observations can be made here. The slopes of the temperature curves vary in each case from being a monotonous rise at higher Reynolds Numbers (Case 12) and flatter profiles at lower Reynolds Numbers. This indicates forced convection dominated flow at higher Reynolds numbers and combined forced convection and partial nucleate boiling flows at lower Reynolds numbers (Tong, 1975). Tong, very elegantly discusses the contribution of each component of heat transfer (evaporative, forced convection and microconvection analogous to our discussion of evaporative, single phase and quenching heat fluxes in that order) and concludes that at low system pressures, high velocities and low heat fluxes, bubble nucleation is suppressed and the forced convection mechanism is favored. This is what is seen in Figure 6.12 and Figure 6.13. The evaporative and the associated quenching heat transfer ratios decrease as the Reynolds number is raised from 550 to 1100. There is lower vapor generation as the Reynolds Number increases and the contribution to the heat transfer comes entirely from the single phase heat transfer mode.

Another important observation that can be made here is the stagnation point heat transfer. The temperature at the stagnation point for Cases 10, 11 and 12 decreases as the Reynolds Number is increased indicating, again, a strong single phase convection effect at the stagnation point. A valid question may arise at this point as to what the benefits of boiling really are if one is able to achieve cooler wall temperatures at simply higher Reynolds Numbers (higher flow velocities). The real benefit of boiling heat transfer lies in the streamwise temperature gradient observed in each case. Shown in Table 6.2 are the wall temperature gradients observed in each case (obtained by subtracting the temperature at the stagnation point from the temperature at the outlet). Clearly, the lower Reynolds Number cases are marked by lower ΔT values when compared to the higher Reynolds Number cases due to the increased importance of boiling heat transfer. The

boiling and the quenching mechanisms are envisioned to dominate the heat transfer mechanism at higher heat fluxes than those studied in this work.

Table 6.2: Streamwise Temperature Gradients versus the Reynolds Number

Case	ΔT (°C)
10	30.6
11	33.5
12	36.5

(6.9) Boiling Effectiveness

To ascertain the effectiveness of boiling especially with variations in the inlet subcooling, the temperature differential between the outlet plane and the stagnation point versus the inlet subcooling was plotted for Cases 1, 2, 3,6,7,8 and 9. These cases were chosen to study the effects of subcooling with the other two parameters, namely, the heat flux and inlet Reynolds number held constant. This is shown in Figure 6.14. It is seen that as the degree of inlet subcooling is decreased for different power levels, a drop in the wall temperature occurs. This is due to the increased boiling that occurs at lower inlet subcooling levels. Boiling tends to reduce the wall temperature variation from the stagnation point to the outlet region resulting in lower temperature differentials. This observation (reduced temperature differentials with decreased inlet subcooling levels) augurs well for electronics cooling design. Often, electronics cooling demands minimal temperature variations across the chip which is not possible with single phase liquid or air cooling systems. Also, the temperature of the incoming fluid is a critical parameter. The results from this analysis show that the same level of cooling can be achieved (same heat

fluxes is slow at first, but an order of magnitude rise is seen as the heat flux is increased and the level of subcooling is decreased. For most of the cases considered in this study, the single phase heat transfer component dominates the other two modes of heat transfer. The evaporative heat transfer component occupies the next spot followed by the quenching heat transfer coefficient, a markedly different result from what is being observed in the literature for higher Reynolds Number jets. Lower subcooling levels are associated with flatter temperature profiles than those with higher subcooling levels. In effect, lower subcooling levels are associated with lower streamwise ΔT values. In a confined microjet impingement arrangement, the liquid velocity profile has considerable effects on the vapor bubble nucleation, vapor drag and the bubble departure diameter. Increases in the Reynolds Number from 550 to 1100 are associated with lower stagnation point temperatures and higher streamwise ΔT values. The vapor generation is suppressed at higher Reynolds Numbers and the heat transfer mechanism appears to be more heavily influenced by forced (single phase) convection.

Chapter 7

Summary and Suggestions for Future Work

(7.1) Summary of Results

(7.1.1) Single Phase Microjet Impingement

Single microjets in the laminar regime with confined outflow arrangements reveal interesting characteristics akin to turbulent jets in conventional sized impingement systems. The stream function plots show primary and secondary recirculation zones that depend on the Reynolds Number. The reattachment points of the recirculation zones are associated with secondary peaks in the Nusselt Number indicative of increased heat transfer. However, with single jets covering only a small area of the heated chip, they may not be very effective in cooling large areas of the heated surface. The remedy to this problem is the use of an array of microjets with an optimized pitch between them to cool large areas. A lot of work is currently being directed in this regard.

(7.1.2) Two-Phase Modeling and Boiling Microjets:

The RPI model and the modified version used in this thesis for laminar subcooled boiling, predict wall temperature values that are close to the limited experimental values that are available in the literature. This is encouraging for future work on numerical simulation of boiling systems. Apart from the reasonable success of the numerical model, the boiling problem results themselves show some interesting characteristics that may have significant import for the design of two-phase cooling systems.

Some limitations of the numerical model include its inability to model beyond nucleate boiling regimes (film boiling for example). The next step would be an extension

of the present model to include film boiling regimes which is an arduous and an unenviable task because of the amount of experimental data needed for verification.

Microjet Impingement cooling of electronics, especially boiling microjets hold considerable promise for high heat flux removal coupled with precise temperature control. Numerical Simulation of these problems has inherent advantages over experimental efforts only, but is limited and seriously impaired by the complexity of the boiling physics. Other possible areas of expansion of this work are the inclusion of ribs and cavities in the flow path which promote local turbulence leading to high heat transfer rates. Depending on their size, they could also potentially act as active nucleation sites promoting nucleate boiling. Turbulence also leads to increased vapor drag and enhances heat transfer by accelerating the removal of vapor from the wall region.

The gross unsteadiness inherent in a partial nucleate boiling regime also calls for a more robust time-averaging technique that represents better time-averaged values of the various heat flux components and the wall temperature. The physics of the boiling problem being complicated and grossly unsteady, especially at higher Reynolds Numbers, even the determination of a better averaging technique may be a complicated task which has a lot of potential for future work.

Other improvements to the current work can be made in the form of modifcations to the various semi-empirical correlations. Of all these correlations, the bubble departure diameter must rank as the highest because it influences the rate of evaporative heat transfer significantly. A variety of other semi-empirical correlations for the bubble departure diameter have been proposed in the literature (Kandlikar, 2004) and an extensive study can be done on the evaluation of these correlations. The same is true for the correlations for the different components of heat transfer and the drag coefficient. The bubble departure diameter and the maximum bubble size in this thesis were limited to the height of the channel. This assumption is valid until the vapor phase in the fluid domain behaves like droplets and do not coalesce to form big vapor slugs. The assumption may fail to predict heat transfer characteristics accurately if vapor slugs form and coalesce

together to block the flow channel at least for a short duration of time until the build-up of liquid pressure at the stagnation point is strong enough to push the vapor slug out of the domain.

For the microjet impingement problem described in this thesis, the bubble departure diameter may be as high as the channel wall width and blocks the channel. When this happens, there is a tremendous amount of vorticity that is created in the wake of the vapor bubble. Also, the bubble size distribution may be different; the vapor phase may exist as discrete bubbles in some areas and continuous vapor slugs in other areas. To resolve such finer details, a multi-field modeling technique is required.

References

Basu, N., Warrier, G.R., and Dhir, V.K., (2002) "Onset of Nucleate Boiling and Active Nucleation Site Density During Subcooled Flow Boiling" *ASME Journal of Heat Transfer*, Vol, 124, pp. 704-712.

Basu, N., Warrier, G.R., and Dhir, V.K., (2005) "Wall Heat Flux Partitioning During Subcooled Flow Boiling: Part 1 – Model Development" *ASME Journal of Heat Transfer,* Vol. 127, pp. 131-140.

Basu, N., Warrier, G.R., and Dhir, V.K., (2005) "Wall Heat Flux Partitioning During Subcooled Flow Boiling: Part 2 - Model Validation" *ASME Journal of Heat Transfer,* Vol. 127, pp. 141-148.

Batchelor, G.K., (1993), "An Introduction to Fluid Dynamics" *Cambridge University Press,* First Edition

Bowers, M.B., and Mudawar, I., (1994) "High Flux Boiling in Low Flow Rate, Low Pressure Drop Mini-Channel and Micro-Channel Heat Sinks" *International Journal of Heat and Mass Transfer*, Vol. 37, pp. 327-332.

Del Valle, M.V.H., and Kenning, D.B.R., (1985), "Subcooled Flow Boiling at High Heat Flux" *International Journal of Heat and Mass Transfer,* Vol. 28(10), pp. 1907-1920.

Dhir. V.K., (2006), "Mechanistic Prediction of Nucleate Boiling Heat Transfer – Achievable or a Hopeless Task". *ASME Journal of Heat Transfer*, Vol. 128, pp. 1-12.

Di Marco, P., Grassi, D., Margrini, A., (1994), "Unsubmerged Jet Impingement Heat Transfer at Low Liquid Speeds", in *10th International Heat Transfer Conference.* Brighton, U.K.

Elison, B., and Webb, B.W., (1994), "Local Heat Transfer to Impinging Liquid Jets in the Initially Laminar, Transitional and Turbulent Regimes" *International Journal of Heat and Mass Transfer*, Vol. 37(8), pp. 1207-1216.

Ellsworth, M.J.Jr., and Simons, R.E., (2005) "High Powered Chip Cooling -- Air and Beyond" *Electronics Cooling*, Vol. 11(3).

Faghri, M., and Sunden, B.,(2004), "Heat and Fluid Flow in Microscale and Nanoscale Structures", *WIT Press*

Fitzgerald, J.A., and Garimella, S.V., (1997), "A Study of the Flow Field of a Confined and Submerged Impinging Jet", *International Journal of Heat and Mass Transfer,* Vol. 41(9), pp. 1025-1034.

Fitzgerald, J.A., and Garimella, S.V., (1997), "Flow Field Effects on Heat Transfer in Confined Jet Impingement" *ASME Journal of Heat Transfer*, 119: p. 630-632.

Garimella, S.V., and Rice, R.A., (1995), "Confined and Submerged Liquid Jet Impingement Heat Transfer". *ASME Journal of Heat Transfer*, Vol. 117, pp. 871-877.

Garimella, S.V., (2000) "Heat Transfer and Flow Fields in Confined Jet Impingement" *Annual Review of Heat Transfer*, Vol. 11, pp. 413-494.

Goodson, K.E., (2003) "Microscale Thermal Engineering of Electronic Systems" in *Rohsenow Symposium of Future Trends of Heat Transfer,* Cambridge, MA.

Hsu, Y.Y., (1962), "On the size Range of Active Nucleation Cavities on a Heating Surface" *ASME Journal of Heat Transfer*, Vol. 84(3), pp. 207-216.

Hall, D.E., Incropera, F.P., and Viskanta, R., (2001), "Jet Impingement Boiling From a Circular Free-Surface Jet During Quenching" *ASME Journal of Heat Transfer*, Vol. 123, pp. 901-910.

Ichimiya, K., and Hosaka, N., (1992) "Experimental Study of Heat Transfer Characteristics due to Confined Impinging Two-Dimensional Jets". *Experimental and Thermal Fluid Science,* Vol. **5**(6), pp. 803-807.

Jiang, L., Wong, M., and Zohar, Y., (2001) "Forced Convection Boiling in a Microchannel Heat Sink", *Journal of Microelectromechanical Systems*, Vol. 10(1), pp. 80-87.

Kandlikar, S.G., (2004), "Heat Transfer Mechanisms During Flow Boiling in Microchannels", *ASME Journal of Heat Transfer*, Vol. 126, pp. 8-16.

Kumar, R., Trabold, T.A., and Maneri, C.C., (2003), "Experiments and Modeling in Bubbly Flows at Elevated Pressures". *ASME Journal of Fluids Engineering*, Vol. 125, pp. 469-478.

Kumar, R., Maneri, C.C., and Strayer, T.D., (2004) "Modeling and Numerical Prediction of Flow Boiling in a Thin Geometry". *ASME Journal of Heat Transfer*, Vol. 26, pp. 22-33.

Kurul, N., and Powdowski, M.Z., (1990) "Multidimensional Effects in Forced Convection Subcooled Boiling" *Proc. International Heat Transfer Conference.* Jerusalem, Israel.

Li, C.Y., and Garimella, S.V., (2004) "Prandtl Number Effects and Generalized Correlations for Confined and Submerged Jet Impingement" *International Journal of Heat and Mass Transfer*,. Vol. 44, pp. 3471-3480.

Lienhard V, J.H., (1995) "Liquid Jet Impingement" *Annual Review of Heat Transfer*, Vol. 6, pp. 199-270

Liu, X., Lienhard V, J.H., and Lombara, J.S., (1991), "Convective Heat Transfer by Impingement of Circular Liquid Jets" *ASME Journal of Heat Transfer,* Vol. 113, pp. 571-582.

Ma, C.F., and Bergles, A.E., (1986) "Jet Impingement Nucleate Boiling", *International Journal of Heat and Mass Transfer*, Vol. 29(8), pp. 1095-1101.

Martin, H., (1977), "Heat and Mass Transfer between Impinging Gas Jets and Solid Surfaces" *Advances in Heat Transfer*, Vol. 13, pp. 1-60.

Monde, M., and Katto, Y., (1978), "Burnout in a High heat-Flux Boiling System with an Impinging Jet", International Journal of Heat and Mass Transfer, Vol. 21, pp. 295-305.

Moraga, F.J., Bonetto, F.J., Lahey, R.T., (1999) "Lateral Forces on Spheres in Uniform Turbulent Shear Flow", *International Journal of Multiphase Flow*, Vol. 25, pp. 1321-1372.

Morris, G.K., and Garimella, S.V., (1998), "Orifice and Impingement Flow Fields in Confined Jet Impingement", *ASME Journal of Heat Transfer*, Vol. 120, pp. 68-72.

Narumanchi, S.V.J., Hassani, V., and Bharathan, D., (2006), "Numerical Simulations of Boiling Jet Impingement Cooling in Power Electronics". in *Proc.IEEE-ITHERM*. San Diego, CA.

Patankar, S.V., (1980), "Numerical Heat Transfer and Fluid Flow", *Taylor and Francis*.

Peng, X.F., and Wang, B.-X.,(1993), "Forced convection and flow boiling heat transfer for liquid flowing through microchannels" *International Journal of Heat and Mass Transfer*, Vol. 36, pp. 3421-3427.

Peng, X.F., Hu, H.Y., and Wang, B-X., (1998) "Boiling Nucleation During Liquid Flow in Microchannels", *International Journal of Heat and Mass Transfer*, Vol. 41, pp. 101-106.

Qu, W., and Mudawar, I., (2002), "Prediction and Measurement of Incipient Boiling Heat Flux in Microchannel Heat Sinks", *International Journal of Heat and Mass Transfer*, Vol. 45, pp. 3933-3945.

Qu, W., and Mudawar, I., (2003), "Measurement and Prediction of Pressure Drop in Two-Phase Micro-Channel Heat Sinks", *International Journal of Heat and Mass Transfer*, Vol. 46, pp. 2737-2753.

Qu, W., and Mudawar, I., (2003), "Flow Boiling Heat Transfer in Two-Phase Micro-channel Heat Sinks – I. Experimental Investigation and Assessment of Correlation Methods", *International Journal of Heat and Mass Transfer*, Vol. 46, pp. 2775-2771.

Qu, W., and Mudawar, I., (2003), "Flow Boiling Heat Transfer in Two-Phase Micro-channel Heat Sinks – II. - Annular Two-Phase Flow Model", *International Journal of Heat and Mass Transfer,* Vol. 46, pp. 2773-2784.

Ragunathan, S., Goering, D.J., (2008), "A Parametric Study of Liquid Microjet Impingement for Electronics Cooling", *Proc. IEEE-ITHERM* , Orlando, Florida.

Ragunathan, S., Goering, D.J., and Karulkar, P.C., (2007) "Heat Transfer in a Three-Dimensional Stacked CSP Module", *Proc. 23rd IEEE SEMI-THERM.* San Jose, CA.

Ranz, W.E., and Marshall Jr, W.R., (1952) "Evaporation From Drops, Part 2", *Chemical Engineering Progress*, Vol. 48(4), pp. 173-180.

Ranz, W.E., and Marshall Jr, W.R., (1952), "Evaporation from Drops, Part 1", *Chemical Engineering Progress*, Vol. 48(3), pp. 141-146.

Stevens, J., and Webb, B.W., (1991) "Local Heat Transfer Coefficients Under an Axisymmetric Single Phase Liquid Jet", *ASME Journal of Heat Transfer*, Vol. 113, pp. 71-78.

Tong, L.S., (1975), "Boiling Heat Transfer and Two-Phase Flow", *Robert E. Krieger Publishing Company.*

Unal, H.C., (1976), "Maximum Bubble Diameter, Maximum Bubble Growth Time and Bubble-Growth Rate During the Subcooled Nucleate Flow Boiling of Water up to 17.7 MN/m^{2}". *International Journal of Heat and Mass Transfer,* Vol. 19, pp. 643-649.

Vader, D.T., Incropera, F.P., and Viskanta, R., (1992), "Convective Nucleate Boiling on a Heated Surface Cooled by an Impinging, Planar Jet of Water", *ASME Journal of Heat Transfer*, Vol. 114, pp. 152-160.

Wang, E.N., *et al.* (2004) "Microjet Impingement Cooling with Phase Change", *Proc. IMECE.* Anaheim, CA.

Wang, E.N., *et. al.*, (2004), "Micromachined Jets for Liquid Impingement Cooling of VLSI Chips", *Journal of Microelectromechanical Systems*, Vol. 48(5), pp. 833-842.

Warrier, G.R., Basu, N., and Dhir, V.K., (2002), "Interfacial Heat Transfer During Subcooled Flow Boiling", *International Journal of Heat and Mass Transfer*, Vol. 45, pp. 3947-3959.

Warrier, G.R., and Dhir, V.K., (2006), "Heat Transfer and Wall Heat Flux Partitioning During Subcooled Flow Nucleate Boiling – A Review", *ASME Journal of Heat Transfer*, Vol. 128, pp. 1243-1256.

Webb, B.W., and Ma, C.F., (1995), "Single Phase Liquid Jet Impingement", *Advances in Heat Transfer*, Vol. 26, pp. 105-217.

Wheeler, J.P., and Neti, S., (1999), "Heat transfer for a Semi-confined Impinging Laminar Jet", *Proc. 33 rd National Heat Transfer Conference.* Alburquerque, New Mexico.

White, F.M., (1991), "Viscous Fluid Flow", McGraw Hill Inc

Wolf, D.H., Incropera, F.P., and Viskanta, R.,(1996), "Local Jet Impingement Boiling Heat Transfer", *International Journal of Heat and Mass Transfer*, Vol. 39(7), pp. 1395-1406.

Womac, D.J., Ramadhyani, S., and Incropera, F.P., (1993), "Correlating Equations for Impingement Cooling of Small Heat Sources With Single Circular Liquid Jets", *ASME Journal of Heat Transfer*, Vol. 115, pp. 106-115.

www.electronics-cooling.com Access Date 10/2008

www.fluent.com Access Date 10/2008

www.ibm.com Access Date 10/2008

www.intel.com Access Date 10/2008

Zhang, L., Wang, E.N., Goodson, K.E., and Kenny, T.W., (2005), "Phase Change Phenomena in Silicon Microchannels", *International Journal of Heat and Mass Transfer*, Vol. 48, pp. 1572-1582.

Zhou, D.W., and Ma, C.F., (2004), "Local jet impingement boiling heat transfer with R113", *Journal of Microelectromechanical Systems*, Vol. 13(5), pp. 833-842.

Zohar, Y., (2003), "Heat Convection in Microducts", *Kluwer Academic Publishers.*

Appendix

A1: User-Defined Function for the Boiling Microjet Impingement Problem

```
#include "udf.h"
#include "sg.h"
#include "sg_mphase.h"
#include "flow.h"
#include "mem.h"
#include "metric.h"


#define relax 0.05    /* underrelaxation factor equal to 0.01-0.05 */
#define threshold 1e-7    /* error tolerance*/
#define Tsub_min 3.    /* minimum liquid subcooling, K*/

#define sigma 58.78e-3 /*surface tension coefficient of vapor-liquid
system, N/m*/
#define gravity 9.8   /* gravity, m/sec2 */
#define L 2256.9e3  /* latent heat at system pressure, J/kg */

#define Ks_silicon  130       /*thermal conductivity of solid material (Silicon) */
#define Ros_silicon 2329.0      /*density of the solid material (Silicon) */
#define Cps_silicon 700.0       /*heat capacity of the solid material (Silicon)*/

#define P_sys 1.01325e5   /*system pressure, Pa */

#define p_min 0.70109e5  /*parameters for boiling curve determination*/
#define p_max 1.4327e5
#define t_min 363.15
#define t_max 383.15

#define domain_index_liq 2 /*domain indexes of phases*/
#define domain_index_vap 3



/* END OF USER INPUTS */
```

```
real evaporative_heat_flux, m_evap_wall, wall_super_heat
        ,quench_to_total_heatflux, heat_coeff_sphase , heat_coeff_quench
        ,Number_evap_wall, dwall, delta,sphase_to_total_heatflux
        ,evap_to_total_heatflux ;

real Ts(real, real);
real dbubw(real , real);
real site_dens(real, real);
real A2f(real, real, real);
real damp(real x);


real Interfacial_area(real,real);

/* this macro is hooked up as a source term for vapor  */
/* continuity equation                                 */

DEFINE_MASS_TRANSFER(vaporisation_condensation1, c,
mixture_thread,from_index,from_species_id,to_index,to_species_id)
{
        Thread **pt = THREAD_SUB_THREADS(mixture_thread);
        real vof_vapor,vof_liquid,total_mass_exchange;
        real dbub,Tsat;
        real reb,urel,Tl, urelx,urely,urelz,Pr,Ai,Nu,H;

        vof_vapor = C_VOF(c,pt[from_index]);
        vof_liquid = 1.-vof_vapor;
        Tl = C_T(c,pt[to_index]);
        urelz =0.;
        urelx = C_U(c,pt[from_index]) -
        C_U(c,pt[to_index]);
        urely = C_V(c,pt[from_index]) -
        C_V(c,pt[to_index]);

#if RP_3D
        urelz = C_W(c,pt[from_index]) -
        C_W(c,pt[to_index]);
#endif

        urel = sqrt(urelx*urelx + urely*urely + urelz*urelz);
        dbub = C_PHASE_DIAMETER(c,pt[from_index]);
        reb = urel * dbub * C_R(c,pt[to_index])/
        C_MU_L(c,pt[to_index]);
        Pr = C_MU_L(c,pt[to_index])*C_CP(c,pt[to_index])
```

```
                / C_K_L(c,pt[to_index]);
        Ai = Interfacial_area(vof_vapor, dbub);
        Nu =  2. + 0.6*pow(reb,0.5)*pow(Pr,0.3) ; /* Ranz Marshall correlation */
        H = C_K_L(c,pt[to_index]) *  Nu / dbub;
      Tsat = Ts(P_sys+C_P(c,mixture_thread),Tl);
        C_UDMI(c,mixture_thread,16) = Tsat;
        total_mass_exchange = ( (Tl-Tsat)*H*Ai/( L + (C_CP(c,pt[to_index])*(Tsat-Tl))
)
                + C_UDMI(c,mixture_thread,6) )*relax + (1-
relax)*C_UDMI(c,mixture_thread,15) ;
        C_UDMI(c,mixture_thread,15) = total_mass_exchange ;
      return -total_mass_exchange;
}

DEFINE_HEAT_FLUX(heat_flux1, f, tf, c, t, cid, cir)
{
        Thread *tm , *ts, *tp, *tm_sol, *t0, *t_sol;
        cell_t c_sol;
        face_t f_sol;
        Domain *d ;
        Thread **pt;
        int index,it,Nit=2000;
        real A[ND_ND], At, vof_l, vof_v, Tl,
                Ul, Mul, Cpl, Kl, cell_volume;
        real Tsub, ratio, bb, phi, multiplier, f0, Ja, prel, Qe,
                Hq, Tsat,Tw,Rol,Rog,pressure,Tsol,Hsol,Csol,Hl,
                q_wall_sol, q_wall_liq, Tmax, Tmin, upper,lower,middle;
        d = THREAD_DOMAIN(t);
        index = DOMAIN_ID(d);

        /* Message("\n %f\n",cid[1]);*/

        /* Message("fluid %d\n", index); */

        if (index == domain_index_liq) /* Wall Energy passed on to the liquid domain
only*/
        {
                tm = THREAD_SUPER_THREAD(t);
                pt = THREAD_SUB_THREADS(tm);
                ts = pt[1];
                tp = pt[0];

                vof_l = C_VOF(c,tp);
```

```
        if ( vof_l > 1e-6) /*check if there is enough liquid to boil*/
        {
                F_AREA(A,f,tf);
                At = NV_MAG(A);
                vof_v = C_VOF(c,ts);
/*Liquid Velocity at each cell*/
                Ul = sqrt(C_U(c,tp)*C_U(c,tp)+C_V(c,tp)*C_V(c,tp));


                cell_volume = C_VOLUME(c,tm);
                Mul = C_MU_L(c,tp);
                Cpl = C_CP(c,tp);
                Kl = C_K_L(c,tp);
                Tsat = Ts(P_sys+C_P(c,tm),C_T(c,t));
                Tl = C_T(c,tp);
                Tsub = Tsat-Tl;
                Rol = C_R(c,tp);
                Rog = C_R(c,ts);
                ratio = Rog/Rol;


/*check for one particular wall (which transfers the heat to the liquid domain)*/

                if ( (THREAD_ID(tf)== 14) )


                {
                        tm_sol =
THREAD_SHADOW(THREAD_SUPER_THREAD(tf));
                        f_sol = F_SHADOW(f,tf);
                        c_sol = F_C0(f_sol,tm_sol);
                        t0 = F_C0_THREAD(f,tf);
                        t_sol = tm_sol -> t0;
                        Tsol = C_T(c_sol,t_sol);
                        Tmax = MAX(Tl,Tsol)+10.;
                        Tmin = MIN(Tl,Tsol)-10.;
                        Hsol = C_UDMI(c,tm,11);
                        Csol = C_UDMI(c,tm,13);
                } /* end of wall if */
                else
                {
                        Tmax = Tl+100.;
                        Tmin = Tl-100.;
                        Hsol = 0.;
```

```
                    Csol = 0.;
                }

                phi = MAX(1.,pow(Ul/0.61,0.47));

/*bb = MAX(0.5*Tsub/(1.-ratio),0.5*MAX(q_wall_sol,1e-3)/(1.-
ratio)/0.0065/Rol/Cpl/Ul*0.001);*/

                if (Tsub > Tsub_min)
                    bb = 0.5*Tsub/(1.-ratio); /* bb is the coefficient b in eqn 21
*/
            else
                    bb = 0.5*Tsub_min/(1.-ratio)*exp((Tsub/Tsub_min)-1.);

            pressure =  MAX(C_P(c,tm)+P_sys,0.05*P_sys);
            multiplier = 0.683e-5*pow(pressure,0.709)
                                *
sqrt(Ks_copper*Ros_copper*Cps_copper)/sqrt(phi*bb)/Rog/(L);

/* Calculation of the bubble departure frequency */
                f0 = sqrt( 4.*gravity*(Rol-Rog)/3./Rol );

/* Calculation of the quenching heat coefficient */
                Hq = 1.13*pow( f0*Kl*Rol*Cpl,0.5 );
                Ja = MAX(Rol*Cpl*MAX(Tsub,0)/Rog/L,0.);
                prel = 0.524*Rog*f0*(L+Cpl*(Tsat- C_T(c,t) )); /* Evaporative
heat flux equation*/
                delta = 1.;
                Qe = 0.;
                for (it = 0; it< Nit; ++it)
                {
                    if (Hsol < 1e-6)
                    {
                        q_wall_sol = WALL_HEAT_FLUX(f,tf)/At;

                    }
                    else
                    {
                        q_wall_sol = Hsol*(Tsol-Tmin) + Csol;
                    }


                    Qe = prel*site_dens(Tmin-Tsat,vof_l)*pow(dbubw(Tmin-
Tsat,multiplier),2.5) *damp(vof_v) ;
```

```
/*Single Phase heat transfer coefficient*/
heat_coeff_sphase = cid[1] / vof_l
                        * (1.-A2f(site_dens(Tmin-Tsat,vof_l),dbubw(Tmin-
Tsat,multiplier),Ja))*damp(vof_v)  ;

/*Quenching heat transfer coefficient*/
                    heat_coeff_quench = Hq * A2f(site_dens(Tmin-
Tsat,vof_l),dbubw(Tmin-Tsat,multiplier),Ja)
                / pow(dbubw(Tmin-Tsat,multiplier),0.25)*damp(vof_v)  ;
            Hl = heat_coeff_sphase + heat_coeff_quench ;
            q_wall_liq = Hl*(Tmin-Tl)+Qe;

            lower = q_wall_sol - q_wall_liq;
            /*Message("\n %g %g %g %g %g %g %g %g
%g\n",Tsol,Tmax,Tmin,Hsol,Csol,q_wall_sol,lower,Tl,heat_coeff_sphase);*/

            if (Hsol < 1e-6)
            {
                        q_wall_sol = WALL_HEAT_FLUX(f,tf)/At;
                    }
                    else
                    {
                        q_wall_sol = Hsol*(Tsol-Tmax)+ Csol;
                    }

                    Qe = prel*site_dens(Tmax-Tsat,vof_l)*pow(dbubw(Tmax-
Tsat,multiplier),2.5) *damp(vof_v) ;

                    heat_coeff_sphase = cid[1] / vof_l
                        * (1.-A2f(site_dens(Tmax-
Tsat,vof_l),dbubw(Tmax-Tsat,multiplier),Ja))*damp(vof_v) ;

                    heat_coeff_quench = Hq * A2f(site_dens(Tmax-
Tsat,vof_l),dbubw(Tmax-Tsat,multiplier),Ja)
                / pow(dbubw(Tmax-Tsat,multiplier),0.25) *damp(vof_v) ;

                Hl = heat_coeff_sphase + heat_coeff_quench ;
                q_wall_liq = Hl*(Tmax-Tl)+Qe;
                upper = q_wall_sol - q_wall_liq;
                Tw = 0.5*(Tmin+Tmax);
                    if (Hsol < 1e-6)
                    {
                        q_wall_sol = WALL_HEAT_FLUX(f,tf)/At;
                    }
```

```
                        else
                        {
                                q_wall_sol = Hsol*(Tsol-Tw)+Csol;
                        }

                        Qe = prel*site_dens(Tw-Tsat,vof_l)*pow(dbubw(Tw-
Tsat,multiplier),2.5)*damp(vof_v)  ;
                        heat_coeff_sphase = cid[1] / vof_1 *
                                (1.-A2f(site_dens(Tw-Tsat,vof_l),dbubw(Tw-
Tsat,multiplier),Ja))*damp(vof_v) ;

                        heat_coeff_quench = Hq * A2f(site_dens(Tw-
Tsat,vof_l),dbubw(Tw-Tsat,multiplier),Ja)
                                /pow(dbubw(Tw-Tsat,multiplier),0.25)
*damp(vof_v) ;

                        Hl = heat_coeff_sphase + heat_coeff_quench ;
                        q_wall_liq = Hl*(Tw-Tl)+Qe;
                        middle = q_wall_sol - q_wall_liq;
                if ( lower * middle < 0. )
                        {
                                Tmax = Tw;
                                delta = fabs(q_wall_sol/(q_wall_liq+1e-3)-1 );
                                if (delta <= threshold) it = Nit;
                        }
                        else if ( upper * middle < 0. )
                        {
                    Tmin = Tw;
                                delta = fabs(q_wall_sol/(q_wall_liq+1e-3)-1 );
                                if (delta <= threshold) it = Nit;

                        }

                        else
                        {
/*Message("it %d\n", it);
Message("lower, upper,middle, Tsol, Tl %g %g  %g  %g  %g \n",lower,
upper,middle,Tsol,Tl );
Message("Hl, Hsol, Qe, Tw  %g %g  %g  %g   \n", Hl, Hsol, Qe, Tw);*/
it = Nit;
                        }

                } /* end of for loop */
```

```
/* Storing the Results */

                        m_evap_wall = Qe * At / cell_volume / (L+Cpl*(Tsat-C_T(c,t))) ;

/* storing the wall superheat for initialization */
                        wall_super_heat = Tw-Tsat;

                        quench_to_total_heatflux =  heat_coeff_quench*(Tw-
C_T(c,t))/(q_wall_liq+1e-3) ;
                        sphase_to_total_heatflux =  heat_coeff_sphase *(Tw-
C_T(c,t))/(q_wall_liq+1e-3) ;
                        evap_to_total_heatflux =    Qe/(q_wall_liq+1e-3) ;
                        Number_evap_wall = m_evap_wall / ( Rog*0.523*pow(
dbubw(Tw-Tsat,multiplier),3.) );
                        dwall = dbubw(Tw-Tsat,multiplier);
                        C_UDMI(c,tm,6)  = Qe * At / cell_volume / (L+Cpl*(Tsat-
C_T(c,t))) ;
                        C_UDMI(c,tm,7)  = delta;
                        C_UDMI(c,tm,10) = Tw-Tsat;
                        C_UDMI(c,tm,18) = heat_coeff_quench*(Tw-C_T(c,t))/
(q_wall_liq+1e-3) ;
                        C_UDMI(c,tm,19) = heat_coeff_sphase *(Tw-
C_T(c,t))/(q_wall_liq+1e-3) ;
                        C_UDMI(c,tm,20) = Qe/(q_wall_liq+1e-3) ;
                        C_UDMI(c,tm,21) = F_T(f,THREAD_SUPER_THREAD(tf)) -
(Tsol+q_wall_sol/Hsol);
                        C_UDMI(c,tm,21) = dwall ;
                        C_UDMI(c,tm,12) = q_wall_liq;
                        cid[0] = Qe * (vof_l+vof_v) ;
                        cid[1] = (heat_coeff_sphase + heat_coeff_quench) * (vof_l+vof_v)
;
                        cid[2] = (heat_coeff_sphase + heat_coeff_quench) * (vof_l+vof_v)
;
                        C_UDMI(c,tm,8) = cid[1] ;
                        C_UDMI(c,tm,9) = cid[0] ;
                } /* end of if vof-liquid >1e-06 loop */
        } /* end of domain-index-liquid loop */
        else if (index == domain_index_vap) /*vapor*/
        {
/*if (f==0)
  {
Message("wall id %d\n", THREAD_ID(tf));
Message("domain id %d\n", index);
Message("Tsol %g\n",Tsol);
```

```
}*/
                cid[0] = 0.;
                cid[1] = 0.;
                cid[2] = 0.;

        }

        else  /*solid part called by mixture thread - need to store heat transfer coefficient
store in
         udmi-11*/
        {

/*check for solid interface*/

                if ( (THREAD_ID(tf)== 5 ) )

                {
                        tm_sol = THREAD_SHADOW(tf);
                        t_sol =tm_sol ->t0;

                        if (FLUID_THREAD_P(t_sol))
                        {
                                f_sol = F_SHADOW(f,tf);
                                c_sol = F_C0(f_sol,tm_sol);
                                t0 = F_C0_THREAD(f,tf);
                                C_UDMI(c_sol,t_sol,11) = cid[1];
                                C_UDMI(c_sol,t_sol,13) = cid[0];
                        }
          }
        }
}

/* function calculating boiling site density */
 real site_dens(real superheat, real liquid_void)
 {
        real f;
        f = 0.;
        if (superheat > 0.)
        {
 /*             f = 0.34e4*pow(superheat,2.0);*/
                f = pow(210.*superheat,1.8)/*(1.-exp(-superheat/250.))*/;

        }
```

```
        return f;
}

/* Function calculating bubble departure diameter, m */
real dbubw(real superheat, real multiplier)
{
        real f = 1.e-6;
        if (superheat > 0.)
                {f = multiplier*pow(superheat,1.);}
         if (f >= 0.0002)
           {
            f = 0.0002;
            }
        return f;

}

/* Function calculating boiling wall portion */
real A2f(real dens, real dbub, real Ja)
{
        real f,eps=4.8*exp(-Ja/80.);
        f = MIN(0.785375*eps*dbub*dbub*dens,1.);
        return f;
}


/* This macro is for bubble diameter  */
DEFINE_PROPERTY(diameter1, c, t)
{
        Thread *tm = THREAD_SUPER_THREAD(t);
        Thread **pt = THREAD_SUB_THREADS(tm);
        real dT = Ts(P_sys+C_P(c,tm),C_T(c,pt[0]))-C_T(c,pt[0]);
        real diam=0.;
/* Assign bubble diameter depending on local superheat */
        if (dT > 13.5)  diam = 0.00015;
        if (dT <= 13.5) diam = 0.0015-1e-4*dT;
        if (dT < 0.)      diam = 0.0015;
      if (diam >= 0.0002)
{
      diam = 0.0002;
}

        return diam;
```

```
}


/*Interfacial Area*/
real Interfacial_area(real alfa_bub, real diameter)
{
        real alfa_gs, Ai, n = 1.;
        alfa_gs = MIN(alfa_bub,0.25);
        Ai = 6. * alfa_gs / diameter * pow((1-alfa_bub)/(1-alfa_gs),n);
        return Ai;
}

/* Saturation Temperature*/
real Ts(real pressure, real Tliq)
{
        real f;
        f = t_min + (t_max-t_min)/(p_max-p_min)*(pressure-p_min);
        f = MAX(f,t_min);
        f = MIN(f,t_max);
        return f;
}

/*Energy into the Liquid to form Vapor*/
DEFINE_SOURCE(energy_liquid1, cell, thread, dS, eqn)
{
        real source;
        Thread *tm = THREAD_SUPER_THREAD(thread);
        source = - C_UDMI(cell, tm, 15)*L ;
        dS[eqn] = 0.;
        return source;
}


#define DAMP_X0 0.999
#define DAMP_X1 1.0
#define DAMP_P3 -1.86666666666667
#define DAMP_P2  0.88
#define DAMP_P1 -0.16
#define DAMP_A   7.32421875
#define DAMP_B   1.07421875

real damp(real x)
{
        if (x<= DAMP_X0)
```

```
        return 1.0;
    if (x> DAMP_X1)
        return 0.0;
    return DAMP_A* (x* (DAMP_P1+ x* (DAMP_P2+ x*(DAMP_P3+ x))))+
DAMP_B;
}
```